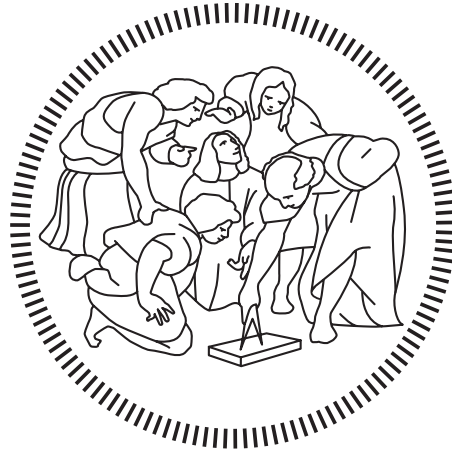


**Politecnico di Milano**

---

SCHOOL OF INDUSTRIAL AND INFORMATION ENGINEERING

Master of Science – Nuclear Engineering



# Derivation and implementation of a point kinetics model for Molten Salt Reactors in GeN-Foam

Supervisor  
**Stefano Lorenzi**

Co-Supervisors  
**Carlo Fiorina**  
**Antonio Cammi**

Candidate  
**ARNALDO SAMUELE MATTIOLI – 920747**

---

Academic Year 2020 – 2021



# Ringraziamenti

Vorrei ringraziare il professor Stefano Lorenzi per il suo indispensabile aiuto in questo lavoro. Ringrazio il professor Antonio Cammi per avermi permesso di lavorare sul progetto di questa tesi e per il suo aiuto durante il suo svolgimento. Sono profondamente grato anche a Carlo Fiorina che mi ha seguito passo dopo passo durante lo svolgimento di questo progetto.

Un ringraziamento speciale lo rivolgo ai miei cari amici Walter, Carmine Bonanni, Valerio, Giulia, Andrea, Nicola, Enrico e Carmine Battistella che mi sono sempre stati vicini e d'aiuto per tutto questo tempo.

Grazie anche agli altri miei amici e ai compagni di studi incontrati durante il mio percorso universitario.

Ringrazio profondamente la mia famiglia che è sempre stata al mio fianco dandomi un indispensabile sostegno e credendo sempre in me.

Ringrazio mio padre Antonio per avermi supportato per tutti questi anni e mia sorella Alice per essere stata enormemente paziente durante i miei periodi di stress.

Infine, devo essere particolarmente grato a mia nonna Elia, che è stata come una madre per me, a mio nonno Arnaldo, che purtroppo non mi vedrà laurearmi, e a mia zia Manuela, che è stata il mio modello di riferimento e sempre lo sarà.

**GRAZIE**



# Abstract

In recent decades, interest in molten salt reactor (MSR) has increased thanks to its entry among the six types of fourth generation (Gen IV) nuclear reactors. Consequently, several models have been developed in order to investigate the physical phenomena present in this type of reactor. The MSR is a circulating fuel reactor (CFR) and the physics due to the re-circulation of the fuel within the system must be considered since it affects, for example, the transport of precursors. In this thesis, a point kinetics model for fluid fuel nuclear systems is developed and presented. In this approach, the precursors are not treated as point quantities but as spatial distributions in the system. In addition to the analytical derivation, the model is implemented in GeN-Foam, an OpenFOAM multiphysics solver for the analysis of nuclear reactor.

Initially, starting from the multi-group diffusion equations and the diffusion and transport equations of the precursors, the analytical derivation is discussed with particular attention to the underlying hypotheses as well as the implementation in the OpenFOAM environment. As verification, the model is tested in a simplified geometry (a mono dimensional channel) and the results compared to an analytical approach. A critical comparison between the new point kinetics model and the multi-group diffusion solver is performed on a two-dimensional geometry representing the molten salt fast reactor (MSFR) to highlight the advantages and disadvantages of the model compared to a standard approach. Two different transients are considered, i.e., an insertion of external reactivity and an exponential reduction of the fuel mass flow rate. As a major outcome, the improved point kinetics models proves to obtain excellent results in reproducing the dynamics of the transients, especially for the distribution of precursors. Finally, a comparison between a one-dimensional and two-dimensional case is carried out considering two different transients. This comparison shows the importance of the spatial description of the precursors, with respect to a point-like approach, and its influence on the evolution of the system.

The results of this investigation are very satisfactory, especially the comparison of the developed model and the diffusion approach, showing the developed solver is able to optimally predict both the dynamics and the final conditions in fluid fuel nuclear systems.



# Sommario

Negli ultimi decenni, l'interesse per il reattore a sali fusi (MSR) è aumentato grazie al suo ingresso tra i sei tipi di reattori nucleari di quarta generazione (Gen IV). Di conseguenza, sono stati sviluppati diversi modelli per studiare i fenomeni fisici presenti in questo tipo di reattore. Il MSR è un reattore a combustibile circolante (CFR) e la fisica dovuta al ricircolo del combustibile all'interno del sistema deve essere considerata poiché influenza, ad esempio, il trasporto dei precursori. In questa tesi viene sviluppato e presentato un modello di cinetica puntiforme per sistemi nucleari a combustibile fluido. In questo approccio, i precursori non sono trattati come quantità puntiformi ma come distribuzioni spaziali nel sistema. Oltre alla derivazione analitica, il modello è implementato in GeN-Foam, un solutore multifisico OpenFOAM per l'analisi di reattori nucleari.

Inizialmente, partendo dalle equazioni di diffusione multi-gruppo e dalle equazioni di diffusione e trasporto dei precursori, si discute la derivazione analitica con particolare attenzione alle ipotesi sottostanti e all'implementazione nell'ambiente OpenFOAM. Come verifica, il modello viene testato in una geometria semplificata (un canale mono dimensionale) e i risultati confrontati con un approccio analitico. Un confronto critico tra il nuovo modello di cinetica puntiforme e il risolutore della diffusione multi-gruppo viene eseguito su una geometria bidimensionale che rappresenta il reattore veloce a sali fusi (MSFR) per evidenziare i vantaggi e gli svantaggi del modello rispetto a un approccio standard. Si considerano due diversi transitori, ovvero un inserimento di reattività esterna e una riduzione esponenziale della portata massica del combustibile. Come risultato principale, i modelli di cinetica puntiforme migliorati dimostrano di ottenere ottimi risultati nella riproduzione della dinamica dei transitori, in particolare per la distribuzione dei precursori. Infine, viene effettuato un confronto tra un caso uni-dimensionale e uno bi-dimensionale considerando due diversi transitori. Questo confronto mostra l'importanza della descrizione spaziale dei precursori, rispetto ad un approccio puntiforme, e la sua influenza sull'evoluzione del sistema.

I risultati di questa indagine sono molto soddisfacenti, in particolare il confronto tra il modello sviluppato e l'approccio di diffusione, mostrando che il solutore sviluppato è in grado di prevedere in modo ottimale sia la dinamica che le condizioni finali nei sistemi nucleari a combustibile fluido.



# Estratto

Grazie al suo ingresso tra i reattori di quarta generazione (Gen IV) e al suo potenziale in materia di sostenibilità, economia, sicurezza, affidabilità e resistenza alla proliferazione, l'interesse per il reattore a sali fusi (MSR) è cresciuto nell'ultimo decennio. Per questo motivo diversi modelli per l'analisi di tali reattori sono stati sviluppati recentemente. Tra i modelli sviluppati ricadono anche i modelli di cinetica puntiforme il cui scopo è studiare - in modo semplificato - l'evoluzione dinamica di tali sistemi durante vari transitori. Infatti, nel MSR la fisica del reattore è strettamente legata al movimento del combustibile fluido e ciò coinvolge anche i precursori che subiscono un processo di trasporto dovuto al movimento del combustibile, oltre alla diffusione dei precursori all'interno del sistema. Questi fenomeni comportano una maggiore complessità delle equazioni da trattare, sia dal punto di vista analitico che numerico. Nella letteratura sono già presenti vari tipi di modelli di cinetica puntiforme, i quali si basano o sulla modifica del modello classico per i reattori convenzionali a combustibile solido, in modo tale da includere i fenomeni del trasporto e della diffusione dei precursori. In alternativa, sono anche presenti derivazioni formali partendo da modelli neutronici più complessi, ad esempio dalle equazioni di diffusione multi-gruppo (MGD). Alcuni lavori presentano una trattazione puntuale dei precursori similmente all'approccio classico. Invece, altri presentano una trattazione dimensionale dei precursori limitandosi però alla direzione assiale (approccio monodimensionale). Per i reattori a combustibile circolante è interessante poter avere e analizzare la distribuzione dei precursori all'interno del sistema poichè influiscono sulla dinamica del sistema durante i transitori. Di conseguenza una trattazione puntuale può essere limitante e portare a risultati erranei. Per quanto riguarda i modelli di cinetica con trattazione uni-dimensionale, oltre ad usare una derivazione non formale, mancano dell'informazione legata all'importanza dei neutroni latenti all'interno del sistema.

In questa tesi un modello di cinetica puntiforme capace di trattare i precursori completamente nello spazio è stato sviluppato, ricavandolo tramite una derivazione formale attraverso una appropriata pesatura dei precursori. Questo comporta l'introduzione di alcune ipotesi necessarie e a una maggiore complessità delle equazioni da risolvere. Partendo dal modello MGD, descritto dal sistema Eq. 1, coerentemente con l'obiettivo di ottenere un modello di cinetica puntiforme, si è deciso di pesare solo l'equazione legata al flusso neutronico:



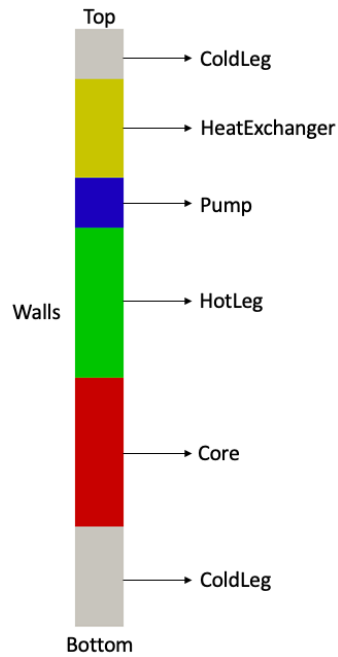


Figure 1: Zone del canale chiuso

	Valore	Unità di misura
Area d'ingresso, $A_{in}$	1	$m^2$
$\dot{m}_{ini}$	3430.6	kg/s
$c_p$	1600	J/(kg)
Conduttanza dello scambiatore, $K$	7.4	MW/(K)
$T_{in,ini}$	963.97	K
$T_{out,ini}$	1144.3	K
$\rho_{0,ini}$	174.01	pcm
$\alpha_{fuel}$	-3.54	pcm/K
$\Lambda$	$1.26 \cdot 10^{-6}$	s

Table 1: Valori principali delle caratteristiche del sistema

I transitori considerati sono due, il primo è un transitorio dovuto a un'inserzione di reattività esterna pari a 57 pcm e l'altro dovuto a una riduzione esponenziale della velocità del fluido nei primi 10 secondi della simulazione con una tempo caratteristico della pompa pari a 2 secondi.

I risultati per il primo transitorio sono mostrati in Tabella 2 :

Inserzione di reattività esterna			
	Cinetica pun- tiforme	Analitico	Errore relativo [%]
$P_{fin}(MW)$	1092.98	1098.20	0.48
$T_{in,fin}(K)$	970.5	970.2	< 0.1
$T_{out,fin}(K)$	1169.5	1170.3	< 0.1
$T_{mean,fin}(K)$	1070	1070.2	< 0.1
$\Delta T_{ml,fin}(K)$	148.4	148.4	< 0.1

Table 2: Risultati del transitorio con un'inserzione di reattività esterna pari a 57 pcm

Per il transitorio con la riduzione di velocità i risultati sono mostrati in tabella 3:

Transitorio con riduzione esponenziale della velocità			
	Cinetica pun- tiforme	Analitico	Errore relativo [%]
$P_{fin}(MW)$	613.66	620.12	1.04
$T_{in,fin}(K)$	908	907.5	< 0.1
$T_{out,fin}(K)$	1221	1223.3	0.19
$T_{mean,fin}(K)$	1064.6	1065.4	< 0.1
$\Delta T_{ml,fin}(K)$	84.8	83.8	1.2

Table 3: Risultati del transitorio con riduzione esponenziale della velocità

Gli errori ottenuti sono ottimi, anche considerando la natura grossolana della mesh (20 centimetri per ogni cella della griglia). Si possono ottenere dei risultati poco più accurati tramite un semplice raffinamento della mesh ma per non aumentare eccessivamente i tempi computazionali delle simulazioni si è deciso di non raffinare la mesh dato che i risultati sono già ottimi.

In seguito, si è effettuato un confronto tra il risolutore sviluppato e quello della diffusione multi-gruppo di GeN-Foam. Quest'ultimo è già un risolutore testato e verificato per l'analisi dei sistemi nucleari. La comparazione ha lo scopo di mostrare come il risolutore sviluppato sia capace di predire correttamente l'evoluzione dinamica di un sistema a combustibile circolante in misura comparabile a quella di ottenibile con una diffusione multi-gruppo. Il confronto è stato fatto su un modello radiale e assiale (Figure 2, quindi bidimensionale, del reattori a sali fusi con spettro neutronico veloce (MSFR).

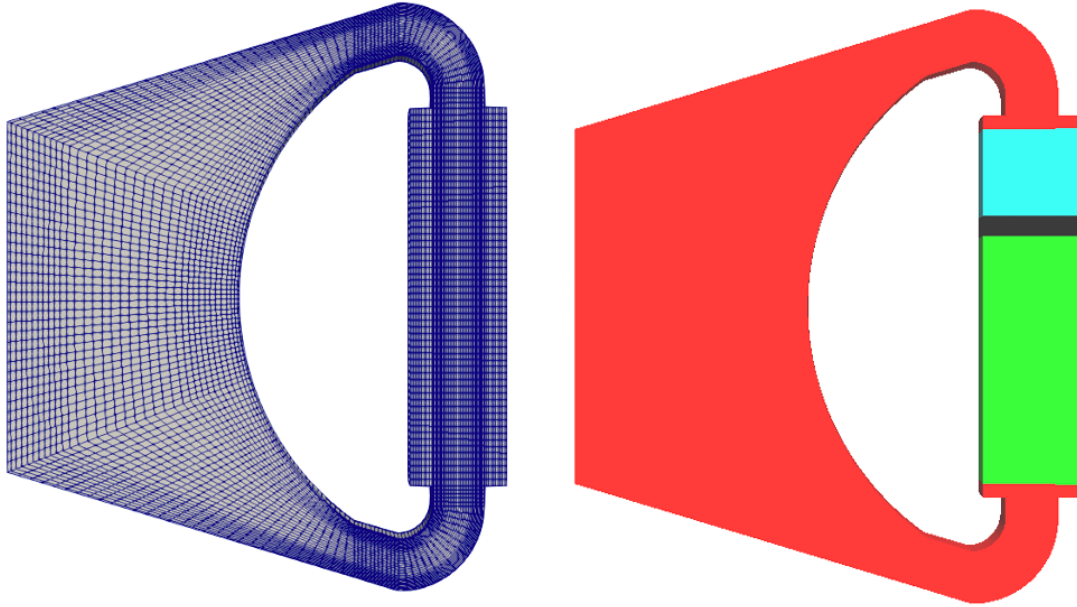


Figure 2: Mesh e zone del modello del 2D-MSFR

I parametri principali del problema sono illustrati in Tabella 4:

	Valore	Unità di misura
Potenza	20	W
$T_{hx}$	900	K
$K_d$	3777.26	pcm
$\alpha_{density}$	4.56	pcm m <sup>3</sup> /kg
$\Lambda$	$1.26 \cdot 10^{-6}$	s

Table 4: Parametri principali del sistema 2D-MSFR

dove i parametri neutronici sono stati ricavati tramite il risolutore della diffusione di GeN-Foam.

Il primo transitorio è dovuto all'inserzione di reattività esterna pari a 53.35 pcm e le evoluzioni ottenute tramite i due risolutori sono confrontate in Figura 3. I transitori successivi sono dovuti a un'esponenziale riduzione della velocità con il tempo caratteristico della pompa uguale a 2 secondi rispettivamente nei primi 10 secondi e nei primi 15 secondi delle simulazioni (Figura 4 e 5).

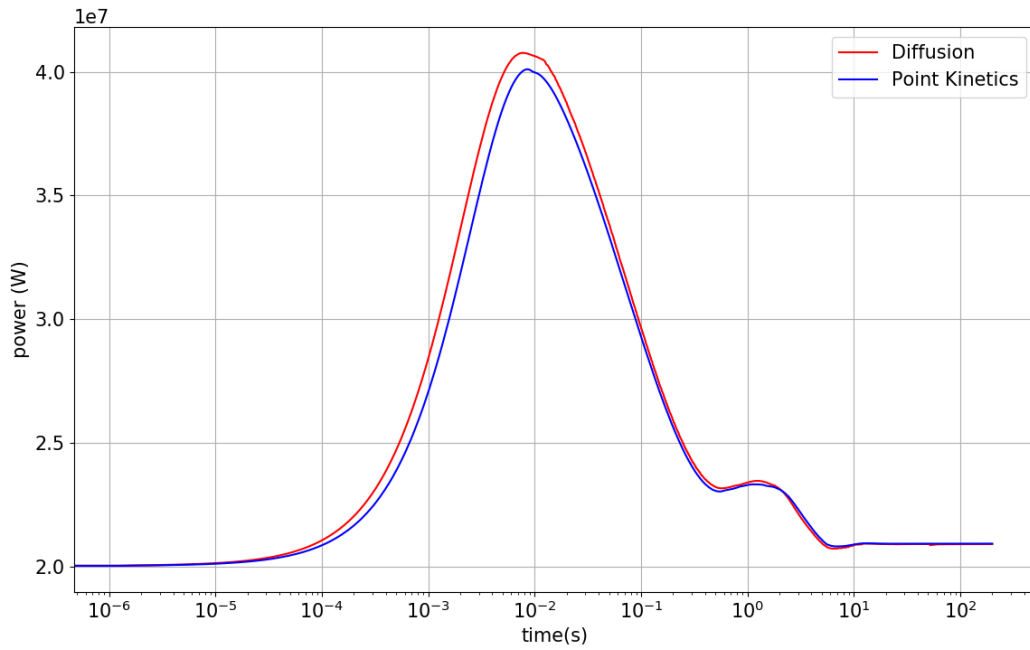


Figure 3: Andamento nel tempo della potenza ottenuto con la cinetica puntiforme e la diffusione nel 2D-MSFR a seguito di un'inserzione di reattività esterna pari a 53.35 pcm

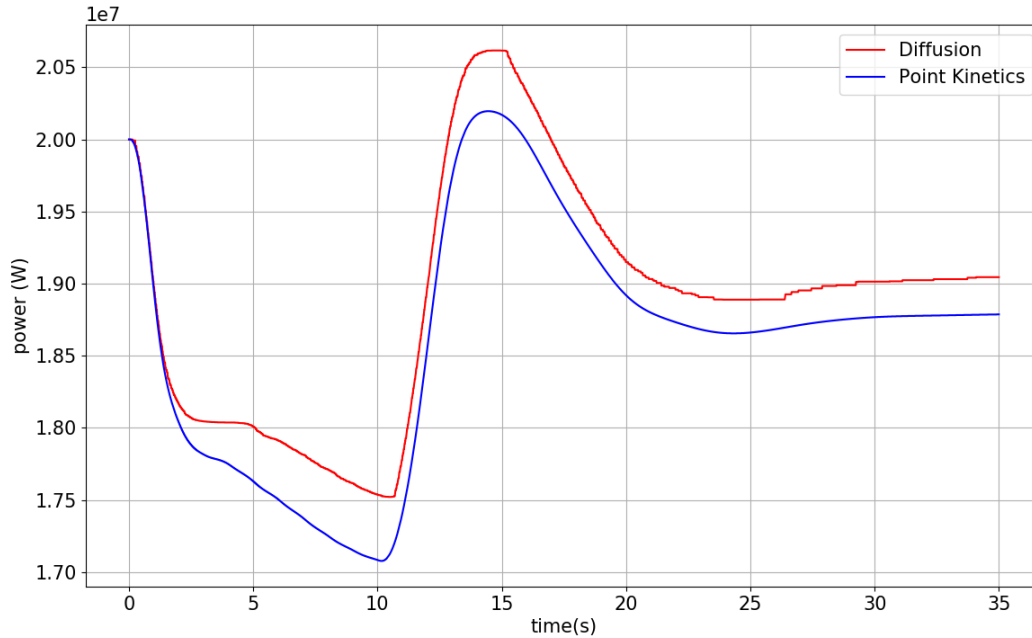


Figure 4: Andamento nel tempo della potenza ottenuto con la cinetica puntiforme e la diffusione nel 2D-MSFR a seguito di una riduzione esponenziale della velocità nei primi 10 secondi di simulazione

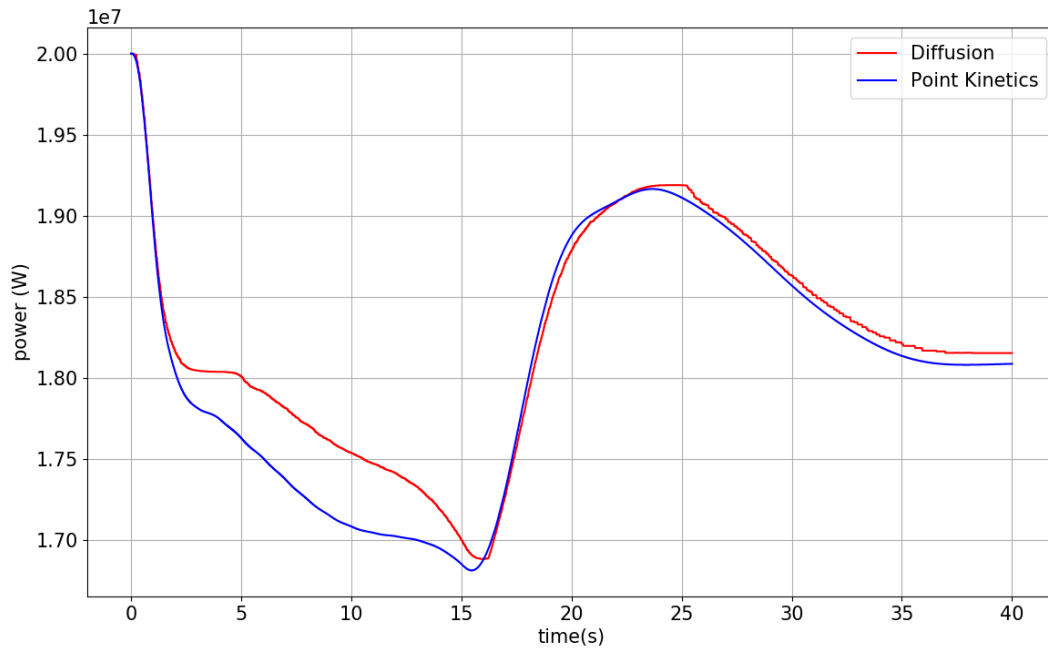


Figure 5: Andamento nel tempo della potenza ottenuto con la cinetica puntiforme e la diffusione nel 2D-MSFR a seguito di una riduzione esponenziale della velocità nei primi 15 secondi di simulazione

Come si può notare dai grafici di confronto il risolutore della cinetica puntiforme riesce a predire l'andamento della potenza nei vari transitori anche se è presente una leggera divergenza dai risultati del MGD. È utile ricordare che il modello della diffusione multi-gruppo è più complesso ma anche più accurato rispetto a un'approccio puntiforme. Anche il confronto riguardante la distribuzione dei precursori ottenuti con i due diversi risolutori è ottimo considerando il buon accordo sulle distribuzioni. Le possibili differenze possono essere spiegate confrontando brevemente i due modelli. Infatti, la cinetica puntiforme descrive i precursori come una potenza su volume, invece, la MGD li descrive semplicemente distribuiti sul volume, e quindi non in termini di potenza:

$$\tilde{C}_i(r, t) = \frac{P_0 v}{\int \phi(0) dV} C_i(r, t) \quad (5)$$

L'ultima parte della tesi è focalizzata sull'investigazione degli effetti dimensionali dei precursori. Tale investigazione è stata fatta tramite un confronto tra la geometria bidimensionale del MSFR e un canale unidimensionale costruito in base al MSFR in modo tale da rispettare i volumi e i tempi di residenza del fluido in ogni zona (Figura 6). Il caso unidimensionale è stato suddiviso poi in due sottocasi, uno con una potenza imposta uniforme sul nucleo (20 MW) e l'altro con una distribuzione di potenza a coseno.

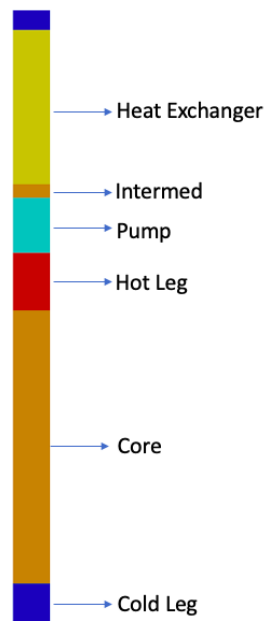


Figure 6: La geometria del 1D-MSFR e le zone della geometria

Il primo transitorio è un transitorio con l'inserzione a parità di reattività esterna in dollari, in questo caso con un'inserzione di 0.1 \$ di reattività (Figure 7).

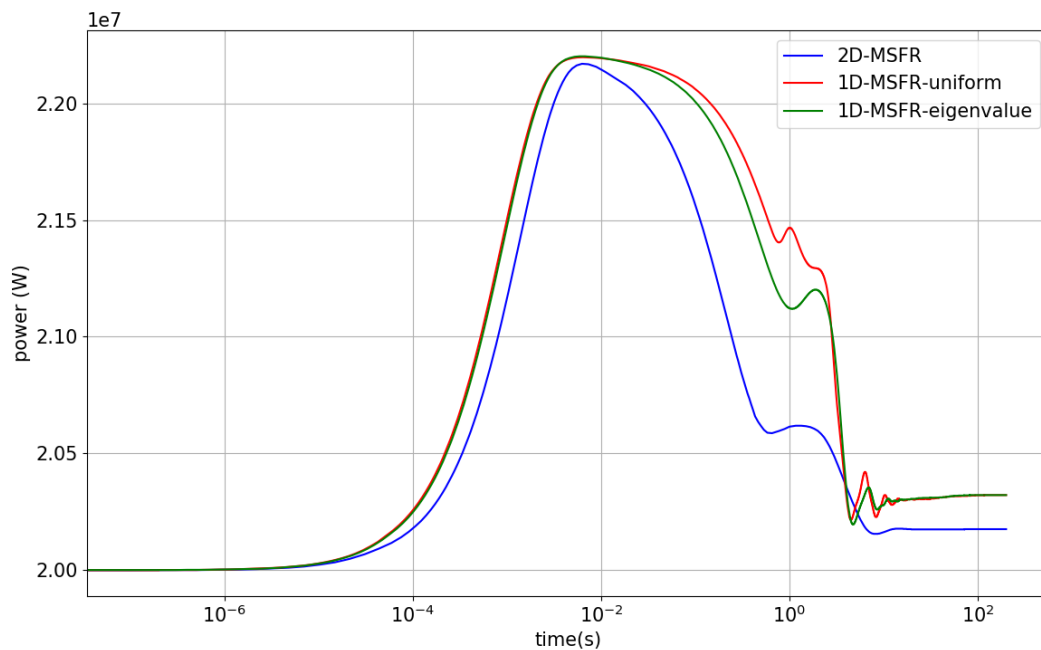


Figure 7: Andamento temporale della potenza per i diversi casi ottenuti con la cinetica puntiforme a seguito di un'inserzione di reattività esterna di 0.1 \$

Si nota come nel caso unidimensionale le oscillazioni dovute al rientro dei precursori nel nucleo sono presenti. Invece, nel caso bidimensionale del MSFR tali oscillazioni non sono presenti, ossia sono smorzate e quindi non sono rilevabili in quest'ultimo caso.

Il transitorio successivo è un transitorio con una riduzione esponenziale della velocità nei primi 10 secondi della simulazione con lo stesso tempo caratteristico della pompa delle precedenti simulazioni, quindi 2 secondi:

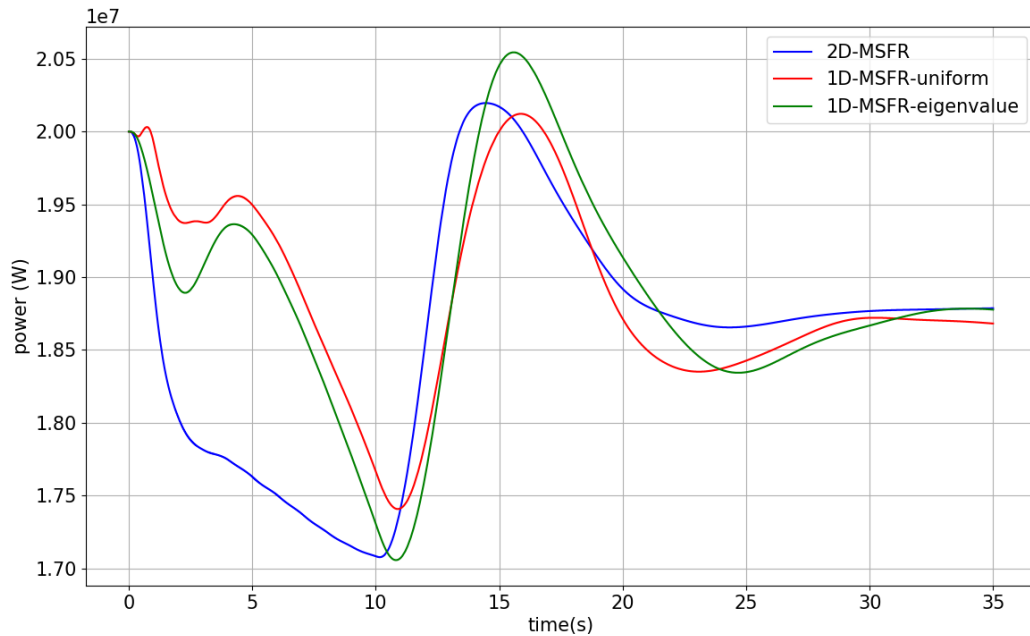


Figure 8: Andamento temporale della potenza per i diversi casi ottenuti con la cinetica puntiforme a seguito di una riduzione esponenziale della velocità nei primi 10 secondi della simulazione

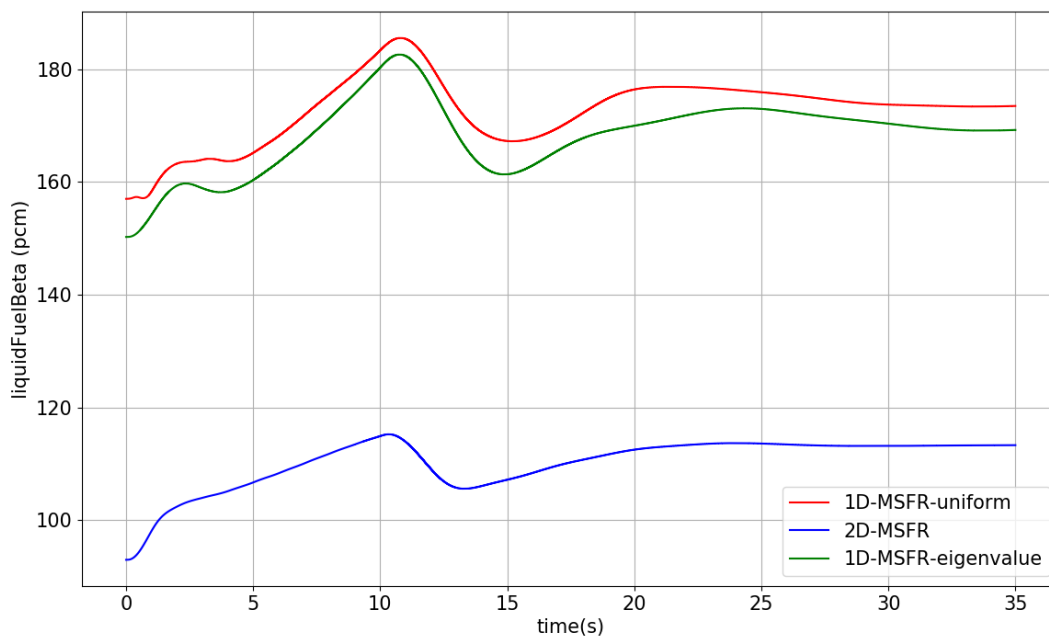


Figure 9: Andamento della reattività dovuta al rientro dei precursori nel nucleo durante il transitorio con la riduzione esponenziale della velocità

Il risultato più importante è la presenza del picco di potenza durante la riduzione di velocità presente nei risultati del sistema unidimensionale. Tali picchi sono dovuti a un maggiore ingresso dei precursori nella regione del nucleo rispetto al caso 2D, come mostrato dai grafici nella Figura 9 seguente che mostra la reattività dovuta al rientro dei precursori nel nucleo durante il transitorio,

In conclusione, in questo lavoro di tesi si è sviluppato un modello cinetico puntiforme per l'analisi di reattori a combustibile circolante (CFR). Tramite le comparazioni con il modello analitico e la diffusione è stato dimostrato come il modello implementato su GeN-Foam riesca a predire lo stato finale e l'evoluzione temporale del sistema in seguito a diverse perturbazioni. Infine, è stato mostrato come tale modello può essere usato come strumento per investigare ed evidenziare gli effetti dimensionali dovuti dalla recircolazione dei precursori all'interno del sistema.

# Contents

<b>Ringraziamenti</b>	<b>iii</b>
<b>Abstract</b>	<b>v</b>
<b>Sommario</b>	<b>vii</b>
<b>Estratto</b>	<b>xviii</b>
<b>Contents</b>	<b>xx</b>
<b>List of Figures</b>	<b>xxiv</b>
<b>List of Tables</b>	<b>xxvi</b>
<b>List of Symbols</b>	<b>xxvii</b>
<b>List of Acronyms</b>	<b>xxxii</b>
<b>1 Introduction</b>	<b>1</b>
1.1 The Molten Salt Reactor . . . . .	1
1.2 GeN-Foam . . . . .	4
1.3 The point kinetics and the state of art for the fluid nuclear system . . . . .	7
<b>2 The point kinetics model for a fluid system</b>	<b>11</b>
2.1 Introduction . . . . .	11
2.2 Analytical derivation of the point kinetics model . . . . .	12
2.3 The model implementation on GeN-Foam . . . . .	18
<b>3 Comparison of the Point Kinetics model with an analytical model</b>	<b>23</b>
3.1 Introduction . . . . .	23
3.2 Description of the analytical model . . . . .	28
3.3 Description of the GeN-Foam model . . . . .	30
3.4 Results . . . . .	34
<b>4 Comparison of the Point Kinetics Model with Diffusion Results</b>	<b>37</b>
4.1 Introduction . . . . .	37
4.2 Test case and numerical modelling . . . . .	38
4.3 The external insertion of reactivity transient . . . . .	45

4.4	The exponential reduction of velocity transient . . . . .	50
4.5	Precursors distributions . . . . .	62
4.6	Conclusion . . . . .	67
<b>5</b>	<b>Investigation of dimensional effects</b>	<b>69</b>
5.1	Introduction . . . . .	69
5.2	The 1D geometry . . . . .	70
5.3	Insertion of external reactivity transients . . . . .	74
5.4	Exponential reduction of velocity transients . . . . .	77
5.5	Conclusion of the comparison . . . . .	80
<b>6</b>	<b>Conclusions</b>	<b>81</b>
<b>A</b>	<b>Appendix</b>	<b>83</b>
A.1	solvePointKineticsLiquidFuel.H . . . . .	83
A.2	computeFeedbackFieldValues.H . . . . .	87
A.3	correctReactivity.H . . . . .	88

# List of Figures

1	Zone del canale chiuso . . . . .	xi
2	Mesh e zone del modello del 2D-MSFR . . . . .	xiii
3	Andamento nel tempo della potenza ottenuto con la cinetica puntiforme e la diffusione nel 2D-MSFR a seguito di un'inserzione di reattività esterna pari a 53.35 pcm . . . . .	xiv
4	Andamento nel tempo della potenza ottenuto con la cinetica puntiforme e la diffusione nel 2D-MSFR a seguito di una riduzione esponenziale della velocità nei primi 10 secondi di simulazione . . . . .	xiv
5	Andamento nel tempo della potenza ottenuto con la cinetica puntiforme e la diffusione nel 2D-MSFR a seguito di una riduzione esponenziale della velocità nei primi 15 secondi di simulazione . . . . .	xv
6	La geometria del 1D-MSFR e le zone della geometria . . . . .	xvi
7	Andamento temporale della potenza per i diversi casi ottenuti con la cinetica puntiforme a seguito di un'inserzione di reattività esterna di 0.1 \$ . . . . .	xvi
8	Andamento temporale della potenza per i diversi casi ottenuti con la cinetica puntiforme a seguito di una riduzione esponenziale della velocità nei primi 10 secondi della simulazione . . . . .	xvii
9	Andamento della reattività dovuta al rientro dei precursori nel nucleo durante il transitorio con la riduzione esponenziale della velocità . . . . .	xvii
1.1	Schematic representation of the Molten Salt Fast Reactor systems in contact with the fuel salt [1] . . . . .	2
1.2	GeN-Foam coupling strategy . . . . .	6
1.3	Schematic representation of feedback in a reactor [2] . . . . .	7
2.1	Flow Chart of the first iteration of the point kinetics solver . . . . .	18
2.2	Flow Chart of the time resolution of the point kinetics solver . . . . .	20
3.1	Zones of the channel . . . . .	24
3.2	Power distribution in the system at steady state . . . . .	25
3.3	The velocity and temperature distributions at steady state . . . . .	27
3.4	Power, total reactivity and fuel temperature predicted by the point kinetics in the closed channel for a reactivity insertion of 57 pcm . . . . .	30
3.5	Power, total reactivity and fuel temperature predicted by the point kinetics in the closed channel for an exponential reduction of velocity in the first 10 seconds . . . . .	31

3.6	Power and average fuel temperature predicted by the point kinetics in the closed channel for an exponential reduction of velocity in the first 10 seconds	32
3.7	Final velocity field after the exponential reduction of velocity . . . . .	33
3.8	Temperature fields: The transient with the exponential reduction of the velocity on the right and the transient with an insertion of reactivity equal to 57 pcm on the left . . . . .	33
4.1	Mesh and the zones of the 2D-MSFR . . . . .	38
4.2	Temperature fields of the steady states: On the right for insertion of external reactivity transient, on the left for the exponential reduction of velocity transient [Left] . . . . .	41
4.3	Spatial distributions of the neutron flux in the steady states: On the right for insertion of external reactivity transient, on the left for the exponential reduction of velocity transient. . . . .	42
4.4	Velocity fields of the steady states: On the right for insertion of external reactivity transient, on the left for the exponential reduction of velocity transient [Left] . . . . .	43
4.5	Check of the steady state for the insertion of external reactivity transient obtained with the diffusion solver . . . . .	45
4.6	Power, total reactivity and average fuel temperature evolutions predicted by the point kinetics in the 2D-MSFR for a reactivity insertion equal to 53.35 pcm . . . . .	46
4.7	Power evolution predicted by the point kinetics and diffusion in the 2D-MSFR for a reactivity insertion equal to 53.35 pcm . . . . .	47
4.8	Final Temperature field and final flux neutron distribution after the transient with insertion of external reactivity equal to 53.35 pcm . . . . .	48
4.9	Check of the steady state for the exponential reduction of velocity transient obtained with the diffusion solver . . . . .	50
4.10	Power, total reactivity and average fuel temperature evolutions predicted by the point kinetics in 2D-MSFR for an exponential reduction of velocity which lasts for the first 10 seconds [PK-10s] . . . . .	52
4.11	Power and average fuel temperature evolutions predicted by the point kinetics in 2D-MSFR for an exponential reduction of velocity which lasts for the first 10 seconds [PK-10s] . . . . .	52
4.12	Velocity evolution in the middle of the heat exchanger for an exponential reduction of velocity which lasts for the first 10 seconds [PK-10s] . . . . .	53
4.13	Power evolution predicted by the point kinetics and the diffusion in 2D-MSFR for an exponential reduction of velocity which lasts for the first 10 seconds [PK-10s] . . . . .	54
4.14	Power, total reactivity and average fuel temperature evolutions predicted by the point kinetics in 2D-MSFR for an exponential reduction of velocity which lasts for the first 15 seconds [PK-15s] . . . . .	55
4.15	Power and average fuel temperature evolutions predicted by the point kinetics in 2D-MSFR for an exponential reduction of velocity which lasts for the first 15 seconds [PK-15s] . . . . .	56

---

4.16	Velocity evolution in the middle of the heat exchanger for an exponential reduction of velocity which lasts for the first 15 seconds [PK-15s] . . . . .	56
4.17	Power evolution predicted by the point kinetics and the diffusion in 2D-MSFR for an exponential reduction of velocity which lasts for the first 15 seconds [PK-15s] . . . . .	57
4.18	Power evolution in the different transients with the two exponential reduction of velocity obtained by the point kinetics [PK-10s vs PK-15s] . . . . .	58
4.19	Final temperature distributions: On the left for the transient with the exponential reduction of velocity which lasts 10 seconds [PK-10s], on the right the one which lasts 15 seconds [PK-15s] . . . . .	59
4.20	Final velocity fields: On the left for the transient with the exponential reduction of velocity which lasts 10 seconds [PK-10s], on the right the one which lasts 15 seconds [PK-15s] . . . . .	60
4.21	Final neutron flux distributions: On the left for the transient with the exponential reduction of velocity which lasts 10 seconds [PK-10s], on the right the one which lasts 15 seconds [PK-15s] . . . . .	60
4.22	Initial distributions of the first group of precursors: On the left the distribution obtained with the diffusion, on the right the one obtained with the PK . . . . .	63
4.23	Initial distributions of the eighth group of precursors: On the left the distribution obtained with the diffusion, on the right the one obtained with the PK . . . . .	63
4.24	Final distributions of the first group of precursors for a reactivity insertion equal to 53.35 pcm: On the left the distribution obtained with the diffusion, on the right the one obtained with the PK . . . . .	64
4.25	Final distributions of the eighth group of precursors for a reactivity insertion equal to 53.35 pcm: On the left the distribution obtained with the diffusion, on the right the one obtained with the PK . . . . .	64
4.26	Final distributions of the first group of precursors obtained with the point kinetics for the exponential reduction of velocity transients: On the left the PK-10s transient, on the right the PK-15s transient . . . . .	66
4.27	Final distributions of the eighth group of precursors obtained with the point kinetics for the exponential reduction of velocity transients: On the left the PK-10s transient, on the right the PK-15s transient . . . . .	66
5.1	The 1D-MSFR geometry and the zones . . . . .	70
5.2	Power distributions at steady states: on the right the one for the imposed power on the core [Imposed Power system] on the core, on the left the one obtained with the eigenvalue calculation [Eigenvalue System] . . . . .	72
5.3	Temperature fields at steady states: on the right the one for the imposed power on the core [Imposed Power system] on the core, on the left the one obtained with the eigenvalue calculation [Eigenvalue System] . . . . .	72
5.4	Check of the steady states through the point kinetics . . . . .	73
5.5	Power evolution for the three cases predicted by the point kinetics for an insertion of reactivity equal to 0.1 \$ . . . . .	75

---

List of Figures

---

5.6	Total reactivity and average fuel temperature evolutions for the three cases predicted by the point kinetics for an insertion of reactivity equal to 0.1 \$	76
5.7	Power evolution for the three cases predicted by the point kinetics for an exponential reduction of the velocity of 10 seconds . . . . .	77
5.8	Total reactivity and average fuel temperature evolutions for the three cases predicted by the point kinetics for an exponential reduction of the velocity of 10 seconds . . . . .	78
5.9	$\beta_{fluid}$ evolution for the three cases predicted by the point kinetics for an exponential reduction of the velocity of 10 seconds . . . . .	79
5.10	Kinetics balance of a fluid fuel nuclear system . . . . .	80

# List of Tables

1	Valori principali delle caratteristiche del sistema . . . . .	xi
2	Risultati del transitorio con un'inserzione di reattività esterna pari a 57 pcm	xii
3	Risultati del transitorio con riduzione esponenziale della velocità . . . . .	xii
4	Parametri principali del sistema 2D-MSFR . . . . .	xiii
3.1	Boundary conditions of the fluid problem . . . . .	24
3.2	Boundary conditions of the neutron problem . . . . .	24
3.3	Table of values used in the analytical problem . . . . .	26
3.4	Results of the transient with an insertion of external reactivity equal to 57 pcm . . . . .	34
3.5	Results of the transient with the exponential reduction of velocity in the first 10 seconds . . . . .	34
4.1	Thermal characteristics of the fluid . . . . .	38
4.2	Characteristics of the heat exchanger . . . . .	39
4.3	Data of the groups of precursors . . . . .	39
4.4	Boundary conditions of the fluid problem . . . . .	40
4.5	Boundary condition of the neutron problem . . . . .	40
4.6	Values obtained and used to compute the feedback coefficients . . . . .	44
4.7	Results for the comparison for a transient with an insertion of external reactivity equal to 53.35 pcm . . . . .	48
4.8	Results for the comparison for the transient with an exponential reduction of velocity which lasts for the first 10 seconds [PK-10s] . . . . .	53
4.9	Result of the $\beta_{fluid}$ for circulating and static fuel obtained with the diffusion model . . . . .	55
4.10	Results for the comparison for the transient with an exponential reduction of velocity which lasts for the first 15 seconds [PK-15s] . . . . .	57
4.11	Results of the two transients with the exponential reduction of velocity . . . . .	58
4.12	Computational times of the simulations of the transients on the 2D-MSFR model . . . . .	61
4.13	Computational advantages between the diffusion and the point kinetics solvers for the simulations of the transients on the 2D-MSFR model . . . . .	61
5.1	Boundary conditions of the fluid problem . . . . .	71
5.2	Boundary conditions of the neutron problem . . . . .	71
5.3	Initial mean values of the initial steady states of the 1D geometry . . . . .	73
5.4	Values of the power of the simulations of the 1D and 2D MSFR . . . . .	74

List of Tables

---

5.5	Final values of the systems at the end of the transient . . . . .	76
5.6	Interesting values of trends power . . . . .	78
5.7	Final values of the systems at the end of the transient . . . . .	78

# List of Symbols

$\alpha$	Albedo coefficient (–)
$\alpha_{density}$	Feedback coefficient of the density of the fluid ( $m^3 kg^{-1}$ )
$\alpha_{fuel}$	Feedback coefficient of the fuel ( $K^{-1}$ )
$\beta$	Total delayed neutron fraction (–)
$\beta_{eff}$	Effective total delayed neutron fraction (–)
$\beta_{fluid}$	Effective fraction of delayed neutron precursors due to the re-circulation (–)
$\beta_{i,eff}$	Effective delayed neutron fraction for the i-th delayed neutron precursor group (–)
$\beta_i$	Delayed neutron fraction for the i-th delayed neutron precursor group (–)
$\chi_{g,i}$	Delayed neutron yield for the g-th group energy of the i-th group of precursors (–)
$\chi_g$	Prompt neutron yield for the g-th energy group (–)
$\Delta T_{ml}$	Logarithmic mean temperature on the heat exchanger ( $K$ )
$\dot{m}$	Mass flow rate ( $kg m^{-3}$ )
$d$	Doppler constant (–)
$\Lambda$	Mean generation time ( $s$ )
$\lambda_i$	Decay constant of the i-th group of precursors ( $s^{-1}$ )
$\nu_g$	Average number of neutrons per fission (–)
$\phi_{g,0}$	Steady state neutron flux of the g-th energy group ( $m^{-2} s^{-1}$ )
$\phi_g$	Neutron flux of the g-th energy group ( $m^{-2} s^{-1}$ )
$\phi_n$	Normalized neutron flux ( $m^{-3}$ )
$\rho$	Reactivity (–)

## List of Symbols

---

$\rho_0$	Equilibrium reactivity (–)
$\rho_{external}$	External reactivity (–)
$\rho_{feedback}$	Reactivity of the feedback (–)
$\rho_{fluid,avg}$	Average density of the fluid ( $kg\ m^{-3}$ )
$\Sigma_{f,g}$	Fission cross section of the g-th energy group ( $m^{-1}$ )
$\Sigma_{R,g}$	Absorption cross section of the g-th energy group ( $m^{-1}$ )
$\Sigma_{s,g'\rightarrow g}$	Group-transfer cross section from the g'-th to the g-th energy group ( $m^{-1}$ )
$\tau_c$	Circulation time of the fluid through the core (s)
$\tau_e$	Circulation time of the fluid through out of primary circuit (s)
$\tilde{C}_i$	Power concentration of the i-th delayed neutron precursor group ( $W\ m^{-3}$ )
$A_{hx}$	Area of the heat exchanger ( $m^2$ )
$c_i^*$	Weighted precursors of the i-th group (W)
$C_i$	Concentration of the i-th delayed neutron precursor group ( $m^{-3}$ )
$c_p$	Specific heat capacity of the fluid ( $J\ kg^{-1}\ K^{-1}$ )
$D_g$	Neutron diffusion of the g-th energy group (m)
$D_{i,f}$	Diffusion constant of the precursor of the i-th group in the fuel ( $m^2\ s^{-1}$ )
$h$	Heat transfer coefficient ( $W\ m^{-2}\ K^{-1}$ )
$J_{in}$	Inlet neutron current ( $m^{-2}\ s^{-1}$ )
$J_{out}$	Outlet neutron current ( $m^{-2}\ s^{-1}$ )
$K$	Conductance ( $W\ K^{-1}$ )
$k_{eff}$	Multiplication factor (–)
$P$	Power (W)
$Q$	Neutron source (–)
$S.F.$	Shape Factor (–)
$S_d$	Delayed neutron source ( $m^{-3}\ s^{-1}$ )
$S_g$	Neutron source of the g-th energy group ( $m^{-3}\ s^{-1}$ )
$S_{n,g}$	Fission neutron source from energy groups other than g-th ( $m^{-3}\ s^{-1}$ )

$S_{s,g}$	Scattering neutron source from neutron energy groups others than the g-th ( $m^{-3} s^{-1}$ )
$T_{fuel,avg}$	Average temperature of the fuel ( $K$ )
$T_{hx}$	Temperature of the heat exchanger ( $K$ )
$T_{in}$	Inlet temperature ( $K$ )
$T_{mean}$	Mean temperature ( $K$ )
$T_{out}$	Outlet temperature ( $K$ )
$u$	Velocity of the fluid ( $m s^{-1}$ )
$v_g$	Average neutron velocity of the g-th energy group ( $ms^{-1}$ )
$V_{hx}$	Volume of the heat exchanger ( $m^3$ )



# List of Acronyms

**CFR** Circulating fuel reactor. v, vii, xviii, xxix, 1, 6, 9

**DNP** Delay neutron precursors. xxix, 9, 10

**Gen IV** Fourth generation. v, vii, ix, xxix

**GeN-Foam** Generalized Nuclear Foam. v, vii, x, xii, xiii, xviii, xix, xxi, xxix, 4–6, 11, 18, 22, 23, 26, 29, 30, 32, 37, 40, 42, 43, 67, 81, 82

**MGD** Multi-group diffusion. ix, xv, xxix, 7

**MPK** Modified point kinetics. xxix, 8, 10

**MSFR** Molten Salt Fast Reactor. v, vii, xii–xvi, xxi–xxiii, xxv, xxix, 2–4, 10, 38, 43, 46, 47, 52, 54–57, 61, 70, 71, 73–78, 81

**MSR** Molten Salt Reactor. v, vii, ix, xxix, 1, 9

**OpenFOAM** Open Field Operation And Manipulation. v, vii, x, xxix, 4, 38

**ORNL** Oak Ridge National Laboratories. xxix, 1

**PK** Point Kinetics. xxii, xxiii, xxv, xxix, 52–60, 63, 64, 66



# Introduction

## 1.1 The Molten Salt Reactor

The main representative of the circulating fuel reactor (CFR) is the molten salt reactor (MSR). The most active development period on the MSR was between the mid 1950s and early 1970s at Oak Ridge National Laboratories (ORNL). However, only after in the new millenium, the interest on this kind of reactor starts to increase because its inclusion as one of six Generation IV reactor types.

The CFRs, in particular the MSR have some differences respect the solid fuel reactor, namely [3]:

- The fission power is directly generated in the fuel which is in liquid form and acts also as a coolant;
- The distribution of the delayed neutron precursors is different to the distribution of the neutron flux due the motion of the fuel. This feature leads to a decrease of their neutronic importance;
- The decay heat is generated in the whole fuel system. This is important for the safety and it must be taken into consideration.

The liquid-fuelled nuclear system has the following advantages over the solid fuel nuclear system [4]:

- A large negative temperature coefficient of the fuel due to the high coefficient of thermal expansion;
- The possibility of continuous fission product removal, making possible to implement an online reprocessing of the fuel and refuelling;
- A better resource utilisation thanks to the higher fuel burn-up than the conventional uranium fuel.

Also the MSRs have other economic, safety, environmental advantages. By listing a few [5]:

- They operate at low pressure and high temperature. Then, these types of reactors are less expensive and they have a higher electrical generation efficiency;

## 1. INTRODUCTION

---

- They can operate as fast or thermal reactor and even as thermal breeder, which operates on the  $U^{233}$ -Th cycle;
- The cladding isn't necessary;
- Obviously, no danger of melting of the fuel;
- No steam explosions;
- They are easier to control and also safer because a lower core excess reactivity can be maintained respect to the traditional reactors.

This thesis is focusing on this type of reactor, in particular the reference reactor will be the Molten Salt Fast Reactor (Figure 4.1). The MSFR is to be operated in the  $Th/U^{233}$  fuel cycle with fluoride salts. The reactor can be started also with the plutonium and minor actinides produced in today's reactors as fissile material.

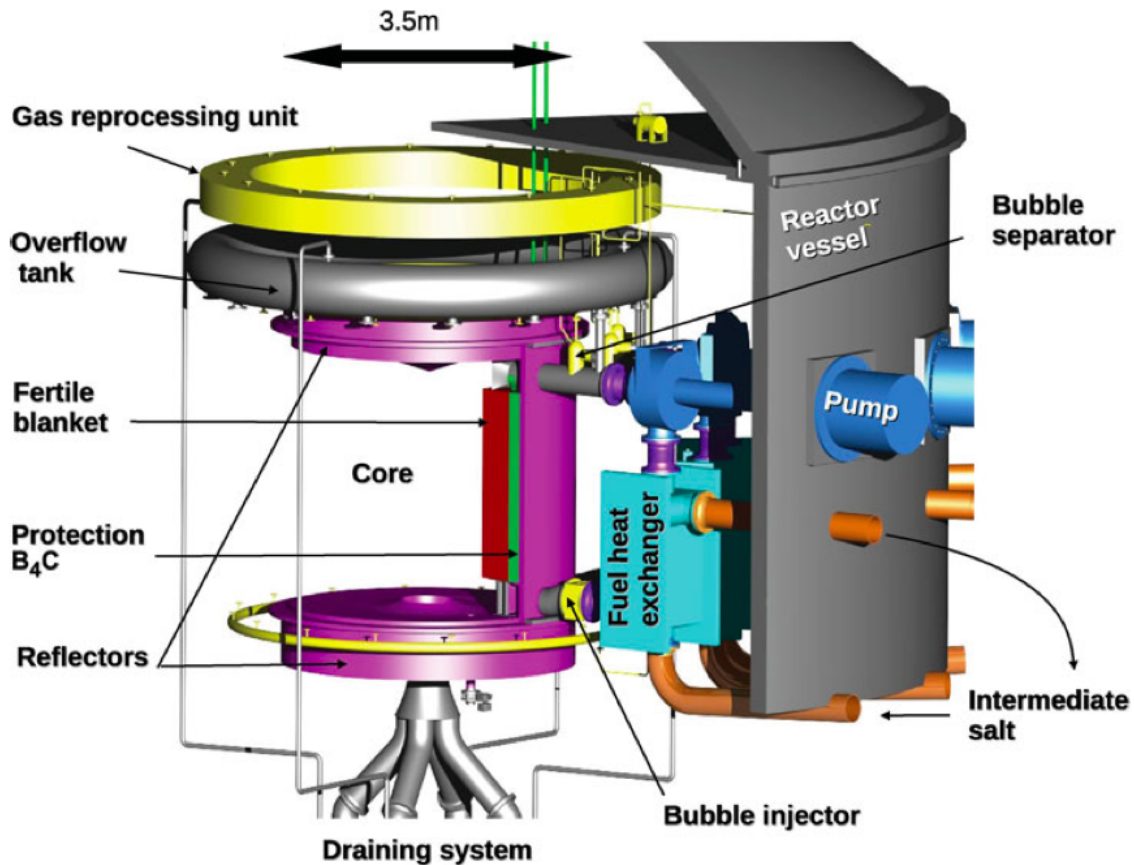


Figure 1.1: Schematic representation of the Molten Salt Fast Reactor systems in contact with the fuel salt [1]

In the following, some components of the MSFR system are briefly described (see Figure 1.1):

- As for the core, a solid moderator is not present. Obviously, in this part of the system, the major part of the fission events occur. Between the the outlet and inlet of the core the difference of temperature is about 100 K with a nominal power of 3 GWth;
- The fuel salt is a mixture of  ${}^7\text{LiF}$  and  $\text{ThF}_4$  at the eutectic point with a proportion of heavy nuclides fixed at 22.5 mol % ( $\text{U}^{233}$  2.5 mol % and  $\text{Th}^{232}$  20 mol %). The neutronic behaviour of the fuel salt is a crucial safety issue. In fact, the safety parameter is the total negative reactivity feedback coefficient related to the fuel temperature and density of the fluid;
- The fertile blanket is necessary to improve the breeding capabilities of the reactor. Here the salt is the same but without any initial fissile material;
- There are two reflectors on the top and on the bottom of the core which can absorb more than 99 % of the leaking neutrons;
- The reactor vessel is present for safety reason;
- A pyrochemical reprocessing unit is meant to remove the lanthanides;
- The bubble injection has the aim to increase the velocity of the bubbling extraction in order to extract insoluble fission products from the salt;
- The pumps and the heat exchangers are organised in 16 units as the bubble injection and the bubble separator.

## 1.2 GeN-Foam

GeN-Foam is a solver based on OpenFOAM [6] which couples together a multi-scale mesh sub-solver for thermal-hydraulics, a sub-solvers in order to solve the neutronic problem. The latter is mainly a multi group diffusion solver and it will be used in the chapter 4 is used. In addition, a displacement based sub-solver is used for the thermal-mechanics problem and a finite-difference model for the evaluation of the temperature field in the fuel [6]. It is used for the analysis of heterogeneous and homogeneous reactors. Then it can be used for example both for thermal reactor and for the fast reactor, as the MSFR. Thanks to the geometrical domain decomposition, all the solvers have parallel computation capabilities. In this description, only the governing equations of the solvers used in this thesis work will be introduced. Also the coupling strategy used by GeN-Foam will be explained briefly.

The thermal-hydraulics solver is based on the standard  $k - \epsilon$  turbulence model for compressible or incompressible flow. However, this solver is extended to a coarse-mesh applications through the use of a porous medium approach for user-selected cell zones inside the mesh. Starting from the turbulent single-phase flow of a fluid in a porous medium solver, the equations are the following:

$$\frac{\partial \gamma \rho}{\partial t} + \nabla(\gamma u_d) = 0 \quad (1.1)$$

$$\frac{\partial \rho u_d}{\partial t} + \frac{1}{\gamma} \nabla(\rho u_d \times u_d) = \nabla(\mu_T \nabla(u)) - \gamma \nabla p + \gamma F_g + \gamma F_{ss} - (\rho u_d \times u_d) \nabla \frac{1}{\gamma} \quad (1.2)$$

$$\frac{\gamma \rho e}{\partial t} + \nabla(u_d(\rho e + p)) = \gamma \nabla(k_T \nabla T) + F_{ss} u_d + \gamma \dot{Q}_{ss} + (k_T \nabla T) \nabla \gamma \quad (1.3)$$

where  $\gamma$  is the porosity term. The solver takes into account only the part of the volume occupied by the fluid, using the Darcy velocity  $u_d$ :

$$u_d = \gamma u \quad (1.4)$$

The terms  $F_{ss}$  and  $\dot{Q}_{ss}$  represent the effect of the sub-scale structures on the fluid flow.  $F_{ss}$  is the drag force exerted by the sub-scale structures on the fluid and it is proportional to the Darcy velocity and this proportionality is represented by the tensor  $k(u_d)$ :

$$F_{ss} = k(u_d) u_d \quad (1.5)$$

$\dot{Q}_{ss}$  is the volumetric heat which is transferred between the fluid and the sub-scale structure:

$$\dot{Q}_{ss} = A_V h(T_{ss} - T) \quad (1.6)$$

$$\rho_{ss} c_{p,ss} \frac{\partial T_{ss}}{\partial t} = \nabla(\gamma k_{ss} \nabla T) + A_V h(T - T_{ss}) \quad (1.7)$$

where  $T_{ss}$  is the local temperature of the sub-scale structure. Also in order to simplify the problem in the heat exchanger, there is the possibility to model this part of the system with a fixed temperature:

$$\dot{Q}_{ss} = A_V h_{eff}(T_{ext} - T) \quad (1.8)$$

The solution of Equations 1.1, 1.2 and 1.3 is achieved through a PIMPLE pressure-based algorithm for compressible flows.

The solver for the turbulence is built starting from the standard  $k - \epsilon$  model for RANS equations. Anyway, the problem of predicting  $k$  and  $\epsilon$  becomes complex in the porous zones. Then, GeN-Foam avoids solving the standard model in the porous zones. In fact, in these zones it forces the values of  $k$  and  $\epsilon$  to converge to the values  $k_0$  and  $\epsilon_0$ , which can be chosen by the user, through a selected convergence rate  $\lambda_{\epsilon/k}$ :

$$\rho \frac{\partial \epsilon}{\partial t} + \nabla(\rho u_d \epsilon) = \rho \lambda_{\epsilon/k} (\epsilon_0 - \epsilon) \quad (1.9)$$

$$\rho \frac{\partial k}{\partial t} + \nabla(\rho u_d k) = \rho \lambda_{\epsilon/k} (k_0 - k) \quad (1.10)$$

The sub-solver for the fuel temperature profile, and also for the cladding temperature profile, is based on the following equations:

$$\rho_f C_{p,f} \frac{\partial T_f}{\partial t} = k_f \frac{\partial^2 T_f}{\partial r^2} + k_f \frac{1}{r} \frac{\partial T_f}{\partial r} + \dot{Q}_f \quad (1.11)$$

$$\rho_c C_{p,c} \frac{\partial T_c}{\partial t} = k_c \frac{\partial^2 T_c}{\partial r^2} + k_c \frac{1}{r} \frac{\partial T_c}{\partial r} \quad (1.12)$$

In this sub-solver the axial-symmetric of the geometry is assumed and the axial heat conduction is neglected.

After having introducing some governing equations of GeN-Foam, it is useful to explain the coupling strategy used by GeN-Foam to couple the difference solvers.

In the Figure 1.2, the coupling strategy can be seen. The simulation starts with the selection of a initial time step. The next time steps are decided based on the requirement between the Courant number condition in the fluid and a maximum allowed power variation. All these values can be chosen by the user and for thermal-hydraulics calculation the Courant number has been set to 1 in the simulations of this thesis. Initially, GeN-Foam starts the simulation following the structure of the PIMPLE loop in order to solve the velocity, pressure and energy. The first equation solved is the mass conservation (Eq. 1.1) followed by the resolution of the  $k - \epsilon$  equations. Then, the velocity predictor step is an optional step based on Eq. 1.2 which uses the pressure field from the previous iteration. After a pressure correction equation is solved in order to correct the non-orthogonality effects.

Then the energy equation is solved in order to obtain the temperature fields and the outer correctors are performed to resolve the coupling of the pressure, velocity and energy. Once the coolant flow and the fluid temperature are obtained, the fuel and cladding are calculated through the equations 1.11 and 1.12, updating the energy equation. Finally after these steps, it solves the thermal-mechanics problem and the neutron one which

## 1. INTRODUCTION

are coupled with the sub-scale temperatures solver and with the sub-solver of the energy equation. It is important to state that GeN-Foam allows to solve only the equations selected by the user, leaving the other fields unaltered. Then, for example, it is possible to solve together the neutronics problem and the thermal-hydraulic one but also it is possible to solve only the neutron one while the other fields remain unaltered.

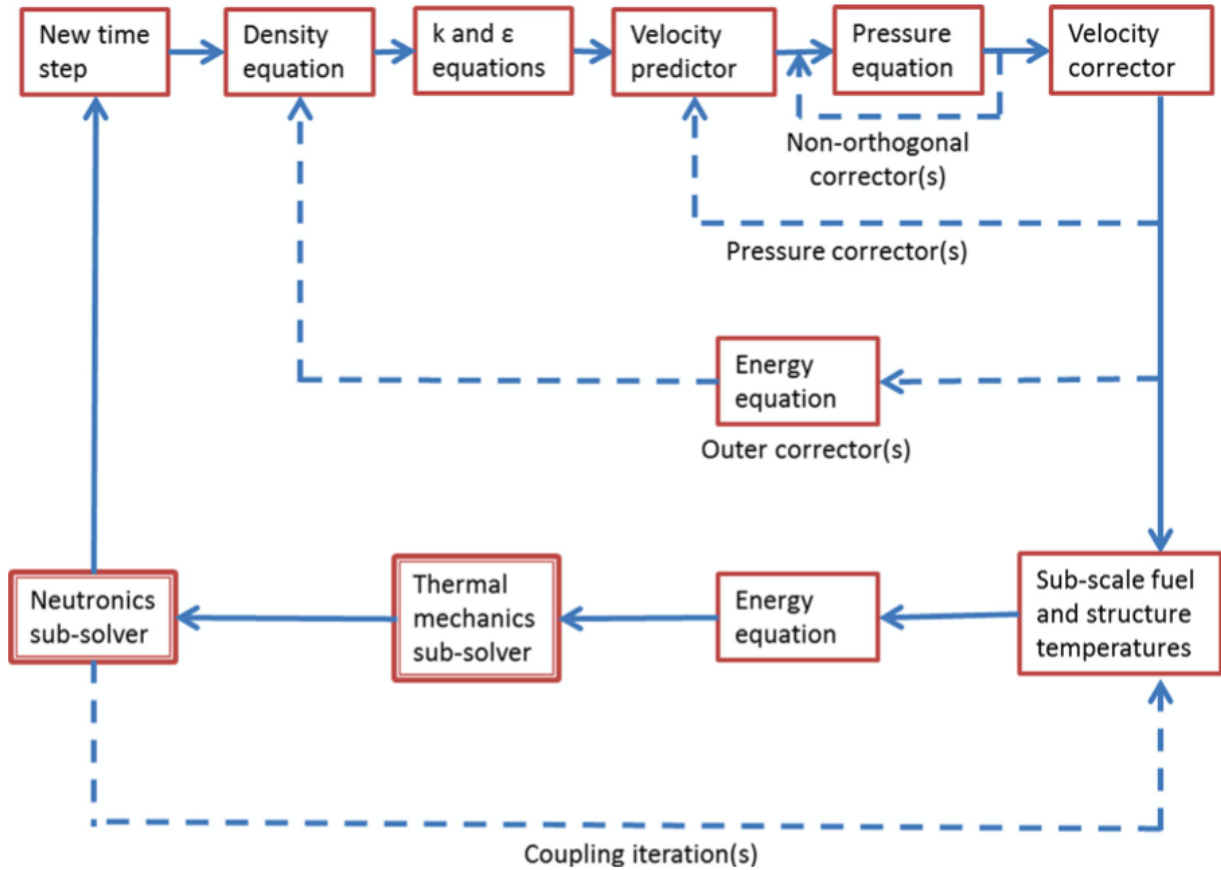


Figure 1.2: GeN-Foam coupling strategy

As said before, the purpose of this thesis is the development of point kinetics model for CFR and its implementation in GeN-Foam in order to solve the neutronics problem without using the multi-group diffusion solver for the calculation of different transients. In particular, the aim is to show that the spatial representation of the precursors is a key issue in the determination of the dynamics of CFR and that a point kinetics model with this spatial modelling can reach satisfactory simulation capabilities.

### 1.3 The point kinetics and the state of art for the fluid nuclear system

The point kinetics model is a set of equations which are used to study the kinetic behaviour of a nuclear system. In this kind of model, the spatial dependence of the quantities of interest (i.e., neutron flux and precursors) is neglected. In fact, in many situation only the dominant features of the time behaviour of the neutron population is important for the problem , for example for the calculation of the power variation during a transient [7]. Furthermore, the point kinetics is simpler to solve than the multi-group diffusion (MGD) equations and therefore it is used to predict the time-response of a nuclear system under given circumstances and perturbations, for example, an insertion of external reactivity or a failure of a pump. Then it is useful both for engineering safety and for stability analysis of the reactor.

The point kinetics model can be obtained with a balance of the prompt and delayed neutrons inside the system or also with a more accurate method, which consists in weighing the equations of the multi-group diffusion equations (MGD) and the equations of precursors with a weight function, for example with the adjoint flux.

For a nuclear system with solid fuel the point kinetics is the following one and it can be obtained with both methods [8]:

$$\begin{cases} \frac{dP(t)}{dt} = \frac{\rho(t) - \beta_{eff}}{\Lambda} P(t) + \sum_{i=1}^R \lambda_i c_i(t) \\ \frac{dc_i(t)}{dt} = \frac{\beta_{i,eff}}{\Lambda} - \lambda_i c_i(t) \quad i = 1, 2, \dots, R \end{cases} \quad (1.13)$$

where  $\rho(t)$  represents the reactivity,  $\Lambda$  is the mean generation time of the system,  $\beta_{i,eff}$  and  $\beta_{eff}$  are the effective delayed neutron fraction for the i-th delayed neutron precursor group and effective total delayed neutron fraction, respectively,  $\lambda_i$  is the decay constant of the i-th precursor group. P is the power of the system and  $c_i$  is the amount of delayed neutron of the i-th precursor group. As one can note the equations of the point kinetics are simpler than those of the multi-group diffusion. The main difficulty of this method is to have the necessary parameters to describe the reactor, as  $\Lambda$  or the feedback coefficients which are used to couple the feedback effects with the point kinetics equations.

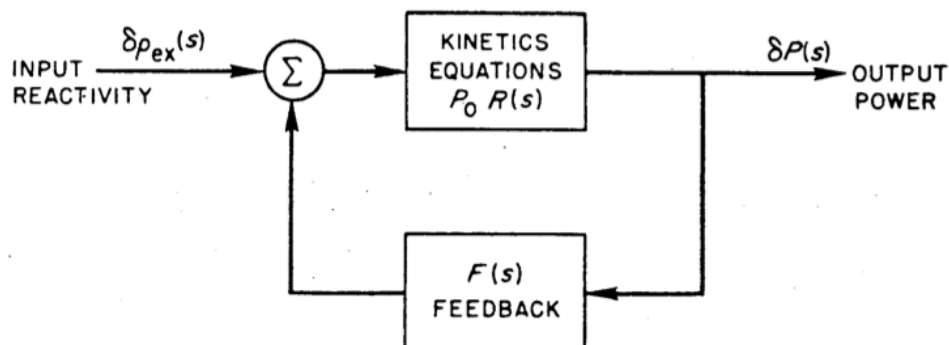


Figure 1.3: Schematic representation of feedback in a reactor [2]

## 1. INTRODUCTION

---

For the liquid fluid nuclear system, the derivation of a point kinetics model is more complex due to the presence of a term of diffusion and a term of transport in the precursors equations.

Considering a balance approach, the classic point kinetics equation for the precursors is modified in a such way that it takes into account the effect of the fuel motion, which causes the transport of precursors. The equations are the following [9]:

$$\frac{dP(t)}{dt} = \frac{\rho(t) - \beta_{eff}}{\Lambda} P(t) + \sum_{i=1}^R \lambda_i c_i(t) \quad (1.14)$$

$$\frac{dc_i(t)}{dt} = \frac{\beta_{i,eff}}{\Lambda} P(t) - \lambda_i c_i(t) - \frac{c_i(t)}{\tau_c} + \frac{c_i(t - \tau_e)}{\tau_c} e^{-\lambda_i \tau_e} \quad i = 1, 2, \dots, R \quad (1.15)$$

This point kinetics formulation can be seen as the result of a balance of neutrons in the entire system where the terms with  $\tau_c$  and  $\tau_e$  represent the effects of the fuel motion on the delayed neutrons precursors.

Considering a weighting approach, the procedure is more complex and several terms need to be introduced as one can see in the following modified point kinetics model (MPK) [10]:

$$\begin{cases} \frac{dP(t)}{dt} = \frac{\rho_s - \tilde{\beta}}{\Lambda_P} P(t) + \sum_{i=1}^R \lambda_i \Gamma_i + \tilde{S} \\ \frac{d\Gamma_i}{dt} = \frac{\tilde{\beta}_i + \rho_i}{\Lambda_i} P(t) - (\lambda_i + \mu_{mu,i} + \mu_{\epsilon,i}) \Gamma_i + \sigma_i \quad i = 1, 2, \dots, R \end{cases} \quad (1.16)$$

This model has been obtained starting from the multi-group diffusion through a weighing made with the adjoint flux for the neutron flux equation and with the adjoint precursors for the equations of the precursors. Regarding the new terms:

- $\Gamma_i$  is the unknown related to the precursors of the  $i$ -th group;
- $\rho_s$  is the sum of  $\rho_0$ , the equilibrium reactivity of the system, and  $\rho_{pert}$ , the reactivity related to the perturbation;
- $\tilde{\beta}_i$  and  $\tilde{\beta}$  are the effective delayed neutrons fraction of the  $i$ -th group and the total fraction of delayed neutrons;
- $\Lambda_P$  and  $\Lambda_i$  are the prompt neutron lifetime and precursor lifetime of the  $i$ -th group related to the motion of the fuel;
- $\rho_i$  is an unconventional precursor reactivity term;
- $\mu_{\mu,i}$  and  $\mu_{\epsilon,i}$  are two constant, the first related to the perturbation of the fluid and the other related to the perturbation of the recirculating time of the fuel;
- $\sigma_i$  is an apparent source which takes into account the recirculation of the fissile material.

### 1.3. THE POINT KINETICS AND THE STATE OF ART FOR THE FLUID NUCLEAR SYSTEM

---

Several new terms related to the motion of the fuel and the transport, and also diffusion, of the precursors appear in this model. Also the definitions of new reactivity appear, where the most important is the equilibrium reactivity. This reactivity can be obtained also with the previous point kinetics model (see Eq. 1.17) and it is equal to zero for a solid fuel nuclear system (it can be seen if the time derivatives of the Eq. 1.13 are neglected).

$$\rho_0 = \beta - \sum_{i=1}^R \frac{\beta_i \lambda_i}{\lambda_i + \frac{1 - e^{-\lambda_i \tau_e}}{\tau_e}} \quad (1.17)$$

The equilibrium reactivity compensates the loss of the delayed neutron precursors (DNP) in the out-of-core part of the primary circuit and it guarantees the steady state condition of the system in the numerical models [11].

In all the point kinetics formulations just seen, the precursors are treated as point quantities even if the motion is accounted for. The main assumption in this regard is a fixed parameters ( $\tau_c$  and  $\tau_e$  in the first one,  $\mu_{e,i}$  and  $\sigma_i$  in the second one) that are constant during the transients. Since in the CFRs the precursors are transported within the system due to the motion of the fuel, the coupling with the velocity is relevant as well as the delayed neutron importance. Consequently, it could be important to have the spatial information related to the precursors also in a point-like approach. This aspect is not faced by the aforementioned models.

This is especially true if we look at the oscillations of power due to the recirculation of the precursors in the system, in particular when the precursors return back in the primary circuit, during a transient or even a case where the fuel velocity field is altered, which leads to a change in the distributions of precursors [12].

As for the spatial distribution of the precursors, in the literature, there are 1D approaches as the following one [13]:

$$\begin{cases} \frac{dN(t)}{dt} = \frac{\rho(t) - \beta}{\Lambda} P(t) + \sum_{i=1}^R \lambda_i C_i(t) \\ \frac{\partial c_i(z,t)}{\partial t} - \frac{\Gamma_1 H^c}{M_f^c} \frac{\partial c_i(z,t)}{\partial z} = \frac{\beta_i}{\Lambda} n(z,t) - \lambda_i c_i(z,t) \quad i = 1, \dots, R \end{cases} \quad (1.18)$$

where  $\Gamma_1$  is the mass flow rate in the primary circuit,  $H^c$  is the height of the core,  $M_f^c$  is the mass of the fuel in the core and  $n(z,t)$  is the neutron density.

To complete the model, a boundary condition has to be imposed on the inlet and on the outlet of the reactor core:

$$c_i(0, t) = c_i(H^c, t - \tau_e) e^{-\frac{\lambda_i}{\tau_e}} \quad i = 1, \dots, R \quad (1.19)$$

In this one-dimensional model, the DNP motion in a MSR can be appreciated in more detail. However, this model leads to a more complex system of equations to solve. In fact, now the partial differential equations must be solved instead of the ordinary differential equation. In this kind of model also the diffusion of precursors is neglected but this can be considered of minor importance with respect to the convective term [14]. Also a link to couple the equations of precursors and the power equation, in this case the neutron population  $N(t)$ , is necessary. This link is obtained by an integration on the axial direction of the system, where the distributions of precursors is discretized [15]:

$$C_i(t) = \int_0^H c_i(z, t) dz \quad i = 1, \dots, R \quad (1.20)$$

Imposing a sinusoidal shape, the neutron density is derived by the neutron population:

$$n(z, t) = \frac{N(t)}{2} \sin \frac{\pi z}{H} \quad (1.21)$$

The introduction of a spatial discretization also in the DNP modelling is important to correctly simulate the shape of the power peak and its evolution, in order to look in more detail the effects of the spatial distributions of the precursors in the fluid fuel nuclear system. In addition, the modelling of the DNP axial distribution notably affects the steady-state reactivity [16]. Hence, the results and the balance of precursors could be altered by changes in the mathematical method used [17].

Anyway, these models are limited to a purely axial description of the precursors, neglecting for example the radial behaviour of the precursors. In system like the MSFR, this can be a remarkable limitation. Furthermore, the axial integration does not allow to take into account the different importance associated with the different axial positions of the reactor [15].

In the next chapter, a point kinetics model is developed starting from a formal derivation, similar to the derivation of the MPK, in order to not neglect any information related to the spatial distributions of the precursors. This way, this approach can be used to study also 2D or 3D geometries.

# The point kinetics model for a fluid system

## 2.1 Introduction

In this chapter, the main aim is to obtain a point kinetics model for the fluid fuel nuclear systems. The fundamental concept of this derivation is not to treat the precursors as point quantities. As a consequence, it will be not possible to use a balance of the system to find the point kinetics equations (Eq. 1.14 and 1.15), but a more accurate method is used in order to achieve this goal, i.e., starting from a more complex neutronics model - the multi-group neutron diffusion - and use a projection approach. However, if we apply the projection both on the neutron and precursors equations, the model will be very similar to that represented by the Eq. 1.16 and the precursors will be treated as point quantities. Hence the path chosen is to weight only the equation related to the prompt neutrons. This way, it is possible to use a point-like approach for the power estimation and, at the same time, to treat the precursors as quantities with a fully spatial distribution in the system. This strategy entails the following issues:

- The necessity to find a quantity capable of coupling the time equation of the power and the spatial time equations of the precursors;
- The presence of some terms which in the field of point kinetics are not used;

The first problem is solved using a weighting of the precursors which is used only in the power equation. Then in this model the weighted precursors are used only as a link between the two family of equations.

The second problem is solved introducing the hypothesis that these terms are constant in the space. This hypothesis allows to manipulate the precursors equations and to find the point kinetics model which can be used in this field.

After, the implementation of this model on GeN-Foam and its fundamental characteristics will be illustrated.

## 2.2 Analytical derivation of the point kinetics model

In order to obtain a point kinetics model for the neutron problem it is necessary to start from the equation of neutron transport or from the simplest equation of the multi-group energy diffusion equation, as in the following discussion.

Considering R-th groups of precursor (index i) and G-th (index g) energy groups for the neutron flux, the neutron diffusion equation is coupled with the transport-diffusion equation of the precursors for a fluid system and the system to solve is the following:

$$\left\{ \begin{array}{l} \frac{1}{v_g} \frac{\partial \phi_g}{\partial t} = (\nabla \cdot D_g \nabla - \Sigma_{R,g}) \phi_g + (1 - \beta) \chi_g \sum_{g'=1}^G (\nu \Sigma_f)_{g'} \phi_{g'} + \sum_{g'=1, g' \neq g}^G \Sigma_{s, g' \rightarrow g} \phi_{g'} + \\ \sum_{i=1}^R \chi_{g,i} \lambda_i C_i + S_g \\ \frac{\partial C_i(r,t)}{\partial t} + u \cdot \nabla C_i = -\lambda_i C_i + \beta_i \sum_{g=1}^G (\nu \Sigma_f)_g \phi_g + \nabla \cdot D_{i,f} \nabla C_i \end{array} \right. \quad (2.1)$$

The main problem of obtaining a point kinetics model is the weighting of the terms of transport and diffusion on the precursors equation. In fact, after the precursors equation is weighted, the information on the spatial distribution of the precursors is lost (or better variation of the spatial distribution cannot be taken into account).

But in this thesis the purpose is to develop a model which does not lose the information related to the spatial distribution of the precursors in the system.

The hypothesis that the neutron flux can be divided into a space-dependent and a time-dependent part,  $T(t)$ , is introduced [18]:

$$\phi_g(r, E, t) = \phi_{g,0}(r, E) T(t) \quad (2.2)$$

$T(t)$  is defined as a weighted integral of the total number of neutrons present in the reactor at any time:

$$T(t) = \int \int \frac{1}{v_g} \phi_g W dV dE = T(t) \int \int \frac{1}{v_g} \phi_{g,0} W dV dE \quad (2.3)$$

Instead below the integral  $L(t)$  is defined, which is the normalized quantity chosen. In fact, it is equal to 1 for each time instant, thanks also to the definition of  $T(t)$ :

$$L(t) = \int \int \frac{1}{v_g} \phi_{g,0} W dV dE = 1 \quad (2.4)$$

$$L(t) = 1 \quad \forall t \quad (2.5)$$

---

## 2.2. ANALYTICAL DERIVATION OF THE POINT KINETICS MODEL

---

Then the quantity of the Eq. 2.6 is added and subtracted in the neutron equation, which is the production term of the precursors due to the neutron flux multiplied for the spectrum of the delay neutrons:

$$\sum_{i=1}^R \sum_{g'=1}^G \chi_i \beta_i (\nu \Sigma_f)_{g'} \phi_{g'} \quad (2.6)$$

After this modification, the neutron equation is multiplied by  $W$ , the weight function (which will be defined after), and integrated on energy and on volume.

Now the usual quantities as the reactivity and the mean generation time must be defined.

The fission rate,  $F(t)$ , is defined as follows and then the neutron equation is divided by the fission rate:

$$F(t) = \sum_{g=1}^G \int \int W [\chi_g (1 - \beta) + \sum_{i=1}^R \chi_{g,i} \beta_i] \sum_{g'} (\nu \Sigma_f)_{g'} \phi_{g'} dV dE \quad (2.7)$$

It can be seen that, after doing the steps above, on the left of the equation the mean generation time  $\Lambda$  is found, which is defined in (Eq. 2.8):

$$\Lambda(t) = \frac{L(t)}{F(t)} \quad (2.8)$$

To derive the reactivity, a reaction rate,  $R(t)$ , must be defined. It takes into account the terms of diffusion, capture and fission, including the quantity added to the equation of diffusion (see Eq 2.6):

$$\begin{aligned} R(t) = & \int \int W (\nabla \cdot D_g \nabla - \Sigma_{R,g}) \phi_{g,0} dV dE + \\ & \int \int W [(1 - \beta) \chi_g \sum_{g'=1}^G (\nu \Sigma_f)_{g'}] dV dE + \\ & \int \int W [\sum_{i=1}^R \sum_{g'=1}^G \chi_i \beta_i (\nu \Sigma_f)_{g'}] dV dE + \\ & \int \int W [\sum_{g'=1, g' \neq g}^G \Sigma_{s,g' \rightarrow g}] \phi_{g',0} dV dE \end{aligned} \quad (2.9)$$

Thanks to the reaction rate the reactivity,  $\rho(t)$ , can be defined:

$$\rho(t) = \frac{R(t)}{F(t)} \quad (2.10)$$

Also the  $\beta_{i,eff}$  and the  $\beta_{eff}$  are defined below:

## 2. THE POINT KINETICS MODEL FOR A FLUID SYSTEM

---

$$\beta_{i,eff} = \frac{\int \int W \sum_{g'=1}^G \chi_i \beta_i (\nu \Sigma_f)_{g'} \phi_{g',0} dV dE}{F(t)} \quad (2.11)$$

$$\beta_{eff} = \sum_{i=1}^R \beta_{i,eff} \quad (2.12)$$

The source with the weighting becomes a point source in the following way:

$$Q(t) = \frac{\int \int W S_g dV dE}{L(t)} \quad (2.13)$$

Having weighed the neutron diffusion equation, a weighted time-dependent form of the precursors is introduced (which it is not dependent on the space). This quantity will be used as the link between the point power equation and the diffusion and transport equation of the precursors. The first form of the weighed precursors is the following:

$$c_i(t) = \frac{\int \int W \chi_{g,i} C_i dV dE}{L(t)} \quad (2.14)$$

Finally the equation for  $T(t)$  is obtained thanks to the previous definitions:

$$\Lambda \frac{dT}{dt} = (\rho(t) - \beta_{eff})T(t) + \Lambda \sum_{i=1}^R \lambda_i c_i + \Lambda Q(t) \quad (2.15)$$

The equation of precursors is presented unchanged with respect to the original system and it can be coupled to the equation for  $T(t)$  just found thanks to the definition of the weighted precursors (Eq.2.14).

So at the end a system with a time-dependent equation coupled with a transport-diffusion equation (so also space-dependent) is found and these two equations have the definition of the weighting precursors as link. So, the two differential equations can be solved together. Until now, the system obtained is the following:

$$\begin{cases} \frac{dT(t)}{dt} = \frac{\rho(t) - \beta_{eff}}{\Lambda} T(t) + \sum_{i=1}^R \lambda_i c_i(t) + Q(t) \\ \frac{\partial C_i(r,t)}{\partial t} + u \cdot \nabla C_i = -\lambda_i C_i + \beta_i \sum_{g=1}^G (\nu \Sigma_f)_g \phi_g + \nabla \cdot D_{i,f} \nabla C_i \end{cases} \quad (2.16)$$

As explained, the goal is to couple the equation for the power, without spatial dependencies (as in the classical point kinetics for a solid fuel system) with the transport-diffusion for the precursors, which are expressed in terms of a power distribution.

But because  $T(t)$  isn't the power, the first equation of the system is multiplied by  $\frac{P(0)}{T(0)}$  and the second equation by  $P(0)$ . Thanks to the definitions on the below system, the system (2.16) is rewritten:

$$\begin{cases} \frac{P(t)}{P(0)} = \frac{T(t)}{T(0)} \\ C_i^*(r, t) = C_i(r, t)P(0) \\ c_i^*(t) = \frac{P(0)}{T(0)}c_i(t) \\ P(t)\phi(0) = P_0\phi(t) \end{cases} \quad (2.17)$$

Also, for simplicity a mono-energetic case is considered and then the equations become:

$$\begin{cases} \frac{dP(t)}{dt} = \frac{\rho(t) - \beta_{eff}}{\Lambda} P(t) + \sum_{i=1}^R \lambda_i c_i^*(t) \\ \frac{\partial C_i^*(r, t)}{\partial t} + u \cdot \nabla C_i^* = -\lambda_i C_i^* + \beta_i \nu \Sigma_f \phi(0) P(t) + \nabla \cdot D_{i,f} \nabla C_i^* \end{cases} \quad (2.18)$$

Also the weighting formula for the precursors is modified because of the introduction of these definitions:

$$c_i^*(t) = \frac{\int W C_i^*(r, t) dV}{T(0)} = \frac{\int W C_i^*(r, t) dV}{\int \frac{1}{v} W \phi(0) dV} \quad (2.19)$$

Now the goal is to eliminate  $\nu \Sigma_f$  in the equation of the precursors. In order not to have the necessity of using neutron quantities, which usually are used in a neutron diffusion model, for this point kinetics model.

A new definition for the precursors is introduced:

$$\hat{C}_i(r, t) = v \cdot C_i^*(r, t) \quad (2.20)$$

The hypothesis, that  $v$ ,  $\nu$  and  $\Sigma_f$  are constant in the space, is made and noting that under these assumptions the mean generation time (Eq 2.8) is equal to:

$$\Lambda(t) = \frac{1}{v \nu \Sigma_f} \quad (2.21)$$

The equation for the precursors can be rewritten as:

$$\frac{\partial \hat{C}_i(r, t)}{\partial t} + u \cdot \nabla \hat{C}_i = -\lambda_i \hat{C}_i + \frac{\beta_i}{\Lambda} \phi(0) P(t) + \nabla \cdot D_{i,f} \nabla \hat{C}_i \quad (2.22)$$

And because  $v$  is constant in the space, the definition of the weighed precursors is rewritten as:

$$c_i^*(t) = \frac{\frac{1}{v} \int W \hat{C}_i(r, t) dV}{\frac{1}{v} \int W \phi(0) dV} = \frac{\int W \hat{C}_i(r, t) dV}{\int W \phi(0) dV} \quad (2.23)$$

## 2. THE POINT KINETICS MODEL FOR A FLUID SYSTEM

---

From a dimensional analysis it can be seen that  $\hat{C}_i$  is a power multiplied by a flux  $[\frac{W}{m^2s}]$ .

Since the purpose of this derivation is to couple a point equation for the power to the distribution equation of the precursors, it is necessary to divide the equation of the precursors by the integral of the flux along the volume.

$$\tilde{C}_i(r, t) = \frac{\hat{C}_i(r, t)}{\int \phi(0) dV} \quad (2.24)$$

So also a normalized flux  $\phi_n$ , which is defined below, is introduced:

$$\phi_n = \frac{\phi(0)}{\int \phi(0) dV} \quad (2.25)$$

And the weighed precursors become:

$$c_i^*(t) = \frac{\int W \hat{C}_i(r, t) dV}{\int W \phi(0) dV} = \frac{\int W \tilde{C}_i(r, t) dV}{\int W \phi_n(0) dV} \quad (2.26)$$

Then finally the problem to solve, taking into account the previous weighting (Eq. 2.26) is the following:

$$\begin{cases} \frac{dP(t)}{dt} = \frac{\rho(t) - \beta_{eff}}{\Lambda} P(t) + \sum_{i=1}^R \lambda_i c_i^*(t) \\ \frac{\partial \tilde{C}_i(r, t)}{\partial t} + u \cdot \nabla \tilde{C}_i = -\lambda_i \tilde{C}_i + \frac{\beta_i}{\Lambda} \phi_n(0) P(t) + \nabla \cdot D_{i,f} \nabla \tilde{C}_i \end{cases} \quad (2.27)$$

Also it is possible to release the hypothesis that the neutron velocity is constant. Restarting from the Eq. 2.18 and 2.19, the system is divided by  $\int \frac{1}{v} W \phi(0) dV$ :

$$C_i^+(r, t) = \frac{C_i^*(r, t)}{\int \frac{1}{v} W \phi(0) dV} \quad (2.28)$$

So the system is rewritten and it becomes:

$$\begin{cases} \frac{dP(t)}{dt} = \frac{\rho(t) - \beta_{eff}}{\Lambda} P(t) + \sum_{i=1}^R \lambda_i c_i^*(t) \\ \frac{\partial C_i^+(r, t)}{\partial t} + u \cdot \nabla C_i^+ = -\lambda_i C_i^+ + \beta_i \int \frac{1}{v} W \phi_0 dV P(t) + \nabla \cdot D_{i,f} \nabla C_i^+ \end{cases} \quad (2.29)$$

Meanwhile, the weighed precursors:

$$c_i^*(t) = \int W C_i^+(r, t) dV \quad (2.30)$$

---

## 2.2. ANALYTICAL DERIVATION OF THE POINT KINETICS MODEL

---

Now remain to fix the precursors equation and it is necessary to treat the term of production related to the power, which is divided and multiplied by  $\int \nu \Sigma_f W \phi(0) dV$ :

$$\beta_i \frac{\nu \Sigma_f \phi(0)}{\int \nu \Sigma_f W \phi(0) dV} \frac{\int \nu \Sigma_f W \phi(0) dV}{\int \frac{1}{v} W(0) dV} P(t) \quad (2.31)$$

Now the hypothesis that  $\nu$  and  $\Sigma_f$  are constant in the space is made and also taking the definition of the mean generation time (Eq. 2.8). Thanks to them the (Eq. 2.31) is reduced in:

$$\frac{\phi(0)}{\int \phi(0) W dV} \frac{\beta_i}{\Lambda} P(t) = \frac{\phi_n}{\int \phi_n W dV} \frac{\beta_i}{\Lambda} P(t) \quad (2.32)$$

At the end, without assuming a constant neutron speed, the following system is obtained:

$$\begin{cases} \frac{dP(t)}{dt} = \frac{\rho(t) - \beta_{eff}}{\Lambda} P(t) + \sum_{i=1}^R \lambda_i C_i^*(t) \\ \frac{\partial C_i^+(r,t)}{\partial t} + u \cdot \nabla C_i^+ = -\lambda_i C_i^+ + \frac{\phi_n}{\int \phi_n W dV} \frac{\beta_i}{\Lambda} P(t) + \nabla \cdot D_{i,f} \nabla C_i^+ \end{cases} \quad (2.33)$$

For this thesis the first derivation (Eq. 2.27 and 2.26) will be implemented and used.

### 2.3 The model implementation on GeN-Foam

After obtaining the point kinetics model for a fluid system, it has been implemented on GeN-Foam.

In this section only the implementation and the features of the neutronic point kinetics model on GeN-Foam will be discussed.

First of all the implementation is based on two main parts:

- The first part which consists in initializing the necessary quantities to solve the time-spatial equations of the precursors and the time equation of the power;
- The second one instead consists in solving the Eq. 2.27 through a coupling between the equation of the power and the equations of the precursors until the convergence is not reached.

In the diagram flux below it can be seen as the code works in the first part, which is the first iteration that the code does.

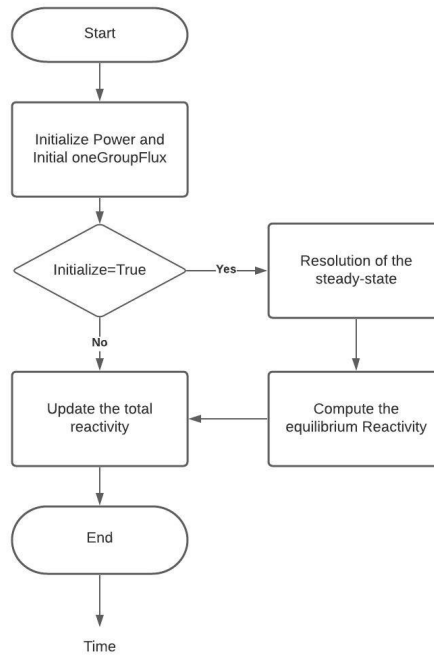


Figure 2.1: Flow Chart of the first iteration of the point kinetics solver

It is important to recall that the problem to solve is meant to be a mono-energetic one. Then, a one group neutron flux field is required as initial condition. This quantity is called *oneGroupFlux* in the flow chart and in the point kinetics model it corresponds with the initial steady state flux,  $\phi(0)$ . Through this flux, the initial normalized flux  $\phi_n(0)$  is computed with the Eq. 2.25.

The user could set the boolean variable, *Initialize*, in this way:

- True if in the simulation the system is a steady state condition and then the resolution of the steady state, from the neutron point of view, is mandatory in order to compute the value of the equilibrium reactivity;
- False in other cases.

The equilibrium reactivity is relevant in liquid fuel systems being the one that counterbalance the reactivity loss due to the precursors drift in a steady-state condition. Its value can be calculated from the system 2.27, where all the time derivatives are set to zero. This way the system to solve isn't anymore a space-time problem but only a spatial one:

$$\begin{cases} \frac{\rho_0 - \beta_{eff}}{\Lambda} P_0 + \sum_{i=1}^R \lambda_i c_{i,0}^* = 0 \\ u \cdot \nabla \tilde{C}_{i,0} = -\lambda_i \tilde{C}_{i,0} + \frac{\beta_i}{\Lambda} \phi_n(0) P_0 + \nabla \cdot D_{i,f} \nabla \tilde{C}_{i,0} \end{cases} \quad (2.34)$$

Firstly, the equations of the precursors are solved since the initial normalized flux was computed before and all the other data are known (e.g., the velocity fields and the initial power of the system).

For the calculation of the weighting precursors, Eq. 2.26, is used but before the weight function,  $W$ , must be defined in the implementation.

The choice on the weight function is a degree of freedom of the model. In the implementation for reasons of unit of measurement and for the purpose of using a reasonable function, the initial normalized flux has been chosen as weight function.

So the Eq. 2.26 can be used to compute the initial weighting precursors,  $c_{i,0}^*$ , and then manipulating the power equation it is possible to compute the equilibrium reactivity:

$$\rho_0 = \beta_{eff} - \frac{\Lambda \sum_{i=1}^R \lambda_i c_{i,0}^*}{P_0} \quad (2.35)$$

After computing this reactivity the only thing to remain to do in this part is the update of the total reactivity,  $\rho(t)$ , in order to include in this quantity the value of the equilibrium reactivity with this formula:

$$\rho(t) = \rho_0 + \rho_{external} + \rho_{feedback} \quad (2.36)$$

Of course when the system is in a steady state condition the external reactivity and the reactivity due to the feedback effects are zero.

## 2. THE POINT KINETICS MODEL FOR A FLUID SYSTEM

---

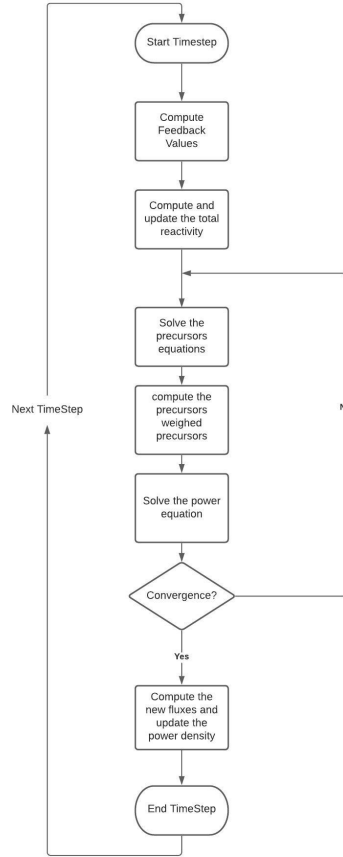


Figure 2.2: Flow Chart of the time resolution of the point kinetics solver

Once calculated the equilibrium reactivity, the full spatial-time dependent system can be solved (Eq. 2.27).

As one can note seeing the flow chart of the Figure 2.2, before solving the system all the feedback values need to be computed, as the average fuel temperature or the average density of the fluid.

These averages values are computed thanks to an integral mean based on the square of the adjoint flux, but it has been hypothesized that the adjoint flux is equal to the mono-energetic neutron flux. For example the average fuel temperature is computed in this way:

$$T_{fuel,avg}(t) = \frac{\int \phi^2(r, t) T_{fuel}(r, t) dV}{\int \phi^2(r, t) dV} \quad (2.37)$$

In a similar way all the other feedback values are computed.

After computing these values the feedback reactivity is computed as the sum of all feedback effects. For example, if we consider a system with neutron feedback effects link to the fuel temperature and to the density of the fluid, the feedback reactivity could be compute in this way:

$$\rho_{external}(t) = \rho_{fuel}(t) + \rho_{density}(t) \quad (2.38)$$

Where it is mandatory to have the feedback coefficients in order to compute the reactivity due to the feedback, for example in this case it is necessary to have  $\alpha_{fuel}$  and  $\alpha_{density}$ .

The previous equation becomes the following one:

$$\begin{aligned} \rho_{external}(t) = & \alpha_{fuel}(T_{fuel,avg}(t) - T_{fuel,avg}(0)) + \\ & \alpha_{density}(\rho_{fluid,avg}(t) - \rho_{fluid,avg}(0)) \end{aligned} \quad (2.39)$$

Of course the initial feedback values are computed with the same integral mean of the Eq. 2.37 and they are found before starting to solve the time problem.

After this the total reactivity is computed through the Eq. 2.36.

For each time step, the equations of the precursors are solved and the weighting precursors are computed. Then having the weighting precursors, the power equation is solved. The power equation and the precursors equations are solve in an iterative way, following the scheme reported in the flow chart of the Figure 2.2, in a cycle which continues until the convergence is reached. The numerical criteria for the convergence of this problem is based on the residuals of the precursors equations. If the maximum of these residuals is less than a chosen residual then the convergence is reached. Alternatively, the cycle is terminated if a maximum number of iterations - which could be modified by the user - is reached.

After the convergence is reached, or in the worst case the maximum number of iterations is reached, the new fluxes, the mono-energetic flux and the power density are updated through the following scale factor:

$$S.F. = \frac{P(t)}{P(t - \Delta t)} \quad (2.40)$$

where  $\Delta t$  is the time step used for the numerical calculation for the current interaction.

After the update, it is possible to continue the simulation at the next time step, following always the flow chart of the the time problem until the end time of the simulation is reached.

As explain, the code is able to compute several interesting quantities. Therefore it is easy to use this solver to monitor the time evolution of the system after a perturbation, in particular the time profiles of the power, of the total reactivity and of the average fuel temperature. Of course it is possible also to check other effects.

This implementation needs the following input data to work:

- The mean generation time,  $\Lambda$ ;
- The neutron feedback coefficients, like  $\alpha_{fuel}$ ;

These quantities must be compute a prior. It needs also a starting steady state condition in order to get reasonable results.

As one can notice that this implementation manages to solve only the neutronics problem. Then it doesn't solve the thermal-hydraulic one and thus, for example, it doesn't compute the new temperature fields which is mandatory for the computation of the

## 2. THE POINT KINETICS MODEL FOR A FLUID SYSTEM

---

average feedback value (see Eq. 2.37). However, this model is implemented in GeN-Foam which is a multi-physics solver and because of that it manages to compute all the physical fields necessary to use the point kinetics model implementation. Concluding the point kinetics model developed has been coupled with the other types of solvers presents in GeN-Foam.

# Comparison of the Point Kinetics model with an analytical model

## 3.1 Introduction

In this section the point kinetics model developed is confronted with an analytical model in order to show that the point kinetics solver gets results very close to the analytical one. This comparison can be seen as the first test of this model implemented in GeN-Foam. The most important figure of merit of this comparison is the calculation of the new steady-state values in terms of temperature reached after the transients considered. The geometry considered in the comparison is a simple closed channel of a height equal of 12 metres (which can be seen in the Figure 3.1), The channel wants to represent a nuclear system. This way the domain is divided in different zones:

- the cold leg (length equals to 3 m);
- the core (length equals to 3 m);
- the hot leg (length equals to 3 m);
- the pump (length equals to 1 m);
- the heat exchanger (length equals to 2 m).

This geometry has been chosen because is simple and also because the mixing effects of the fluid are not present. Furthermore, as one of the features of the point kinetics model is to investigate the dimensional effects due to the spatial distributions of the precursors, this simple configuration has been chosen in order to minimize these effects.

Before introducing the physical problem, it is important to underline the boundary conditions used in the simulation. They are reported in the tables below (Tables 3.1 and 3.2).

It is to be known that the calculated boundary condition is not designed to be evaluated. It is assumed that the value is assigned via field assignment, and not via a call to e.g. `updateCoeffs` or `evaluate`.

### 3. COMPARISON OF THE POINT KINETICS MODEL WITH AN ANALYTICAL MODEL

---

Boundary Condition of the fluid region			
	Top	Bottom	Walls
U	cyclic	cyclic	slip
p	cyclic	cyclic	calculated

Table 3.1: Boundary conditions of the fluid problem

Boundary Condition of the neutron region			
	Top	Bottom	Walls
defaultFlux	cyclic	cyclic	zeroGradient

Table 3.2: Boundary conditions of the neutron problem

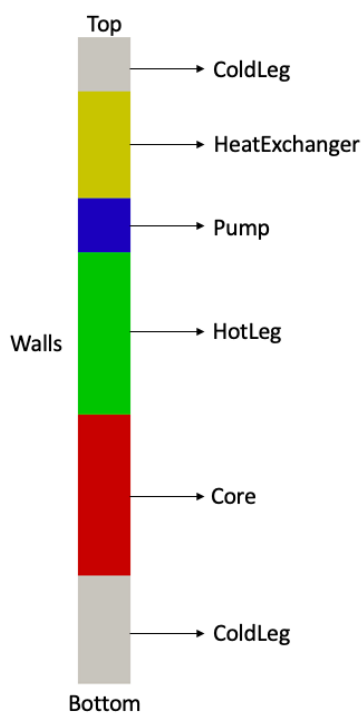


Figure 3.1: Zones of the channel

Obviously, as one can see in the Figure 3.1, the bottom is the inlet of the system and the top is the outlet. Then the cyclic boundary condition, used both for the fluid dynamics problem both for the neutron problem, allows to have a closed system. In fact, this kind of condition is used to link two identical parts of the geometry, in this case the bottom and the top.

The last thing to say is that despite using a not very fine mesh the results are good. In fact, there are 640 cells for 12 metres, so about 20 centimetres for any cells. By further refining the mesh, the computational time increases but the errors decrease slightly compared to those obtained.

The comparison is run against two transients, one with an insertion of external reactivity and the other with an exponential reduction of the velocity, mimic a malfunction of the pump. As told before, this comparison has the goal to verify the consistency of the results of the modified point kinetics model with respect to analytical results. In particular, the comparison is made with the inlet and outlet temperatures on the core, the average fuel temperatures and the logarithmic average temperatures on the heat exchanger and the final power of the system.

In order to have a difference between the inlet and outlet temperatures on the core region in the range 100-200 K, an uniform power of 990 MW has been chosen, as one can see in the Figure 3.2.

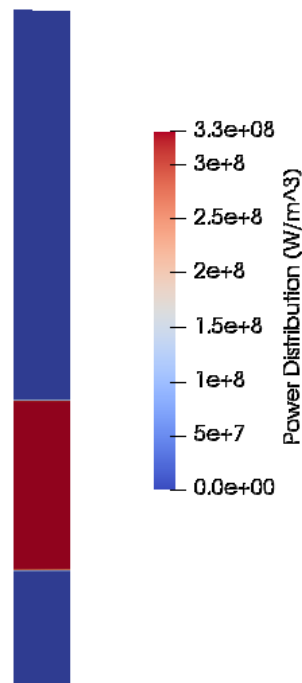


Figure 3.2: Power distribution in the system at steady state

### 3. COMPARISON OF THE POINT KINETICS MODEL WITH AN ANALYTICAL MODEL

---

Then in the table 3.3 are listed all the values request to solve the analytical problem:

	Value	Unit of Measure
Initial inlet velocity, $u$	0.8317	m/s
Density of the fluid, $\rho_{fluid}$	4125	kg/m <sup>3</sup>
Inlet Area, $A_{in}$	1	m <sup>2</sup>
Initial mass flow rate, $\dot{m}_{ini}$	3430.6	kg/s
Specific heat capacity, $c_p$	1600	J/kg*K
Heat transfer coefficient, $h$	1850	W/K*m <sup>2</sup>
Area of the heat exchanger, $A_{hx}$	400	m <sup>2</sup>
Temperature of the heat exchanger, $T_{hx}$	900	K
Neutron fuel feedback coefficient, $\alpha_{fuel}$	-3.54	pcm/K
Mean generation time, $\Lambda$	$1.26 \cdot 10^{-6}$	s

Table 3.3: Table of values used in the analytical problem

It is important to underline that the following quantities are constant both for the analytical model and for the simulations:

- The density of the fluid,  $\rho_{fluid}$ ;
- The specific heat,  $c_p$ ;
- The heat transfer coefficient on the heat exchanger,  $h$ ;
- The temperature of the heat exchanger,  $T_{hx}$ ;
- The fuel feedback coefficient,  $\alpha_{fuel}$

Before showing the analytical model, it is important to explain how the initial conditions of the system, or better the conditions of the system before the beginning of the transient, have been obtained, for the example the initial temperatures and the velocity of the fluid in the core region.

These initial conditions are found thanks to a steady state calculation with the fluid-dynamics solver implemented in GeN-Foam. Thanks to it the following quantities of interest for the comparison and also the initial fields of velocity and temperature, Figure 3.3, are obtained:

- The initial inlet temperature,  $T_{in,ini}$ , equal to 964 K;
- The initial outlet temperature,  $T_{out,ini}$ , equal to 1144.3 K;

- The initial average temperature,  $T_{mean,ini}$ , equal to 1053.6 K;
- The initial average logarithmic temperature,  $\Delta T_{ml,ini}$ , equal to 133.8 K;
- The initial equilibrium reactivity,  $\rho_{0,ini}$ , equal to 174.01 pcm.

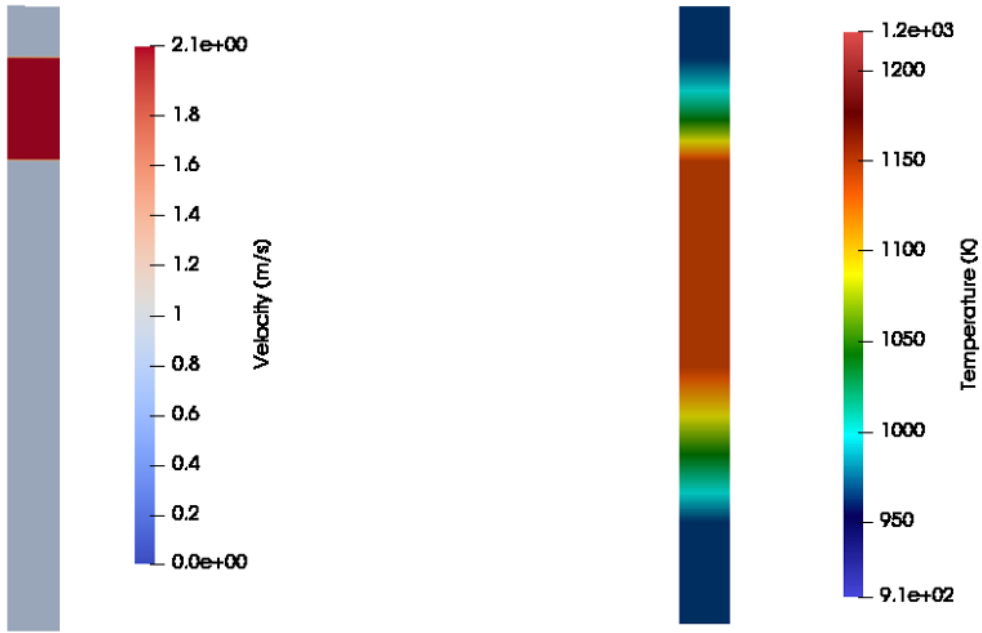


Figure 3.3: The velocity and temperature distributions at steady state

## 3.2 Description of the analytical model

The analytical model used in the comparison is based on the following balances and definitions:

- A power balance on the core;
- A power balance on the heat exchanger;
- A balance of reactivity between the beginning and the end of the transient;
- The definition of  $T_{mean}$  as the average of inlet and outlet temperatures;

So the system to solve analytical is the following one:

$$\left\{ \begin{array}{l} P_{fin} = \dot{m}_{fin} c_p \cdot (T_{out,fin} - T_{in,fin}) \\ P_{fin} = K \cdot \Delta T_{ml,fin} \\ \Delta \rho = \alpha_{fuel} \cdot (T_{mean,fin} - T_{mean,ini}) + \rho_{external} \\ T_{mean,fin} = \frac{(T_{out,fin} + T_{in,fin})}{2} \end{array} \right. \quad (3.1)$$

To solve the system in a closed way the definition of logarithmic temperature must be used:

$$\Delta T_{ml} = \frac{T_{out} - T_{in}}{\ln \frac{T_{out} - T_{hx}}{T_{in} - T_{hx}}} \quad (3.2)$$

It is important to remember that the system works with a heat exchanger with a constant temperature,  $T_{hx}$ .

As for the conductance,  $K$ , it can be calculated in the following way:

$$K = h \cdot A_{hx} = 7.4 \text{ MW/K} \quad (3.3)$$

As told before the unknowns of the problem are the final power and the final temperatures and having all the necessary data the system can be solved in a closed way in the following way:

$$\left\{ \begin{array}{l} T_{mean,fin} = \frac{\Delta \rho - \rho_{external}}{\alpha_{fuel}} + T_{mean,ini} \\ T_{in,fin} = \frac{T_{mean,fin} + 0.5 \left( e^{\frac{K}{\dot{m}c_p}} - 1 \right) T_{hx}}{0.5 \left( e^{\frac{K}{\dot{m}c_p}} - 1 \right) + 1} \\ T_{out,fin} = 2T_{mean,fin} - T_{in,fin} \\ P = \dot{m}c_p (T_{out,fin} - T_{in,fin}) \end{array} \right. \quad (3.4)$$

The transients taken into consideration for the comparison are two:

- The first is a transient with an insertion of reactivity;
- The second one is a transient with an exponential reduction of the velocity.

Regarding the first transient, the velocity field is unchanged so it is not necessary to calculate a new mass flow rate. Also the equilibrium reactivity should not change for the same reason, then the  $\Delta\rho$  is imposed equal to zero for this kind of transient. The external reactivity inserted in the system is equal to 57 pcm.

For this transient, an increase in power and in temperatures is expected.

Instead, for transient with the reduction of velocity, a new mass flow rate must be calculated, due to the exponential reduction of velocity. This exponential reduction lasts ten seconds and the characteristic time of the pump is equal to two seconds. Because the value of the inlet velocity after the exponential reduction is about 0.3 m/s (as one can see in the Figure 3.7), a new mass flow rate is computed and it is equal to 1227.20 kg/s .

Also the  $\Delta\rho$ , which is the difference between the equilibrium reactivity of the final and initial steady states, must be calculated. In this situation the two equilibrium reactivity are 174.01 pcm, as reported before for the initial steady state (then it is the initial equilibrium reactivity), and its value when the transient is exhausted, which is reported after (this is the final equilibrium reactivity of the system), it has been computed through GeN-Foam. It is expected that the final equilibrium reactivity is less than the initial one. In fact, more the velocity of the fluid decrease, more the problem tends to be like a one of a solid fuel system where the precursors distribution is frozen with the flux distribution and where the equilibrium reactivity is equal to zero. There isn't insertion of external reactivity hence the  $\rho_{external}$  is imposed to zero.

Now it is possible to solve the analytical problem for both transients and after the results can be compared with those obtained with the point kinetics solver implemented on GeN-Foam.

### 3.3 Description of the GeN-Foam model

Regarding the simulations, the insertion of external reactivity transient is done as first case. In the figure below (Figure 3.4) the time trends of the power, of the total reactivity and of the neutron average fuel temperature can be seen. A peak of power equal to 1.98 GW can be seen in the power plot. Obviously it is due to the insertion of the external reactivity and the system reaches this peak in about a tenth of second. After this peak, the power of the system decreases due to the negative feedback of the fuel, then the average fuel temperature increases at the same time, until a new steady state condition is reached, as one can see in the plot after about twenty seconds. One can note from the total reactivity plot that when the transient is exhausted, the total reactivity is equal to the initial equilibrium reactivity as supposed in the analytical model for this kind of transient.

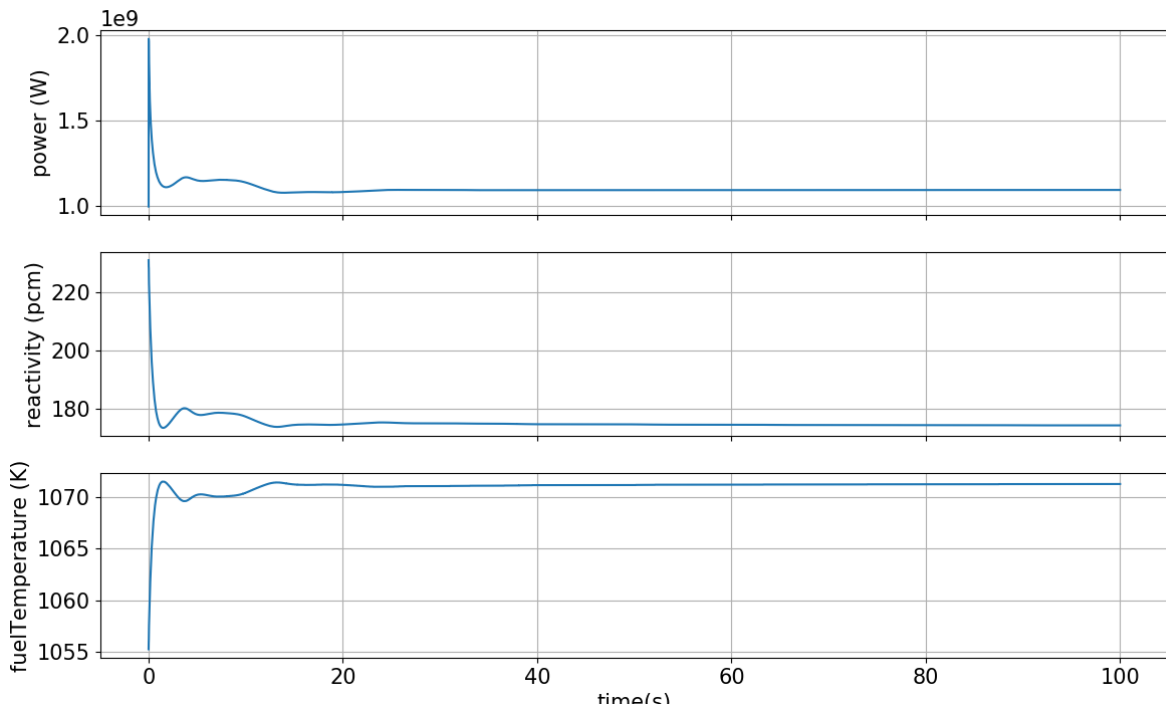


Figure 3.4: Power, total reactivity and fuel temperature predicted by the point kinetics in the closed channel for a reactivity insertion of 57 pcm

Considering the trends reported, the final power and the temperatures are greater than the initial values, as expected in a nuclear system when there is an insertion of external reactivity. The velocity field does not change and therefore with the increase of the power also the average temperature of the fuel increases. Another feature to underline is that the equilibrium reactivity after the transient is equal to the one at the starting steady state. This result is in line with the hypothesis made in the analytic case.

Also for the second transient the time evolution is reported, in the Figure 3.5. The decrease of the power with simultaneous increase of the average fuel temperature during the transient can be seen in the Figure 3.6. This behaviour goes on until the exponential reduction of velocity doesn't finish. After that the minimum of power and the maximum

of the fuel temperature are reached. During this transient there is also the decrease of the reactivity, due to neutron fuel feedback, until when it reached its minimum value.

For completeness these value are reported:

- The minimum of the power is equal to 606.96 MW;
- The maximum of the fuel temperature is equal to 1069.4 K;
- The minimum of reactivity is equal to 124.28 pcm.

After this point the system tries to reach its new steady state and a little increase of the power can be noticed together with the little decrease of the fuel temperature (Figure 3.6). Instead at the end of the transient, the reactivity reaches the value of the new equilibrium reactivity, 134.19 pcm (re-see 3.5. This is line with the hypothesis made in the analytical model for this kind of transient. In fact, if the velocity decreases (as one can see in the Figure 3.7) a decrease of the equilibrium reactivity of the system will be expected. Then, this new equilibrium reactivity will be used also for the computation of the  $\Delta\rho$  for the balance of reactivity of the analytical model.

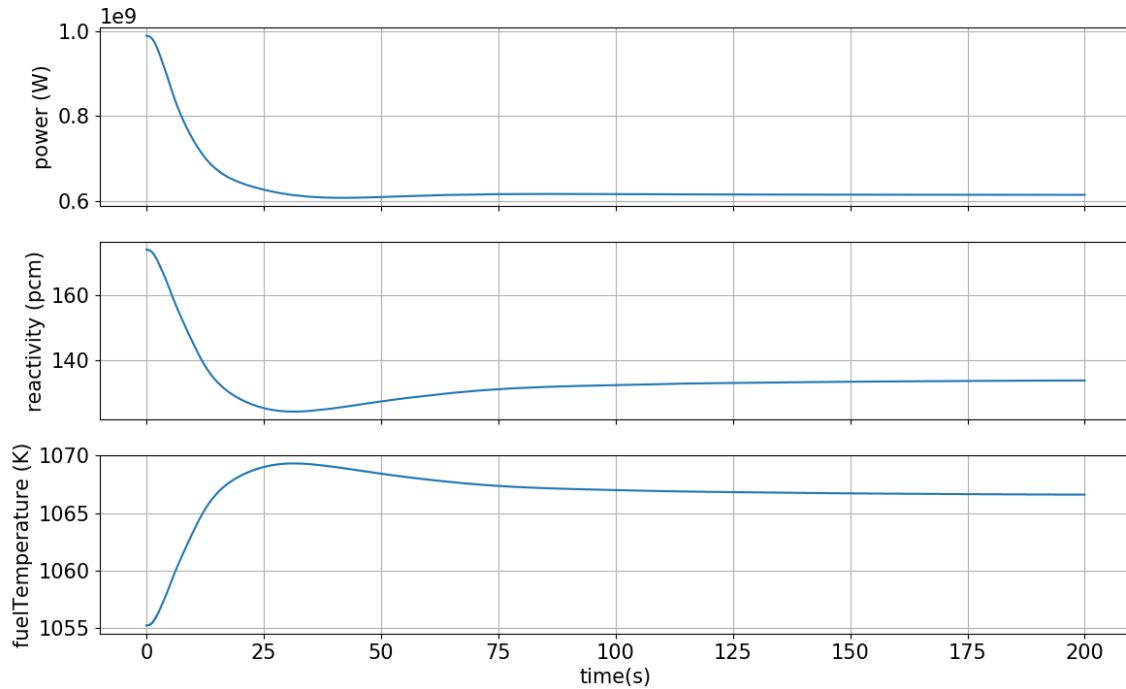


Figure 3.5: Power, total reactivity and fuel temperature predicted by the point kinetics in the closed channel for an exponential reduction of velocity in the first 10 seconds

### 3. COMPARISON OF THE POINT KINETICS MODEL WITH AN ANALYTICAL MODEL

---

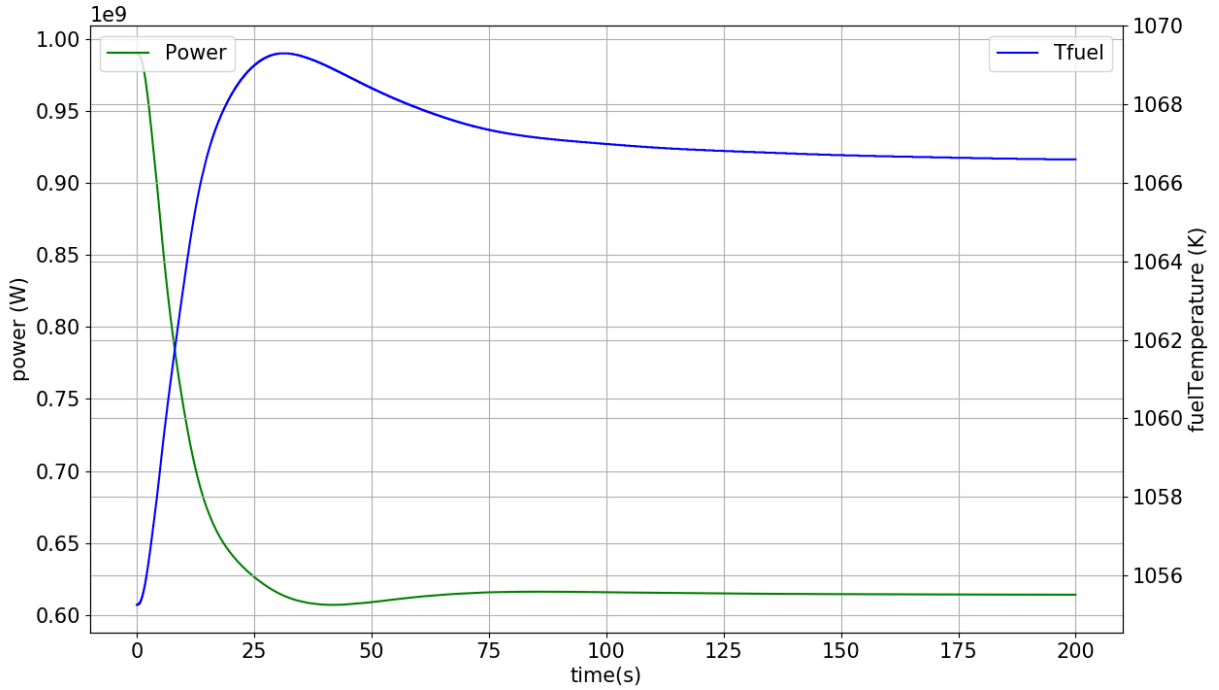


Figure 3.6: Power and average fuel temperature predicted by the point kinetics in the closed channel for an exponential reduction of velocity in the first 10 seconds

In conclusion, also for this transient the final result are in line with the physics of the system. In fact, the final power is less than the initial one. However, the average temperature increases due to the neutron feedback of the fuel. Then, these results must be investigated in more details during the comparison. In the Figure 3.8 one can note the decrease of the inlet temperature and the increase of the outlet temperature.

It is important to notice that in both the simulations the neutron fuel feedback is necessary to counterbalance the perturbations given to the system, in one case the external reactivity and in the other the reduction of the velocity. Of course, this task of the fuel feedback can be noticed also in the balance of reactivity of the Eq. 3.1.

The last thing to underline is about the mean generation time. As said in the section 2.3 it is necessary in order to use the point kinetics implementation on GeN-Foam. Even if it isn't present in the analytical model it is essential for the calculation of the two equilibrium reactivity through GeN-Foam, see Eq. 2.35.

Regarding the simulations, where it is used, it must be said that the mean generation time does not affect the values of the system when the transient is exhausted but only the dynamics of the system, for example the power peak and the time when the system reaches it.

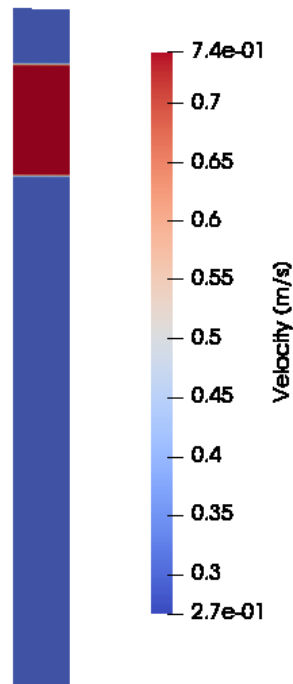


Figure 3.7: Final velocity field after the exponential reduction of velocity

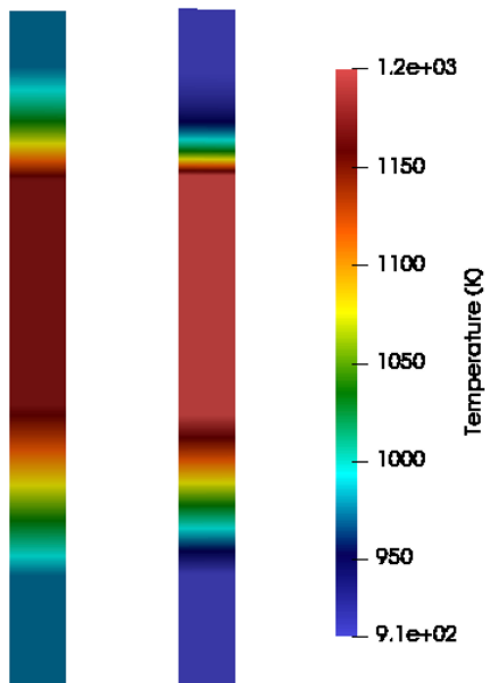


Figure 3.8: Temperature fields: The transient with the exponential reduction of the velocity on the right and the transient with an insertion of reactivity equal to 57 pcm on the left

### 3.4 Results

For the transient with the insertion of reactivity the results are listed in the table 3.4:

Insertion of reactivity transient			
	Simulation	Analytical	Error [%]
$P_{fin}[MW]$	1092.98	1098.20	0.48
$T_{in,fin}[K]$	970.5	970.2	<0.1
$T_{out,fin}[K]$	1169.5	1170.3	<0.1
$T_{mean,fin}[K]$	1070	1070.2	<0.1
$\Delta T_{ml,fin}[K]$	148.4	148.4	<0.1

Table 3.4: Results of the transient with an insertion of external reactivity equal to 57 pcm

As expected the insertion of reactivity makes the power increase and also all temperatures increase also in the analytical model. They are expected results because the power increase due to the insertion of external reactivity while the mass flow rate doesn't change. As results the temperature must be increase for the energy balance.

Moving on to the comparison, one can see that in this case the analytical and numerical values computed are very closed even if the mesh is not very fine. If the mesh is refined more the results will be slightly more accurate, but the computation time will increase too much. Then, because the errors obtained are already lower than the one per cent, it makes sense to use the actual mesh for the comparison.

For the reduction velocity transient, the results are:

Exponential reduction of velocity transient			
	Simulation	Analytical	Error [%]
$P_{fin}[MW]$	613.66	620.12	1.04
$T_{in,fin}[K]$	908	907.5	<0.1
$T_{out,fin}[K]$	1221	1223.3	0.19
$T_{mean,fin}[K]$	1064.6	1065.4	<0.1
$\Delta T_{ml,fin}[K]$	84.8	83.8	1.2

Table 3.5: Results of the transient with the exponential reduction of velocity in the first 10 seconds

As said before this transient is more complex than the previous one and it can be seen from the results. In fact, the power decrease as expected but the inlet and

outlet temperatures behave differently. The inlet temperature decreases and the outlet temperature increase (this behaviour can be seen also in the Figure 3.8).

The reason of these results can be understood looking better at the analytical model (see Eq. 3.4). Of course, the power should decrease due to the reduction of the mass flow rate, which is the quantity most important in this transient and in this geometry. First, starting from the reactivity balance, the average fuel temperature of the system increases due to the decrease of the equilibrium reactivity, also it is due to the negative nuclear feedback of the nuclear system.

In fact, the system tends to increase its average temperature in order to counterbalance the decrease of its total reactivity, as one can see also in the plot of the simulation. However even if this temperature increased by more of 10 K, the mass flow rate decrease of about 35.77 % of its initial value. For this reason the term below is greater than before:

$$A = 0.5(e^{\frac{K}{\dot{m}c_p}} - 1) \quad (3.5)$$

In fact, before the transient this term is equal to 1.42 and at the end of the transient its value is 21.16 and it is the dominant term in the inlet temperature equation and it depends on the mass flow rate. In fact, more this term increases and therefore more the mass flow rate decreases, more the inlet temperature decreases.

So the final inlet temperature decrease for this reason which is related to the thermal-hydraulic problem, but the final average temperature increase for neutron reasons as explained before. Then, the sum of these effects is the reason of the increase of the outlet temperature on the core, which represent the maximum temperature in the system.

However even if the difference between the inlet and outlet temperatures increase, the reduction of the mass flow rate remains the dominant effect also for the final value of the power, which decreases.

Respect to the previous transient, the only difference that can be noted from these results is an increase of the error on the power and on the average logarithmic temperature of the heat exchanger. These differences can be due to the decrease of the velocity field, and therefore they are linked to the resolution of the fluid mechanics problem too, unlike the previous case. The same idea of refining the mesh in order to minimise the error can be proposed but the errors are good enough to avoid it.

So with this comparison it has been pointed out that even if the mesh is coarse, this point kinetic model for a liquid system is able to get results very close to those of analytical model for different types of transients, as one can note from the two tables above.

In fact, good results have been obtained both for a simple transient as the insertion of reactivity case and for a more complex transient with a reduction of mass flow rate in the pump region where the fluid dynamics problem has to be solved again.

### 3. COMPARISON OF THE POINT KINETICS MODEL WITH AN ANALYTICAL MODEL

---

# Comparison of the Point Kinetics Model with Diffusion Results

## 4.1 Introduction

In this section, the implementation of the point kinetics solver is compared with the diffusion solver already implemented in GeN-Foam. The diffusion solver is based on the multi-group diffusion equations [19]:

$$\begin{cases} \frac{1}{v_g} \frac{\partial \phi_g}{\partial t} = \nabla D_g \nabla \phi_g + \frac{\nu \Sigma_{f,g}(1-\beta_t) \chi_{p,g}}{k_{eff}} \phi_g - \Sigma_{r,g} \phi_g + \frac{S_{n,g}(1-\beta_t) \chi_{p,g}}{k_{eff}} + S_d \chi_{d,g} + S_{s,g} \\ \frac{\partial C_i}{\partial t} + \nabla \cdot (u C_i) = \frac{\beta_i \sum_j \nu \Sigma_{f,j} \phi_j}{k_{eff}} - \lambda_i C_i \end{cases} \quad (4.1)$$

Where  $S_{n,g}$ ,  $S_d$ ,  $S_{s,g}$  are the explicit source terms:

$$\begin{cases} S_{n,g} = \sum_{j \neq g} \nu \Sigma_{f,j} \phi_j \\ S_d = \sum_i \lambda_i C_i \\ S_{s,g} = \sum_{j \neq g} \Sigma_{j \rightarrow g} \phi_j \end{cases} \quad (4.2)$$

The diffusion solver is able to do both time and eigenvalue calculations. In this comparison the eigenvalue calculation will be used in order to find the initial steady state of the system before the start of the transient and also to compute the neutron quantities necessary to use the point kinetics model. In the model the eigenvalue equations can be obtained by setting all the time derivatives to zero.

Regarding the multiplication factor,  $k_{eff}$ , it can be computed by an eigenvalue calculation or set by the user, for example to insert reactivity into the system. For this comparison it has been computed thanks to an eigenvalue calculation in order to find the right multiplication factor of system in the initial steady state.

This comparison is very important because it allows to test the modified point kinetics model with a more complex neutron code which is also verified both for thermal reactor and for fast reactor. However there are a little difference between the two models regarding the precursors distribution. As explain in the section 2.2, the point kinetics model computes the spatial distributions of the precursors as a power distributions,  $\frac{W}{m^3}$ . Instead the diffusion computes the precursors as a simple spatial distributions,  $\frac{1}{m^3}$ . Anyway the comparison will be based mainly on the trends of the powers obtained with the two solvers.

## 4.2 Test case and numerical modelling

For the comparison the molten salt fast reactor has been chosen as the comparison case, which can be seen in the Figure 4.1.

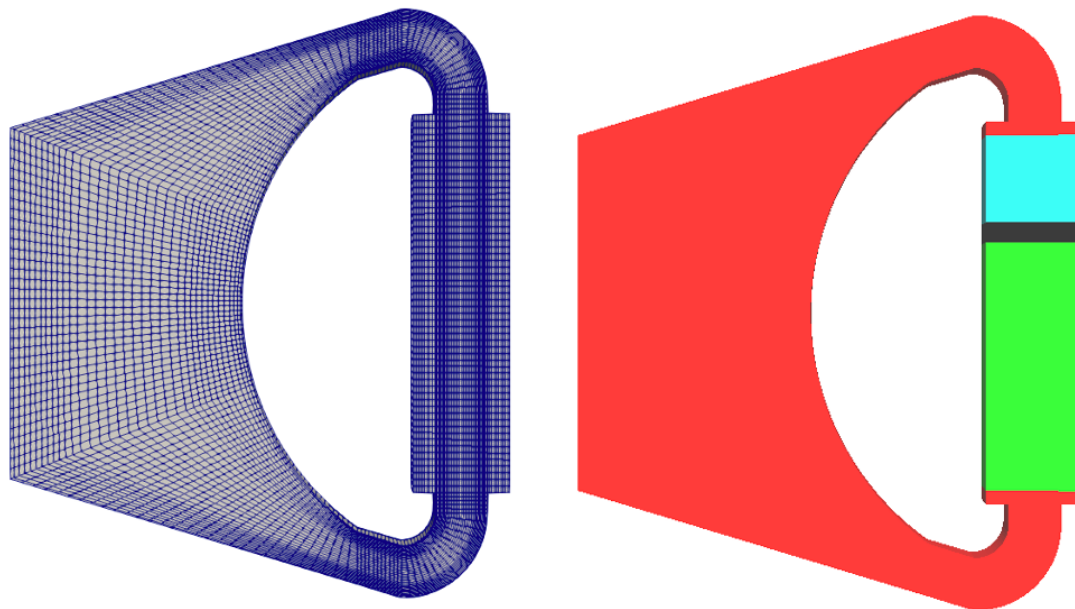


Figure 4.1: Mesh and the zones of the 2D-MSFR

This mesh for the MSFR is a two dimensional one and the system is divided in four main section, which are defined as cellZones in OpenFOAM:

- The main (the red zone), which include the core, the cold leg and the hot leg;
- The pump (the blue zone);
- The intermed (the black zone), which is between the pump and the heat exchanger;
- The heat exchanger (the green zone).

The thermal characteristics of the fluid are reported in the Table 4.1:

	Value	Unit of Measure
Specific heat capacity, $c_p$	1600	J/kg · K
$\beta_{0,fluid}$	$2 \cdot 10^{-4}$	
Reference density for the fluid, $\rho_{fluid,0}$	4125	kg/m <sup>3</sup>
Reference temperature for the fluid, $T_{fluid,0}$	900	K

Table 4.1: Thermal characteristics of the fluid

Instead, the heat exchanger has the characteristics shown in the table below (Table 4.2:

	Value	Unit of Measure
Heat transfer coefficient, $h$	1000	W/K*m <sup>2</sup>
volumetric Area, $\frac{A_{hx}}{V_{hx}}$	200	m <sup>2</sup> /m <sup>3</sup>
Temperature of the heat exchanger, $T_{hx}$	900	K

Table 4.2: Characteristics of the heat exchanger

Regarding the neutron physics, there are six energy groups and eight types of precursors with the following decay constants and  $\beta_i$ :

Group of precursor	$\beta_i$ (-)	$\lambda_i$ (1/s)
1-st group	2.11 10 <sup>-4</sup>	1.25 10 <sup>-2</sup>
2-nd group	4.23 10 <sup>-4</sup>	2.83 10 <sup>-2</sup>
3-rd group	3.74 10 <sup>-4</sup>	4.25 10 <sup>-2</sup>
4-th group	5.79 10 <sup>-4</sup>	1.33 10 <sup>-1</sup>
5-th group	8.93 10 <sup>-4</sup>	2.92 10 <sup>-1</sup>
6-th group	1.43 10 <sup>-4</sup>	6.66 10 <sup>-1</sup>
7-th group	1.93 10 <sup>-4</sup>	1.63
8-th group	3.74 10 <sup>-5</sup>	3.10

Table 4.3: Data of the groups of precursors

Regarding the thermal-hydraulic problem, the main boundary conditions for the pressure, velocity and temperature fields are reported in the Table 4.4.

where the boundary condition "wedge" is used in the front and back of the geometry in order to have the symmetry among the two faces. This kind of boundary condition will be used also in the neutron problem as one can read after.

#### 4. COMPARISON OF THE POINT KINETICS MODEL WITH DIFFUSION RESULTS

---

Boundary Condition of the fluid region						
	front	back	TopWall	BottomWall	reflector	hx
U	wedge	wedge	fixedValue uniform (0,0,0)	fixedValue uniform (0,0,0)	fixedValue uniform (0,0,0)	fixedValue uniform (0,0,0)
p	wedge	wedge	calculated	calculated	calculated	calculated
T	wedge	wedge	zeroGradient	zeroGradient	zeroGradient	zeroGradient

Table 4.4: Boundary conditions of the fluid problem

Instead the main boundary conditions for the neutron problem are:

Boundary Condition of the fluid region						
	front	back	TopWall	BottomWall	reflector	hx
Flux	wedge	wedge	albedoSP3 uniform 1	albedoSP3 uniform 1	albedoSP3 uniform 1	albedoSP3 uniform 1
Flux2	wedge	wedge	fixedValue uniform 0	fixedValue uniform 0	fixedValue uniform 0	fixedValue uniform 0
Prec	wedge	wedge	zeroGradient	zeroGradient	zeroGradient	zeroGradient

Table 4.5: Boundary condition of the neutron problem

The boundary condition "albedoSP3" is a particular boundary condition implemented in GeN-Foam which can simulate the boundary condition based on the ratio between incoming and outgoing partial neutron current in that boundary:

$$\alpha = \frac{J_{in}}{J_{out}} \quad (4.3)$$

There are two transients taken into consideration for this comparison:

- The first transient is one with an insertion of external reactivity;
- The second transient is one with an exponential reduction of velocity:

As one can note these transients are the same of the chapter 3 but unlike before now the geometry is more complex and the mesh is a two dimensional one. Therefore these simulations are more realistic nuclear cases than those seen in the previous chapter.

Before proceeding with the comparison, it is necessary to compute the initial steady state of the system both from the fluid dynamic point of view and from the neutron point of view.

As done in the chapter 3, a calculation to find the thermal-hydraulic steady state was made. Anyway this is only the first calculation in order to find the right steady state. In fact, in this condition the initial multiplication factor can be set only by the user, hence for the diffusion the right multiplication coefficient is missing. The same is true for the initial distributions of neutron fluxes. Then it is simple to understand that after this first step a coupling between the different types of solvers is necessary.

So the next step is an eigenvalue calculation with the diffusion solver which is coupled:

- Only with the energy solver for the case of the first transient;
- Also with the fluid-mechanics solver for the case of the second transient.

For the insertion of reactivity transient it is not necessary to include the resolution of the fluid dynamics physics because it was already done in the first calculation. However the second transient is more complex than the first one. Then, it is better to do a further eigenvalue calculation with the solver of the fluid dynamics in order to find a better steady state. In fact the second transient included also this kind of physics, that it is very important, respect to the insertion of reactivity case where the velocity field doesn't change. In the first case this further calculation has been avoided in order to reduce the computational time.

So, the important parameters to take into consideration to find the steady states are:

- The initial power of the system set to 20 MW;
- The initial condition for the temperature field is set to 900 K;

So in the way just explained it was possible to find the two starting steady states for the two transient cases.

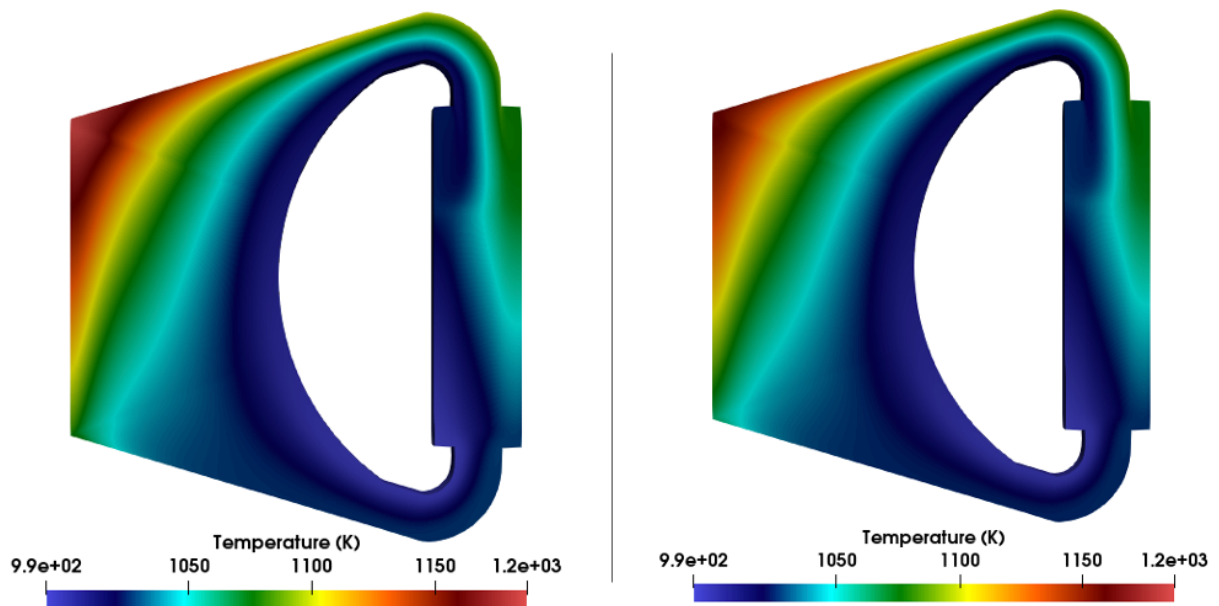


Figure 4.2: Temperature fields of the steady states: On the right for insertion of external reactivity transient, on the left for the exponential reduction of velocity transient [Left]

#### 4. COMPARISON OF THE POINT KINETICS MODEL WITH DIFFUSION RESULTS

---

The Figure 4.2 shows the initial spatial distributions of the temperature fields for the steady states computed with the two eigenvalue calculations. There aren't evident differences in the two spatial distributions and the same goes for the spatial distributions of the total neutron flux in the system, shown in the Figure 4.3. The same goes for the power density distributions which should be the same for the two cases.

However in the velocity fields, shown in the Figure 4.4, there are some little differences near the reflector of the system and near the bottom of the core.

These differences is certainly due to a better calculation with the fluid-dynamic solver of GeN-Foam.

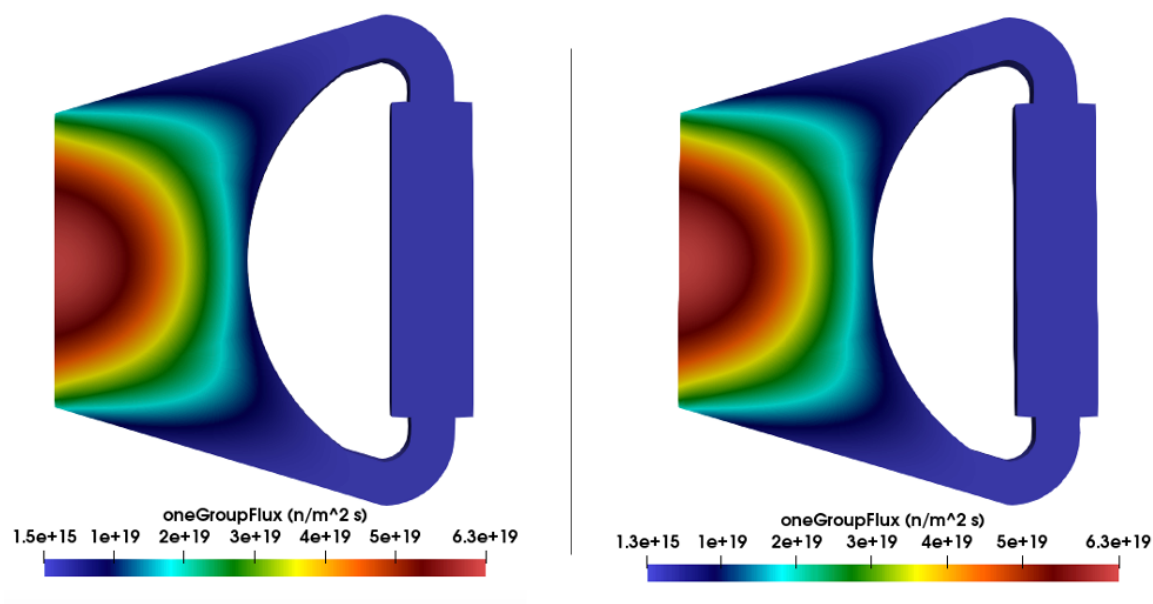


Figure 4.3: Spatial distributions of the neutron flux in the steady states: On the right for insertion of external reactivity transient, on the left for the exponential reduction of velocity transient.

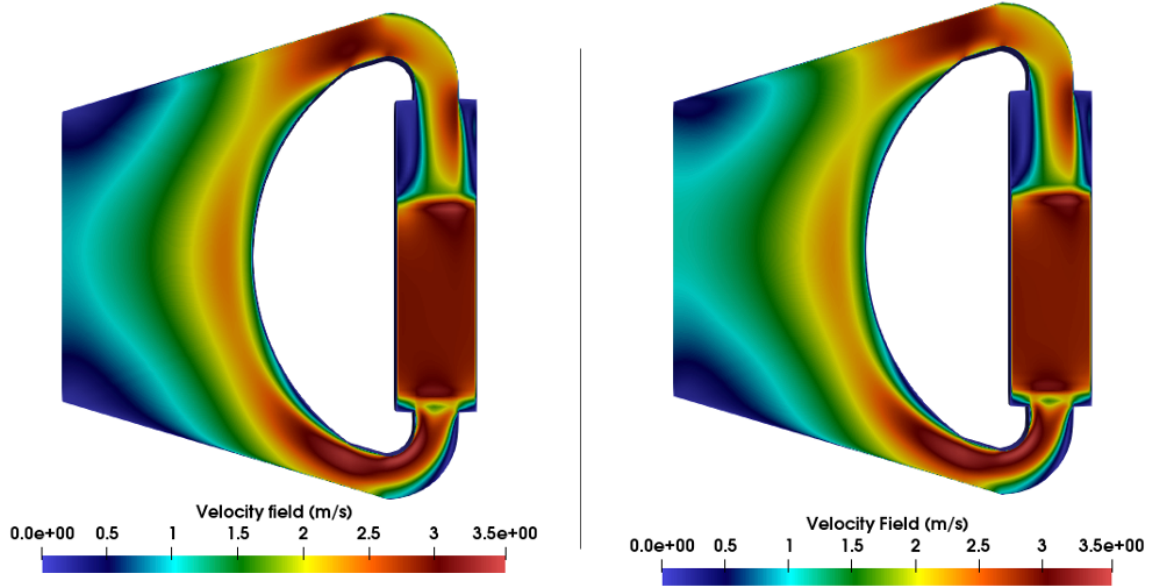


Figure 4.4: Velocity fields of the steady states: On the right for insertion of external reactivity transient, on the left for the exponential reduction of velocity transient [Left]

As told in the section 2.3, this point kinetics solver needs the values of the neutron parameters of the system, in particular in this case:

- The mean generation time,  $\Lambda$ ;
- The fuel doppler constant (for fast reactor),  $K_d$ ;
- The density feedback coefficient,  $\alpha_{density}$

For the mean generation time, the equation 2.8 is used and the input data for the equation are taken from the initial steady state of the insertion of reactivity case. Regarding the weight function  $W$ , as in the implementation of the point kinetics model in GeN-Foam, is equal to  $\phi_n$ .

For the feedback coefficients, in the model of MSFR there are two types of neutron feedback:

- One related to the fuel temperature;
- The other related to the density of the fluid.

These parameters can be computed a priori with the diffusion solver with two separate simulations.

First the two effects are separated in two sub-problems of the molten salt fast reactor. Then separately two new starting steady states are found in the same way used to find the steady state of the insertion of reactivity case. Then, transient calculations with an insertion of external reactivity in the system with the diffusion code were made for the two sub-problems. Thanks to these calculations the final average values are computed

#### 4. COMPARISON OF THE POINT KINETICS MODEL WITH DIFFUSION RESULTS

---

in the two sub-problems. At the end with these values and the initial average values, reported in the table below, it is possible to use the Eq. 4.4 and the Eq. 4.5 to compute the coefficients required for the point kinetics solver. The same external reactivity has been used in the two sub-problems and it is equal to 53.35 pcm.

$$\rho_{external} = -K_d \cdot \ln \left( \frac{T_{fuel,avg,fin}}{T_{fuel,avg,ini}} \right) \quad (4.4)$$

$$\rho_{external} = -\alpha_{density}(\rho_{fluid,avg,fin} - \rho_{fluid,avg,ini}) \quad (4.5)$$

	Initial	Final
$T_{fuel,avg}$ [K]	1058.8	1073.8
$k_{eff,fuel}$ [-]	0.966044	0.965529
$\rho_{fluid,avg}$ [kg/m <sup>3</sup> ]	3994.4	3982.7
$k_{eff,density}$ [-]	0.966434	0.965918

Table 4.6: Values obtained and used to compute the feedback coefficients

Also the initial and final multiplication factors of the two sub-problem are reported in the table for completeness.

Then the values of the neutron data are:

- $\Lambda$  equal to 1.26  $\mu$ s;
- $K_d$  equal about to 3777.26 pcm;
- $\alpha_{density}$  equal about to 4.56 pcm·m<sup>3</sup>/kg.

Now it is possible to proceed with the comparison. In fact, in this way the diffusion and the point kinetics models can work with the same neutron conditions and with reasonable initial steady states.

### 4.3 The external insertion of reactivity transient

In this section the transient with the insertion of external reactivity is discussed.

About the initial steady state, some important values are useful to be stated:

- The equilibrium reactivity,  $\rho_0$ , equal to 183.532 pcm;
- The initial average fuel temperature,  $T_{fuel,avg,ini}$ , equal to 1058 K;
- The initial average density of the fluid,  $\rho_{fluid,avg,ini}$ , equal to 3994.7 kg/m<sup>3</sup>.

For the diffusion the most important quantity is the multiplication factor,  $k_{eff}$ , which is equal to 0.960284.

Before proceeding with the comparison, it is useful to check if the initial steady state is a good one with the diffusion solver. As it can be seen in the Figure 4.5, if there aren't perturbations on the system, the system will remain in stationary condition. It is a further proof that the the steady state computed is a good starting point for a transient simulation.

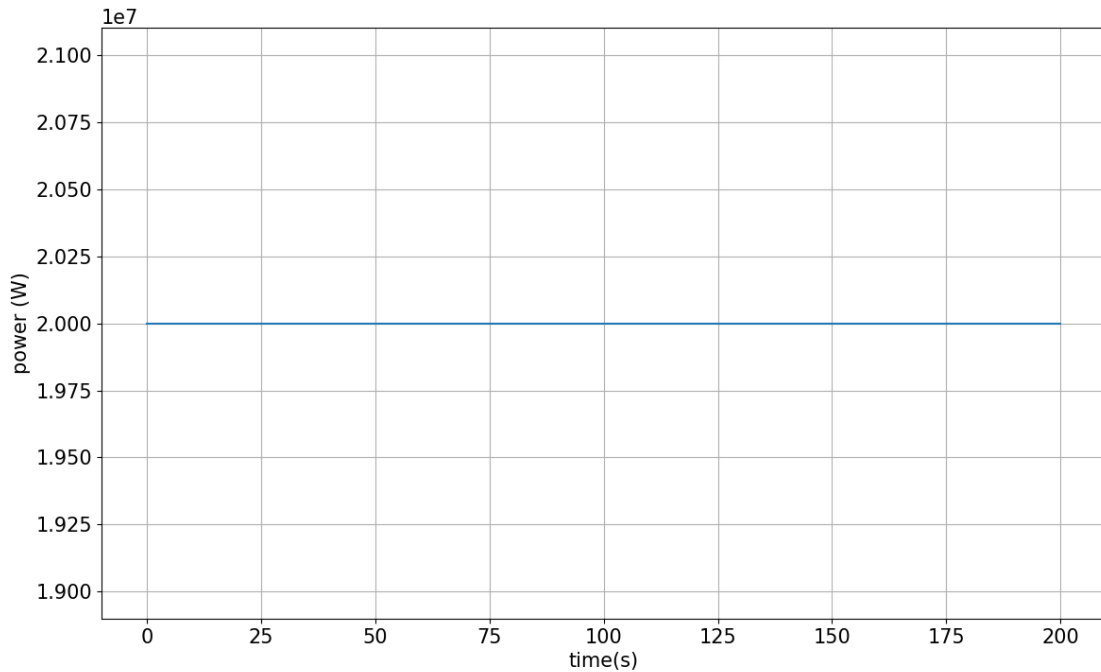


Figure 4.5: Check of the steady state for the insertion of external reactivity transient obtained with the diffusion solver

## 4. COMPARISON OF THE POINT KINETICS MODEL WITH DIFFUSION RESULTS

---

Then an external reactivity equal to 53.35 pcm is inserted in the reactor. This external reactivity can be seen as an external perturbation imposed on the system hence a dynamics evolution of the system is expected before that it reaches a new steady state. The time dynamics evolution obtained with the point kinetics solver (in terms of power, total reactivity and average fuel temperature) can be seen in the Figure 4.6.

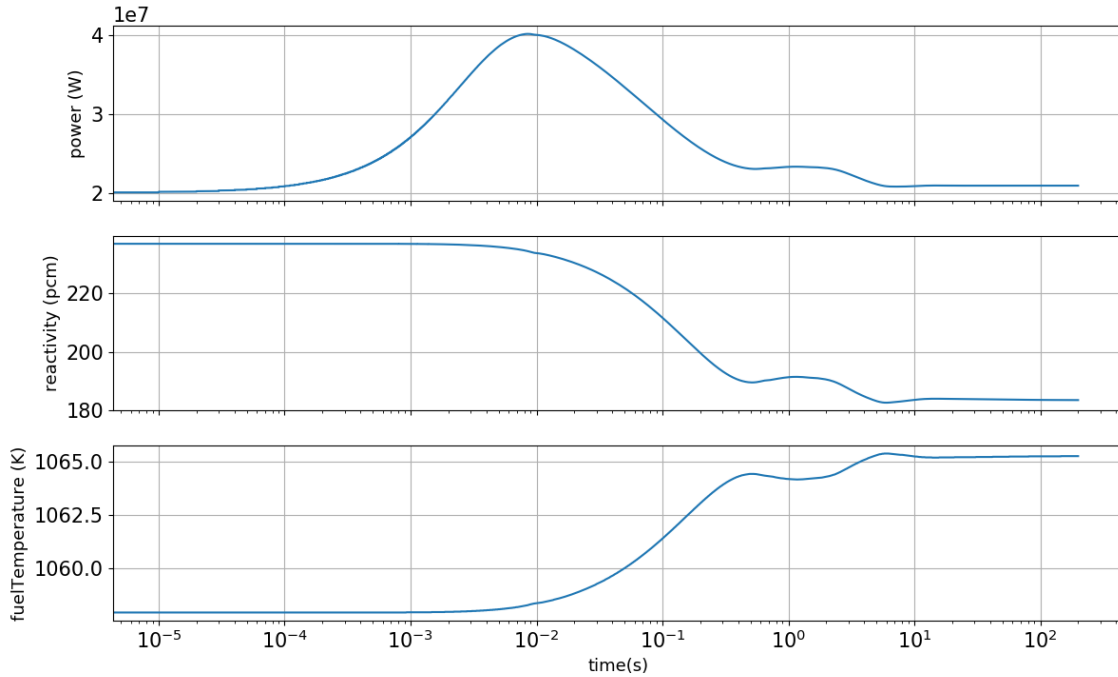


Figure 4.6: Power, total reactivity and average fuel temperature evolutions predicted by the point kinetics in the 2D-MSFR for a reactivity insertion equal to 53.35 pcm

The trend of power shows a typical behaviour of a nuclear system after an insertion of an external reactivity. Indeed, a peak power can be seen immediately after the insertion of reactivity. Then the power decrease due to negative neutron feedback of the fuel temperature and of the density of the fluid until the system doesn't reach the new steady state.

Just have a look on the trends of the total reactivity and the average fuel temperature. Obviously, the initial total reactivity is equal to equilibrium reactivity plus the external one. Then a increase of the temperature can be seen due to the increase of the power. Meanwhile the total reactivity decrease, always due to the neutron feedback, until to reach about the value of the initial equilibrium reactivity of the system. At the end of the transient the external reactivity will be balanced by the feedback effects and its final value will be the value of the equilibrium reactivity, except for numerical error. Regarding the power, its final value is greater than the initial one as expected in this kind of transient. Also for the average temperature the result is the expected one. In fact, there is an increase of the mean temperature.

### 4.3. THE EXTERNAL INSERTION OF REACTIVITY TRANSIENT

Below are reported the most important values when the transient is exhausted and also the value of the power peak during the transient:

- Power at the end of the transient, 20.923 MW;
- Power peak, 40.157 MW after 8.49 ms;
- The final average fuel temperature,  $T_{fuel,avg,fin}$ , equal 1065.2 K;
- The final average density of the fluid,  $\rho_{fluid,avg,fin}$ , equal to 3988.7 kg/m<sup>3</sup>.

For the diffusion simulation the reactivity can be inserted by modifying the multiplication coefficient with the following formula:

$$k_{eff,pert} = k_{eff,steady}(1 - \rho_{external}) \quad (4.6)$$

In fact, looking at the Eq. 4.1 an insertion of reactivity can be obtained in the diffusion case only decreasing the multiplication factor.

The trend of the power for the diffusion against the one for the point kinetics can be seen in the Figure 4.7:

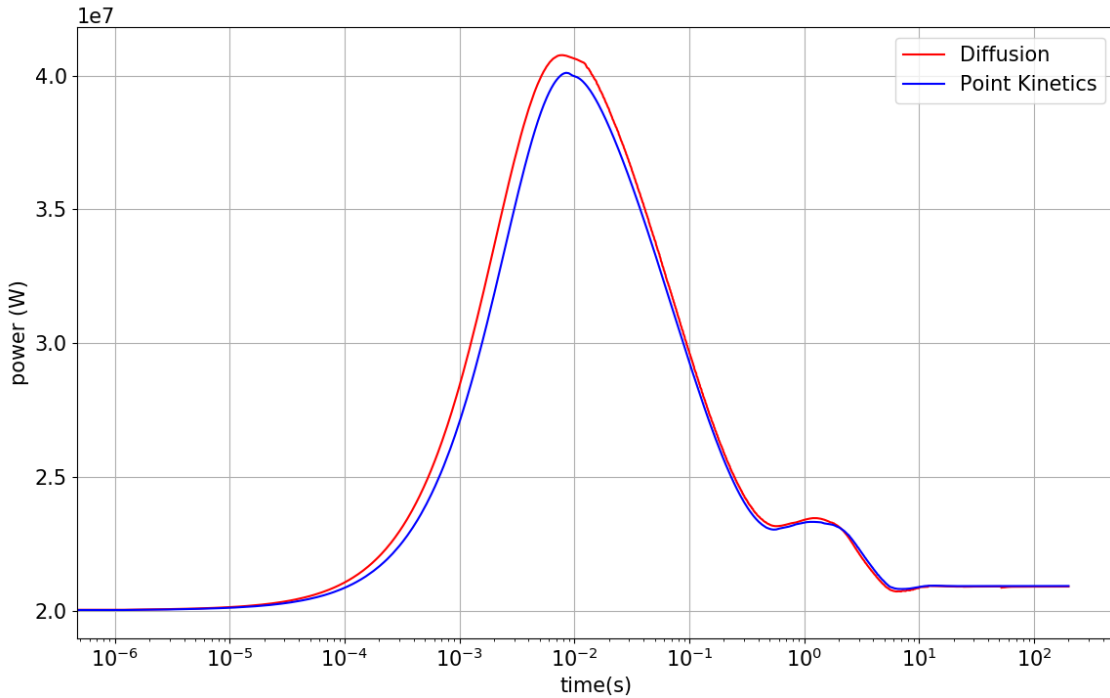


Figure 4.7: Power evolution predicted by the point kinetics and diffusion in the 2D-MSFR for a reactivity insertion equal to 53.35 pcm

So comparing the power peaks, the two trends of the power and the powers at the end of the transient, the two solvers are compared for a case with the insertion of external reactivity. Look at Table 4.7 for the precise values of the peaks and final powers.

#### 4. COMPARISON OF THE POINT KINETICS MODEL WITH DIFFUSION RESULTS

	Point Kinetics	Diffusion
Peak Power [MW]	40.108	40.753
Time of the peak [ms]	8.4882	7.5385
Final Power [MW]	20.923	20.900

Table 4.7: Results for the comparison for a transient with an insertion of external reactivity equal to 53.35 pcm

So as one can note seeing the summary table (Table 4.7) and the Figure 4.7, the diffusion and the point kinetics solvers give results which are very close. Regarding the peak power, it must be said that its value, and obviously also the time when it is reached, depends on the mean generation time in the point kinetics simulation. In fact, if the mean generation time is decreased by the user the peak of power will be higher than before and the peak power will be reached in less time. However the mean generation time has no influence on the final value of the power because it is important only for the dynamic evolution of the system. Then, in the point kinetics the final power depends on the feedback coefficients. These behaviours underline the importance of working with the same neutron conditions if the two numerical solvers have to be compared in a correct way as done in this chapter.

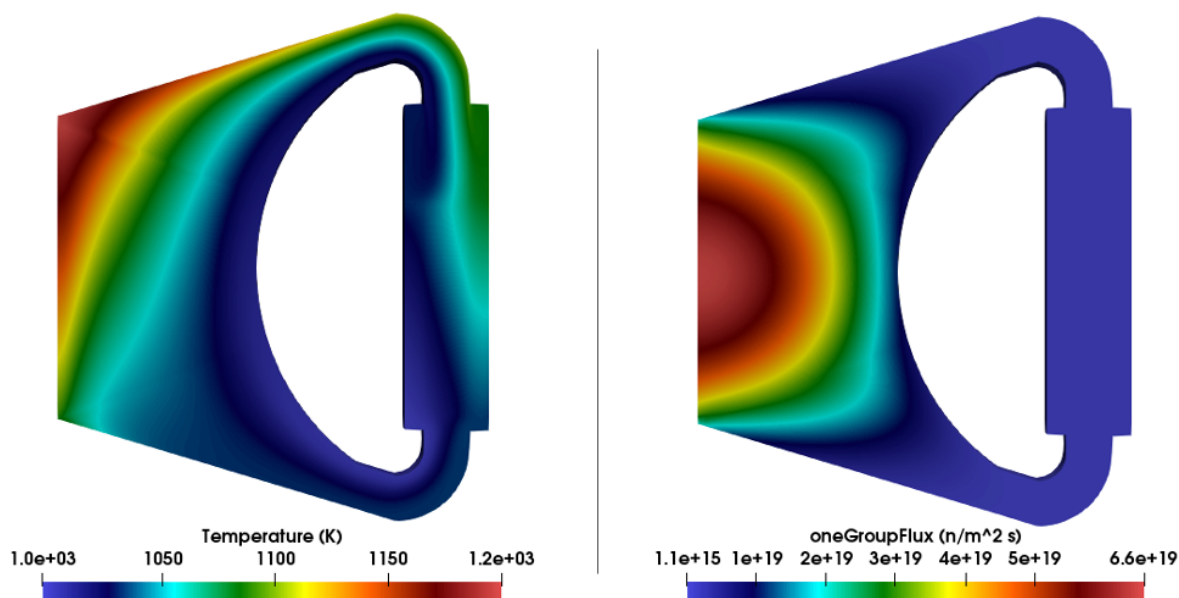


Figure 4.8: Final Temperature field and final flux neutron distribution after the transient with insertion of external reactivity equal to 53.35 pcm

Looking at the Figure 4.8 one can note that the temperature field doesn't change much, there is only a little increase of the temperature, in particular in the core region, how it is expected looking at the values of the initial and final average fuel temperatures.

### 4.3. THE EXTERNAL INSERTION OF REACTIVITY TRANSIENT

---

Indeed about the flux distribution, its shape remains the same of the starting steady state but obviously there is an increase of the neutron flux in the core region due to the increase of the power.

## 4.4 The exponential reduction of velocity transient

As said before, a further eigenvalue calculation, that it is coupled with the fluid dynamics solver, was made in order to find a better initial steady state for this transient case.

Obviously, as done for the previous steady state, a check of the initial steady state just computed isn't a bad idea. The result of this test can be seen on the Figure 4.9. As before this steady state is a good starting point for the next transient simulation.

Also for this case the most important values of the steady state are listed:

- The equilibrium reactivity,  $\rho_0$ , equal to 192.31 pcm;
- The initial average fuel temperature,  $T_{fuel,avg,ini}$ , equal to 1054.1 K;
- The initial average density of the fluid,  $\rho_{fluid,avg,ini}$ , equal to 3997.9  $kg/m^3$ .

Regarding the multiplication factor, it is higher than the previous steady state. The new multiplication factor is equal to 0.960475.

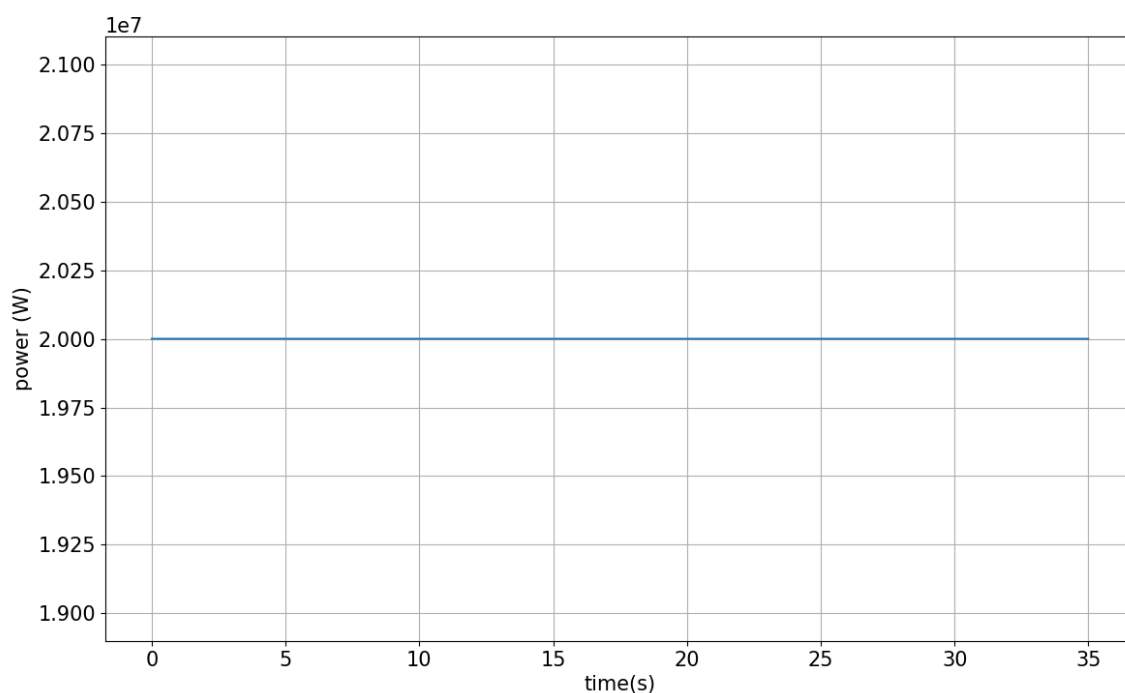


Figure 4.9: Check of the steady state for the exponential reduction of velocity transient obtained with the diffusion solver

Regarding the characteristics of the transient, it is the same of the chapter 3. Therefore an exponential reduction of the velocity field which lasts ten seconds with a pump with a characteristic time equal to two seconds.

The Figure 4.12 shows the time evolution of the velocity in the middle of the heat exchanger during all the simulation. The exponential reduction can be seen in the first ten seconds and then the velocity remains constant for the rest of simulation.

---

#### 4.4. THE EXPONENTIAL REDUCTION OF VELOCITY TRANSIENT

---

Instead in the figures 4.10 and 4.11, the most interesting trends over time of the system are plotted. There is a net decrease of the total reactivity at the end of the transient as expected in a case where the velocity reduces, as in the comparison with the analytical model. In this case the total reactivity includes only the contribution of the equilibrium reactivity, which is a constant value in the Eq. 2.36, and of the feedback reactivity. For this reason the final value of the total reactivity is the value of the equilibrium reactivity of the new steady state when the transient is exhausted.

At the end of the simulation the total reactivity, which is the new equilibrium reactivity of the system, is about 20 pcm less than the starting one.

The total decrease of reactivity is due the decrease of the equilibrium reactivity and both temperature and density feedback counterbalance this behaviour, the results is an increase of the average fuel temperature. The two reactivity feedback are almost equal to a decrease of 10 pcm on the total reactivity for each feedback.

Also a peak can be seen in the reactivity plot and it is related to the peak power and the decrease of the temperature in that range of time when a relative minimum of the temperature can be noted.

Looking at the Figure 4.11, a decrease of the power and the simultaneous increase of the average fuel temperature can be seen in the first ten seconds of simulation. These results are expected. In fact, a reduction of velocity means a reduction of the mass flow rate. Also there is a change on the temperatures of the fuel. Then, the total results is a decrease of the power respect the initial value.

It is important to remember that the system works with an heat exchanger with a constant temperature, equal to 900 K and with a constant heat transfer coefficients, equal to  $1000 \text{ W/m}^2 \text{ s}$ . Then the same conclusion done in the chapter 3 for the same kind of transient can be done. In fact, there is the increase of the average fuel temperature in order to counterbalance the decrease of the equilibrium reactivity, while the power decrease during the exponential reduction of the mass flow rate. This behaviour is expected and it continues until the minimum of power isn't reached. Meanwhile the total reactivity decrease until a minimum value.

After this minimum of power, that it is reached after the reduction of velocity, the system tries to reach a new steady state. The power starts to increase and so the temperature decrease because of the energy balance, in this moment of the simulation the mass flow rate remain constant. This decrease of the average fuel temperature causes an increase of the total reactivity due the usual neutron feedback. This behaviour of the system continues until a peak of the power is reached, which corresponds to the relative minimum of the fuel temperature and the relative maximum of the reactivity. Then the system reaches its new stability conditions and at the end of the transient a net decrease of the power and of the reactivity can be noted. Also a net increase of the fuel temperature, of a few kelvins, can be noted.

#### 4. COMPARISON OF THE POINT KINETICS MODEL WITH DIFFUSION RESULTS

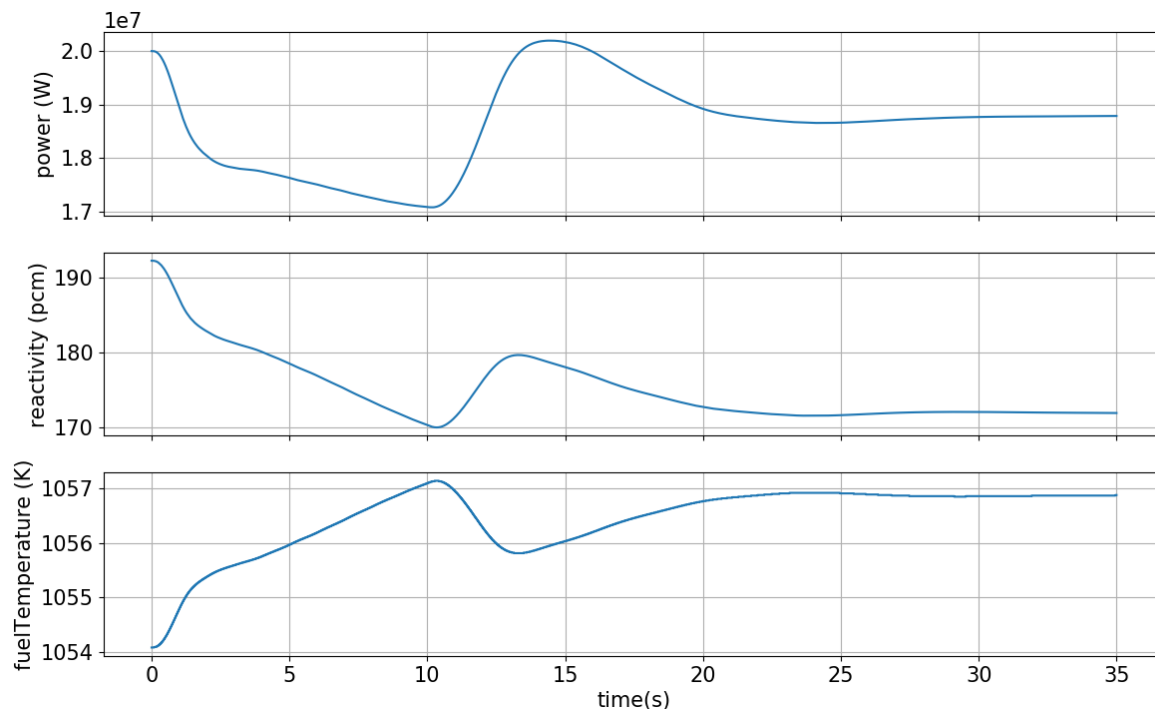


Figure 4.10: Power, total reactivity and average fuel temperature evolutions predicted by the point kinetics in 2D-MSFR for an exponential reduction of velocity which lasts for the first 10 seconds [PK-10s]

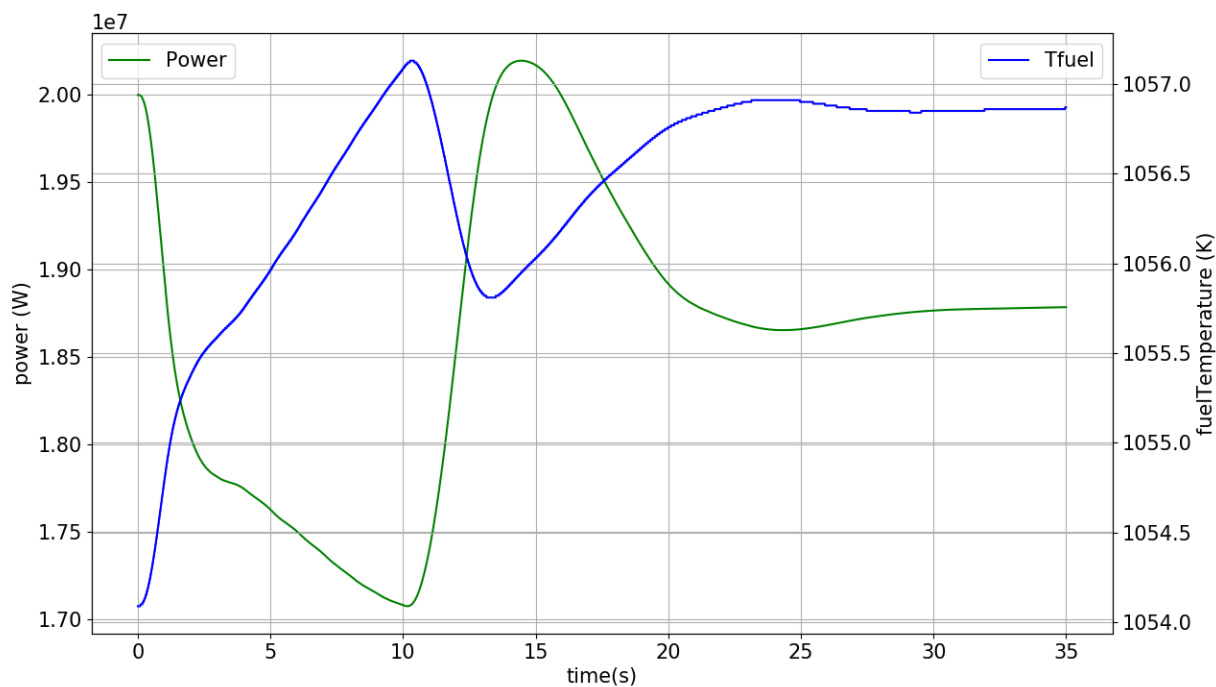


Figure 4.11: Power and average fuel temperature evolutions predicted by the point kinetics in 2D-MSFR for an exponential reduction of velocity which lasts for the first 10 seconds [PK-10s]

#### 4.4. THE EXPONENTIAL REDUCTION OF VELOCITY TRANSIENT

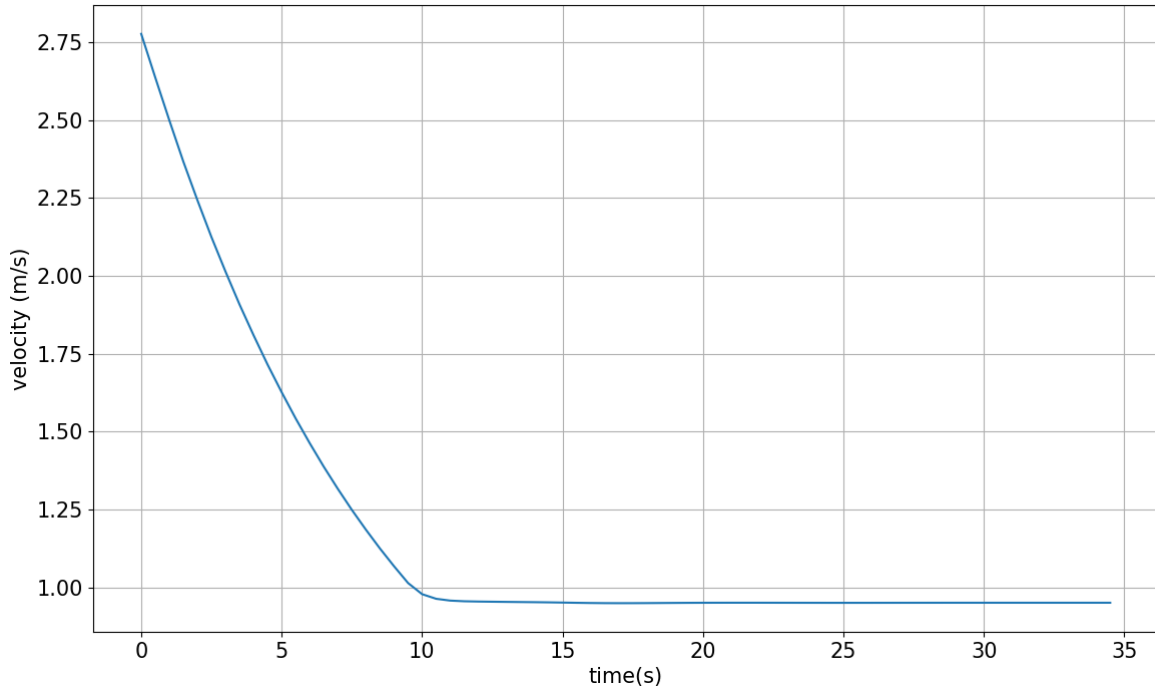


Figure 4.12: Velocity evolution in the middle of the heat exchanger for an exponential reduction of velocity which lasts for the first 10 seconds [PK-10s]

Thence with the point kinetics solver the final conditions of the molten salt reactor are the following:

- Power at the end of the transient, 18.787 MW;
- New equilibrium reactivity,  $\rho_{0,fin}$ , equal to 171.967 pcm;
- The final average fuel temperature,  $T_{fuel,avg,fin}$ , equal 1056.9 K;
- The final average density of the fluid,  $\rho_{fluid,avg,fin}$ , equal to  $3995.6 \text{ kg/m}^3$ .

For the simulation with the diffusion solver the behaviour of the system is the same as one can see in the Figure 4.13.

	Point Kinetics	Diffusion
Minimum Power [MW]	17.078	17.521
Time of the minimum [s]	10.13	10.43
Peak Power [MW]	20.196	20.617
Time of the peak [s]	14.39	14.59
Final Power [MW]	18.787	19.045

Table 4.8: Results for the comparison for the transient with an exponential reduction of velocity which lasts for the first 10 seconds [PK-10s]

#### 4. COMPARISON OF THE POINT KINETICS MODEL WITH DIFFUSION RESULTS

---

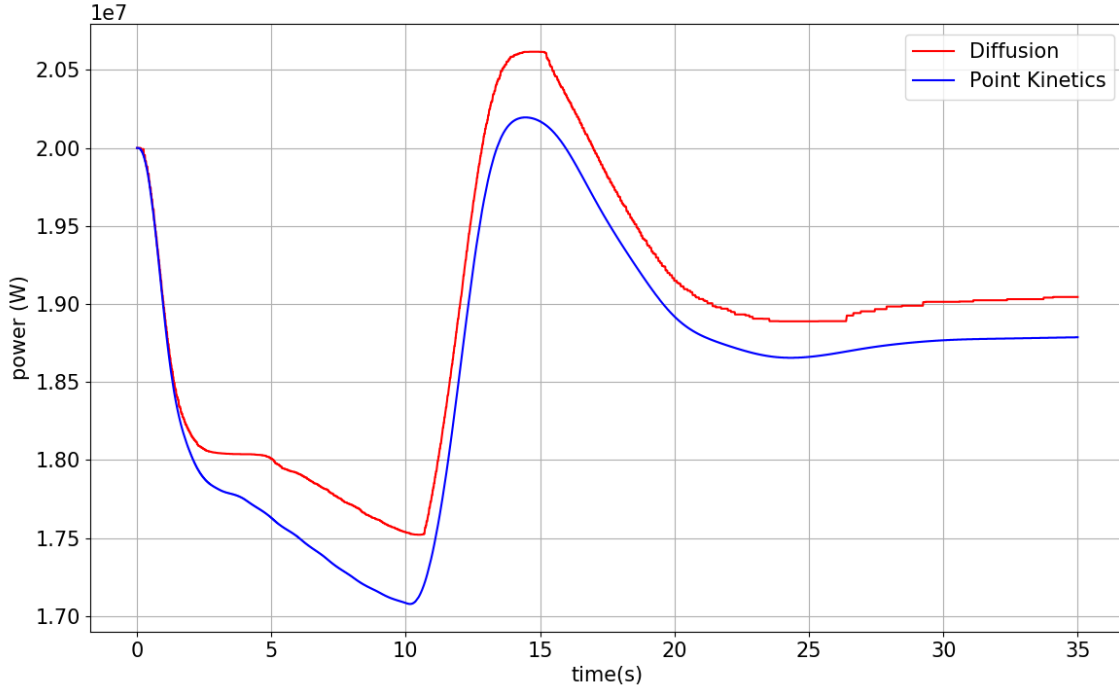


Figure 4.13: Power evolution predicted by the point kinetics and the diffusion in 2D-MSFR for an exponential reduction of velocity which lasts for the first 10 seconds [PK-10s]

At the end the comparison with the diffusion approach can be done comparing the trends of the power of the two approaches and also the most important values during the transient, also look at the Table 4.8.

Focusing on the Figure 4.13 one can note that the time trends of the power are very similar. The differences in minimum location are negligible. The mainly difference between the two trends is that the power obtained thanks to the diffusion solver is always greater than the one obtained with the point kinetics, after the first few seconds of the simulation.

The differences in the power trends originate from a different prediction of circulating beta for the case with circulating fuel, which is equal to 88.9 (as one can see on the Table 4.9) and 93.0 (computed with the Eq. 4.7) in the diffusion and point-kinetic models, respectively. A lower beta in the diffusion case results in a higher reactivity insertion during a loss-of-flow transient, where its value tends to approaches the  $\beta_{eff}$  (which is equal to about 285.3 pcm) for a static fuel (which is the same in the two cases). The higher reactivity insertion during the loss-of-flow transient is the cause of a higher power in the diffusive model. This difference prediction on  $\beta_{fluid}$  between the solvers can be due to the multi-group vs the one-energy approximations for neutrons. Furthermore, this difference is more visible in the transients with a variable mass flow rate.

$$\beta_{fluid}(0) = \frac{\Lambda \sum_{i=1}^R \lambda_i \tilde{c}_{i,0}}{P_0} \quad (4.7)$$

#### 4.4. THE EXPONENTIAL REDUCTION OF VELOCITY TRANSIENT

	$k_{eff}$ with precursors	$k_{eff}$ without precursors	$\beta_{fluid}(0)$ [pcm]
Circulating fuel	0.960475	0.959586	88.9
Static Fuel	0.973857	0.971116	274.1

Table 4.9: Result of the  $\beta_{fluid}$  for circulating and static fuel obtained with the diffusion model

However it isn't a bad idea to try to compare again the two solvers with a different transient of the same kind to see the differences.

The next transient chosen is the same type as the one just discussed but as one can see from the Figure 4.16, in this simulation the exponential reduction lasts fifteen seconds instead of ten seconds. In fact, the final velocity in this simulation is less than the velocity of the previous transient. The characteristic time of the pump remains the same.

The usually plots are reported and they show the same behaviour of the previous simulation as expected (see the plots of the Figure 4.14 and the Figure 4.15).

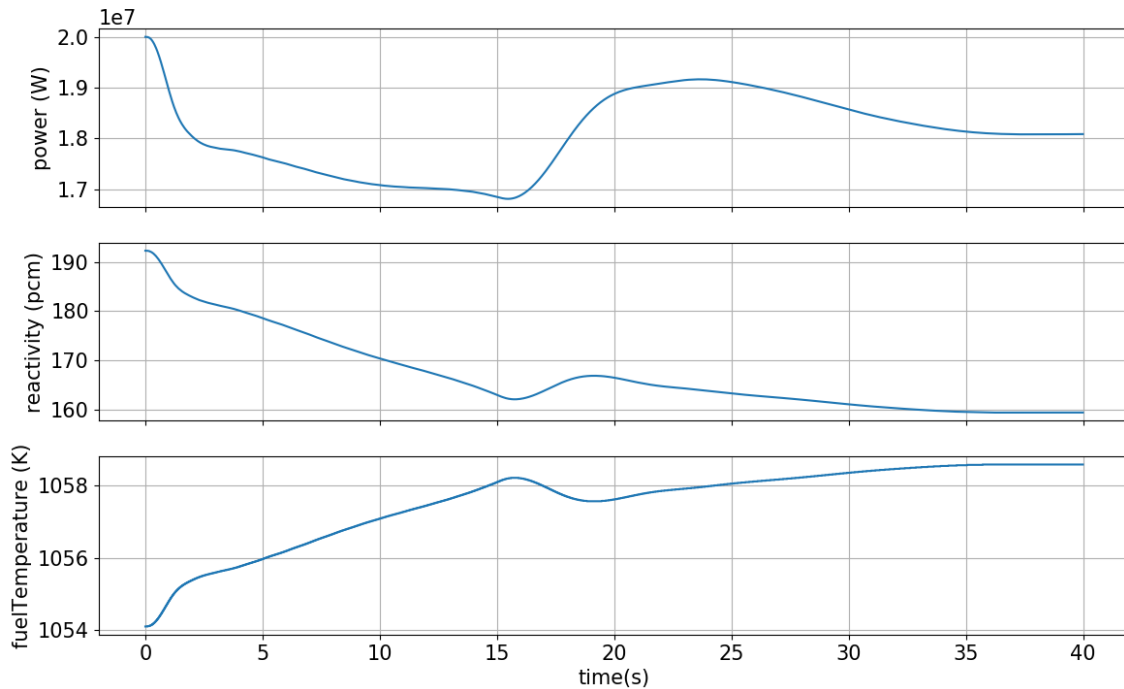


Figure 4.14: Power, total reactivity and average fuel temperature evolutions predicted by the point kinetics in 2D-MSFR for an exponential reduction of velocity which lasts for the first 15 seconds [PK-15s]

#### 4. COMPARISON OF THE POINT KINETICS MODEL WITH DIFFUSION RESULTS

---

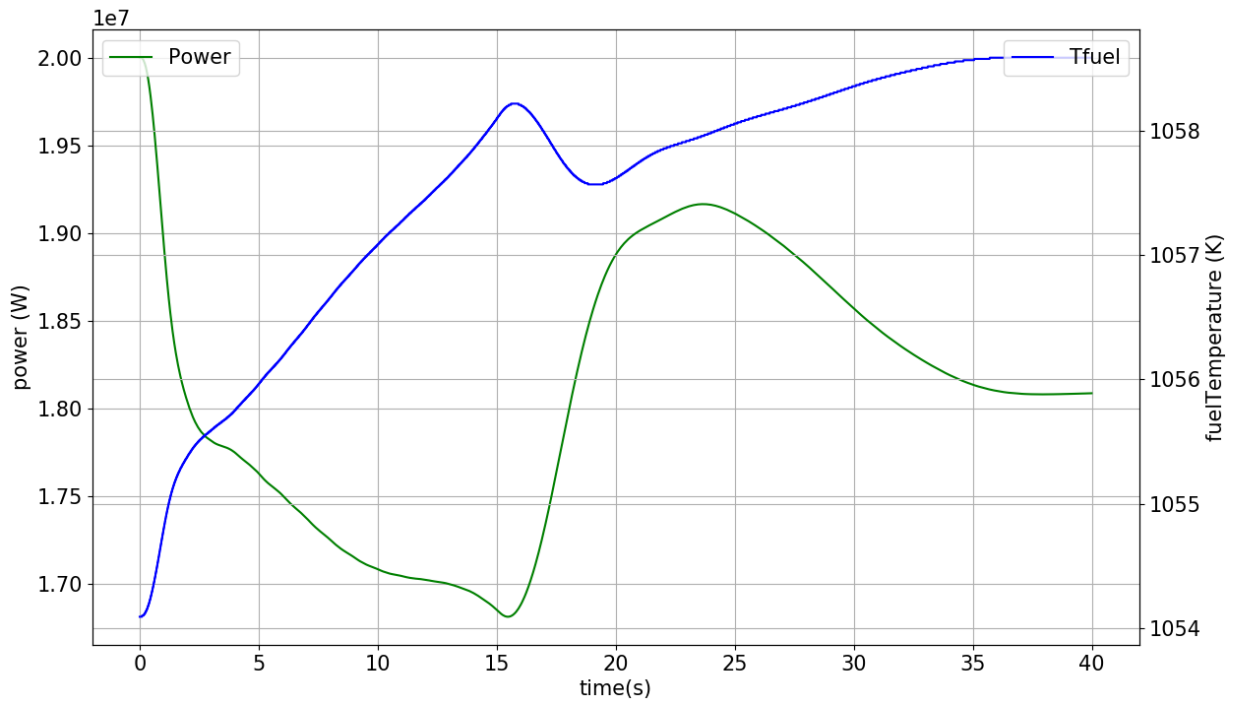


Figure 4.15: Power and average fuel temperature evolutions predicted by the point kinetics in 2D-MSFR for an exponential reduction of velocity which lasts for the first 15 seconds [PK-15s]

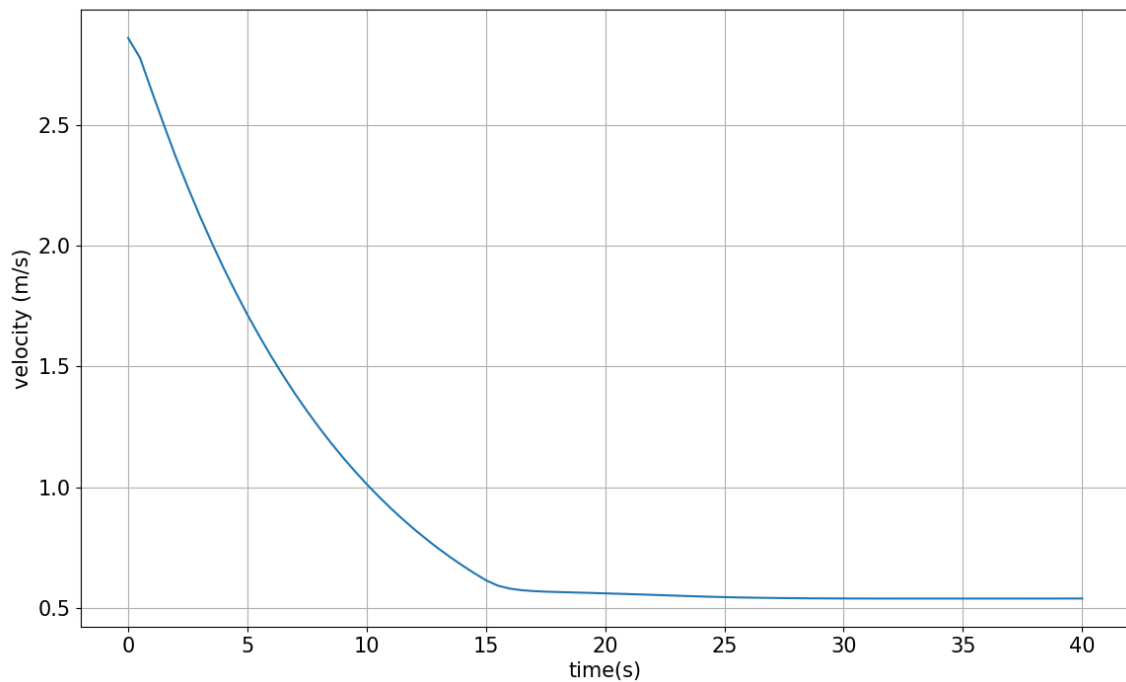


Figure 4.16: Velocity evolution in the middle of the heat exchanger for an exponential reduction of velocity which lasts for the first 15 seconds [PK-15s]

#### 4.4. THE EXPONENTIAL REDUCTION OF VELOCITY TRANSIENT

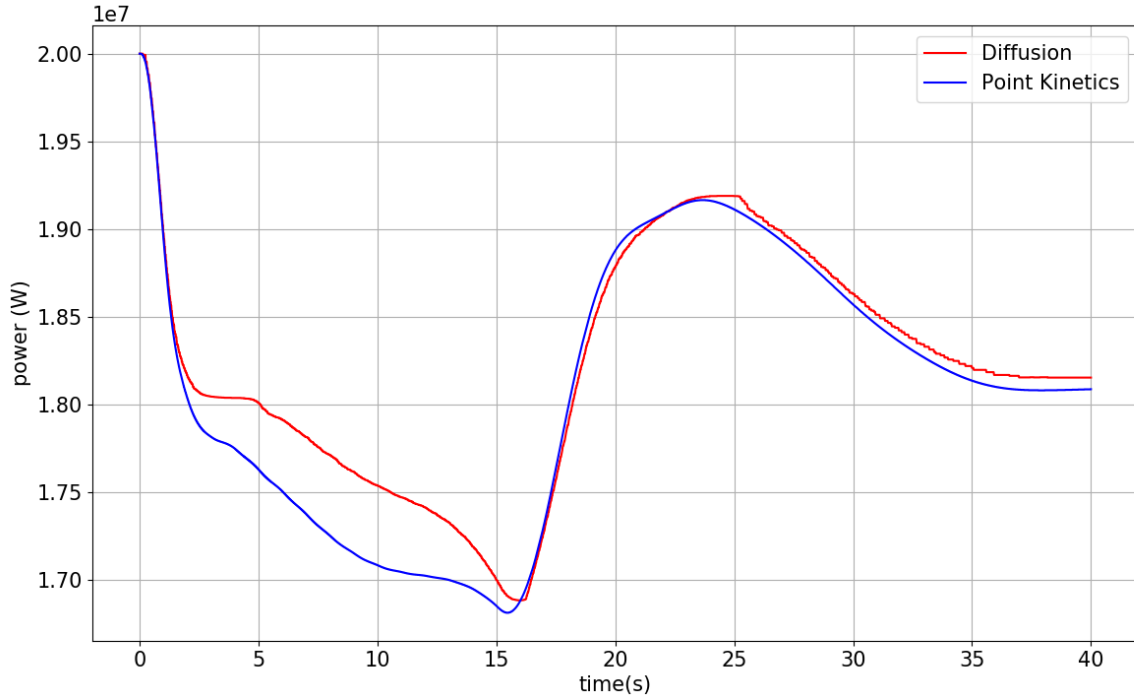


Figure 4.17: Power evolution predicted by the point kinetics and the diffusion in 2D-MSFR for an exponential reduction of velocity which lasts for the first 15 seconds [PK-15s]

For this transient the final conditions of the reactor are:

- Power at the end of the transient, 18.066 MW;
- New equilibrium reactivity,  $\rho_{0,fin}$ , equal to 159.342 pcm;
- The final average fuel temperature,  $T_{fuel,avg,fin}$ , equal 1058.6 K;
- The final average density of the fluid,  $\rho_{fluid,avg,fin}$ , equal to  $3994.2 \frac{kg}{m^3}$ .

The values at the end of the transient are those expected if they are compared with the previous results as it is done after.

	Point Kinetics	Diffusion
Minimum Power [MW]	16.812	16.883
Time of the minimum [s]	15.43	15.90
Peak Power [MW]	19.17	19.19
Time of the peak [s]	23.55	23.98
Final Power [MW]	18.087	18.153

Table 4.10: Results for the comparison for the transient with an exponential reduction of velocity which lasts for the first 15 seconds [PK-15s]

#### 4. COMPARISON OF THE POINT KINETICS MODEL WITH DIFFUSION RESULTS

---

As can be seen from the Figure 4.17 and from the results of the Table 4.10, one can deduce the same conclusion done on the previous simulation for the comparison between the diffusion and the point kinetics solvers. In fact, the trends are very similar and also the same goes for the final results when the system has reached its new steady state. However a difference can be seen than before. It is that from the minimum of the power until the end of the transient the two trends are more closer than the two in the Figure 4.13, as can be notice also from the table.

	Point Kinetics-15s	Point Kinetics-10s
Minimum Power [MW]	16.812	17.078
Time of the minimum [s]	15.43	10.13
Peak Power [MW]	19.165	20.196
Time of the peak [s]	23.55	14.39
Final Power [MW]	18.087	18.787

Table 4.11: Results of the two transients with the exponential reduction of velocity

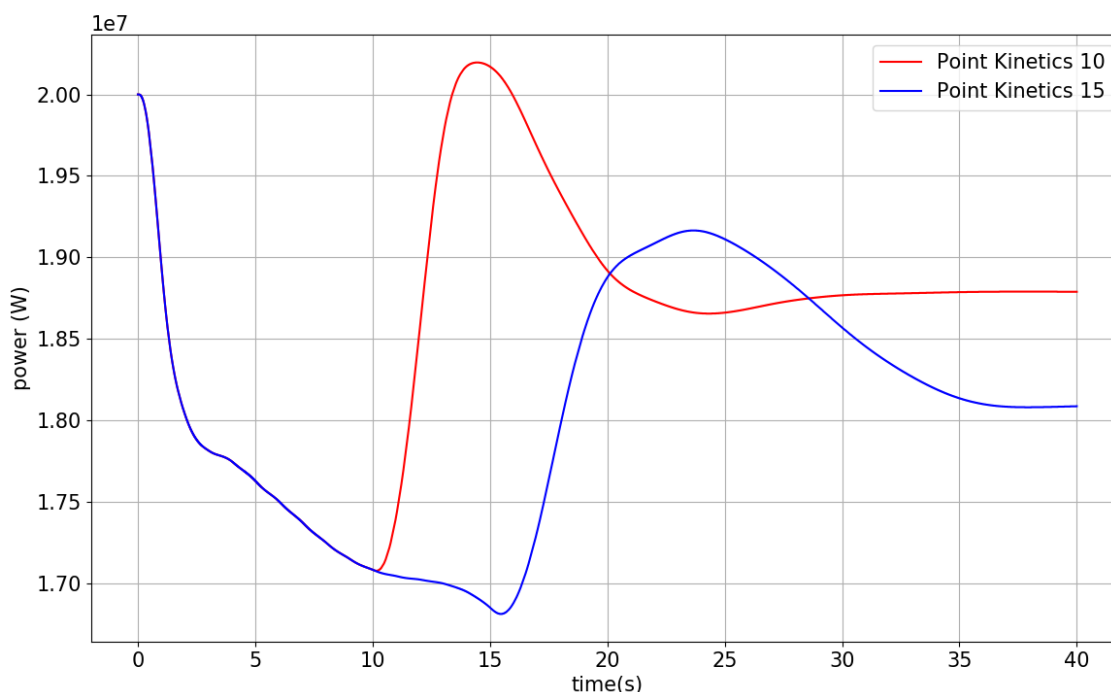


Figure 4.18: Power evolution in the different transients with the two exponential reduction of velocity obtained by the point kinetics [PK-10s vs PK-15s]

Furthermore a comparison between the two transients can be done. From the Figure 4.18, one can see that for the first 10 seconds the two trends are equal as expected. Also

#### 4.4. THE EXPONENTIAL REDUCTION OF VELOCITY TRANSIENT

the values of the minimums and of the peaks of power, reported in the Table 4.11, seems in accordance due to the strong reduction of the velocity in the second simulation (and the same applies for the power peak and its final value). Also the values of the two final equilibrium reactivity are reasonable. In fact, for the first simulation the final equilibrium reactivity obtained is equal 171.967 pcm and for the second it is equal to 159.342 pcm.

Again, these results were expected because of the more reduction of the velocity field in the second simulation. These expectations on the equilibrium reactivity are also justified by the average fuel temperatures (reported previously). In fact even if their difference isn't high, about 2 K, the final average fuel temperature of the second case is higher than the first one. Of course this little difference in the temperatures affects the difference between the two final reactivity. In fact in the first case there is a reduction of the total reactivity of about 10 pcm due to both the fuel neutron feedback and of the density feedback. Instead, in the second transient the reduction due to the fuel temperature, always the same goes for the density feedback, is equal to about 16 pcm.

Furthermore the final spatial distributions of the temperatures of the two cases are different, as one can see from the Figure 4.19. An increase of the temperature field near the region of the pump and of the heat exchanger can be noted for the second transient as expected. This behaviour can be related also to the reduction of the velocity profiles due to the different reduction of velocity (see Figures 4.12 and 4.16), reported in the Figure 4.20, in the same regions. Regarding the core region, there is an increase of temperature fields but also there is a great reduction of the velocity near the reflector zone. In fact a zero velocity of the fluid can be seen near the boundary of the reflector.

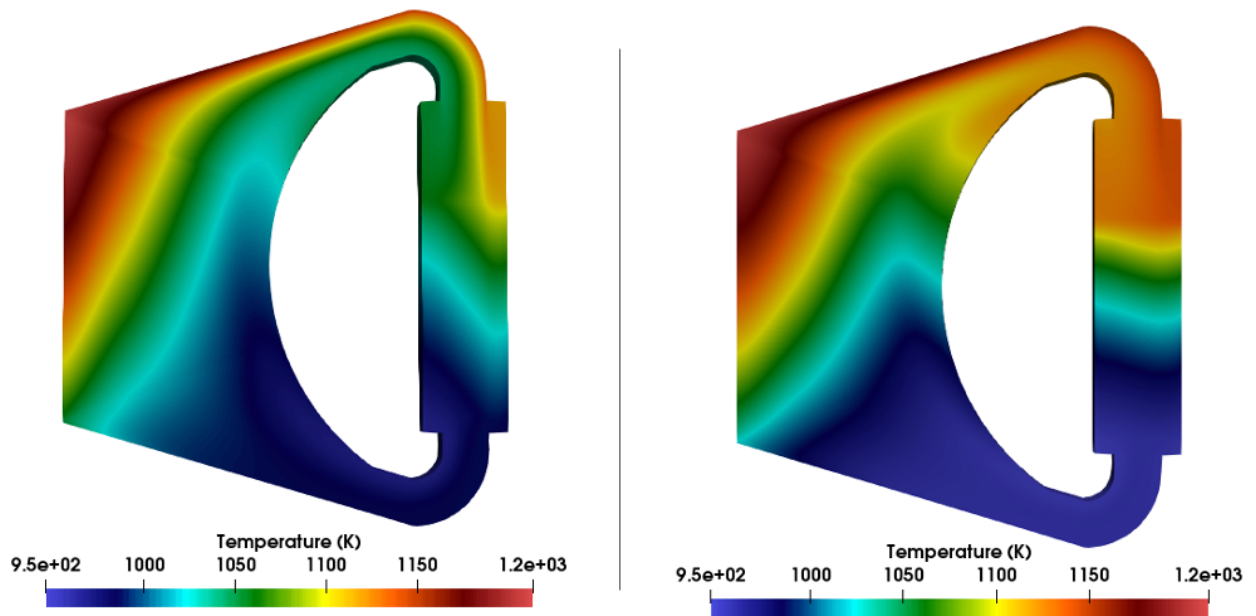


Figure 4.19: Final temperature distributions: On the left for the transient with the exponential reduction of velocity which lasts 10 seconds [PK-10s], on the right the one which lasts 15 seconds [PK-15s]

#### 4. COMPARISON OF THE POINT KINETICS MODEL WITH DIFFUSION RESULTS

---

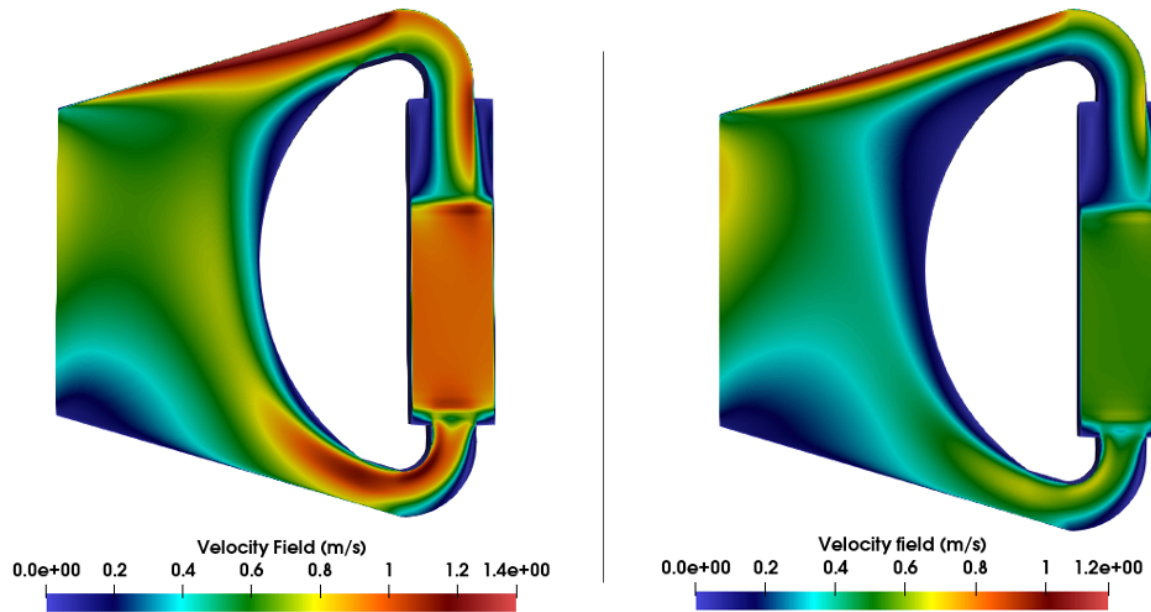


Figure 4.20: Final velocity fields: On the left for the transient with the exponential reduction of velocity which lasts 10 seconds [PK-10s], on the right the one which lasts 15 seconds [PK-15s]

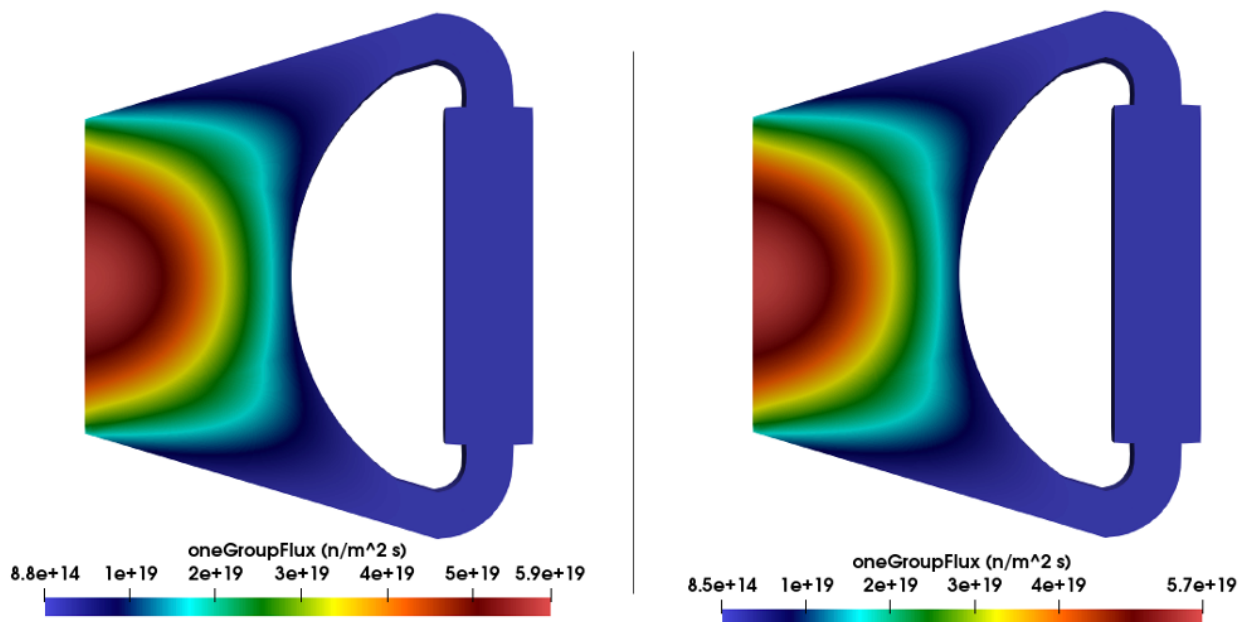


Figure 4.21: Final neutron flux distributions: On the left for the transient with the exponential reduction of velocity which lasts 10 seconds [PK-10s], on the right the one which lasts 15 seconds [PK-15s]

Instead for the flux distribution, the shapes are the usual, see Figure 4.21. Of course the only difference is the magnitude of the fields but it can be understood by comparing

---

#### 4.4. THE EXPONENTIAL REDUCTION OF VELOCITY TRANSIENT

---

the final powers. In fact, for the left side a power equal to 18.787 MW and for the right side the power is 18.087 MW.

Also this modified point kinetics model has the advantage of having shorter computational times than those of the diffusion solver, as one can note from the Table 4.12, and a high computational advantage over a diffusion model (see Table 4.13, computed in the following way:

$$\frac{t_{diffusion} - t_{pointkinetics}}{t_{diffusion}} \quad (4.8)$$

	Computational time [h]
Diffusion [Insertion external reactivity]	0.26
Point Kinetics [Insertion external reactivity]	0.14
Diffusion-10s [Exponential reduction of mass flow rate]	3.24
Point Kinetics-10s [Exponential reduction of mass flow rate]	2.89
Diffusion-15s [Exponential reduction of mass flow rate]	3.99
Point Kinetics-15s [Exponential reduction of mass flow rate]	3.18

Table 4.12: Computational times of the simulations of the transients on the 2D-MSFR model

	Computational advantage [%]
Insertion of external reactivity transient	46.54
Exponential reduction of the mass flow rate [10s]	10.89
Exponential reduction of the mass flow rate [15s]	20.25

Table 4.13: Computational advantages between the diffusion and the point kinetics solvers for the simulations of the transients on the 2D-MSFR model

## 4.5 Precursors distributions

With these simulations, it is possible to investigate a further feature of this model, which is generally not present in a point approach, that is the computation of the spatial distributions of the precursors in the entire system.

For simplicity only the spatial distributions of the first and eighth groups of precursors will be reported, because the first group has the minor decay constant and the eighth group has the major one.

In the Figures 4.22 and 4.23 one can see that the distributions of the precursors in the stationary conditions obtained with the diffusion and for the point kinetics solvers are similar in the shape. There is to say that the only difference in these situations is the order of magnitude of the precursors but it can be easily explained by remembering briefly a little difference between the two models. In fact, the point kinetics computes a precursor distribution in terms of power unlike diffusion which computes this as a simple spatial distribution. This can be seen from the equation below:

$$\tilde{C}_i(r, t) = \frac{P_0 v}{\int \phi(0) dV} C_i(r, t) \quad (4.9)$$

From the Figure 4.22 one can note that the precursors are less distributed on the heat exchanger as expected and they are more present at the bottom of the core. This can be seen also in the Figure 4.23 where the distribution of the precursors is much more similar to the power distribution (see Figure 4.3) of the system thanks the high decay constant. Also from the precursors of the first group the concentration seems to be higher where the velocity is lower and the temperature is higher (compare with Figures 4.2 and 4.4). Then, after seeing that the distributions of precursors are equal at the starting point both for the diffusion and both for the point kinetics, it is time to compare the results between the solvers for the transients done in this chapter.

Starting from the simple transient, that is the transient with the insertion of external reactivity, from the Figures 4.24 and 4.25 one can note that there are no modifications on the shapes of distributions of the precursors respect the initial ones. In fact, these shapes are also related to the velocity field and in this kind of transient this field doesn't change. Anyway for both groups of precursors an increase in precursors can be noted, which is a uniform increase in the whole system even in the heat exchanger.

The results concerning the other groups are not reported but obviously they are almost the same.

Instead for the transients with the reduction of velocity the comparison between diffusion and point kinetics isn't reported because the results are the same, that is the behaviour of the precursors is the same for both models also for these cases. Consequently, an interesting behaviour to look at is the difference between the two different transients of the section 4.4.

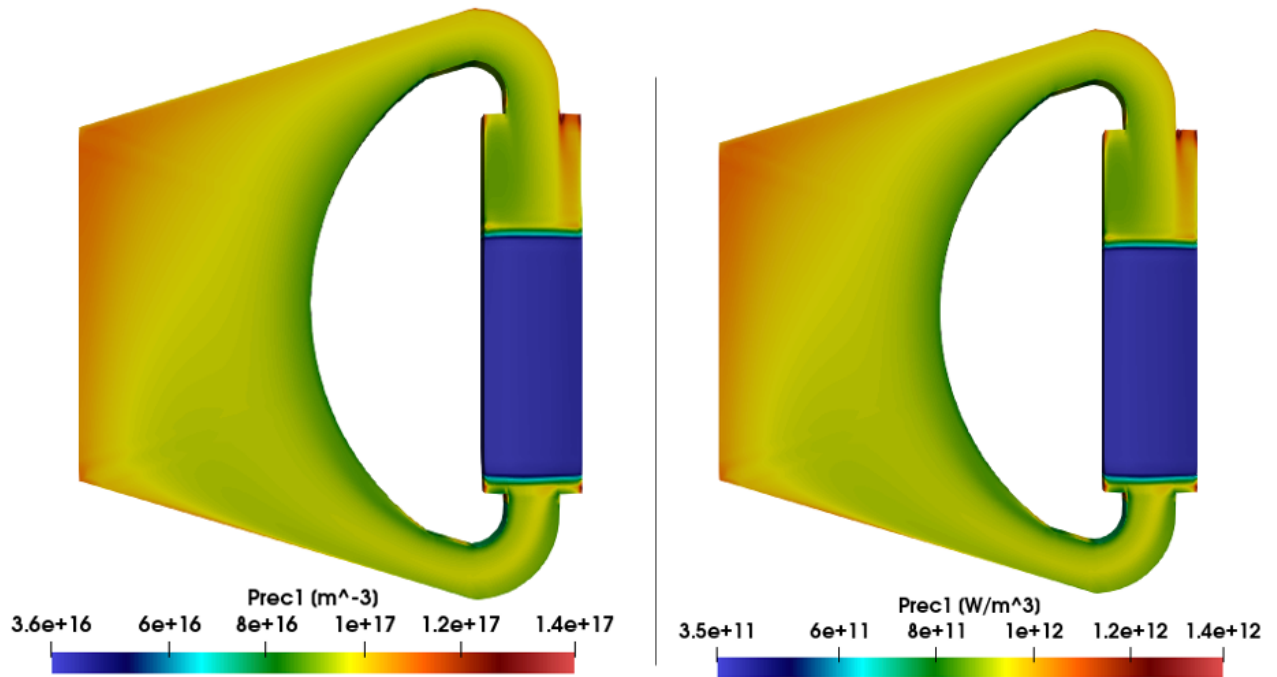


Figure 4.22: Initial distributions of the first group of precursors: On the left the distribution obtained with the diffusion, on the right the one obtained with the PK

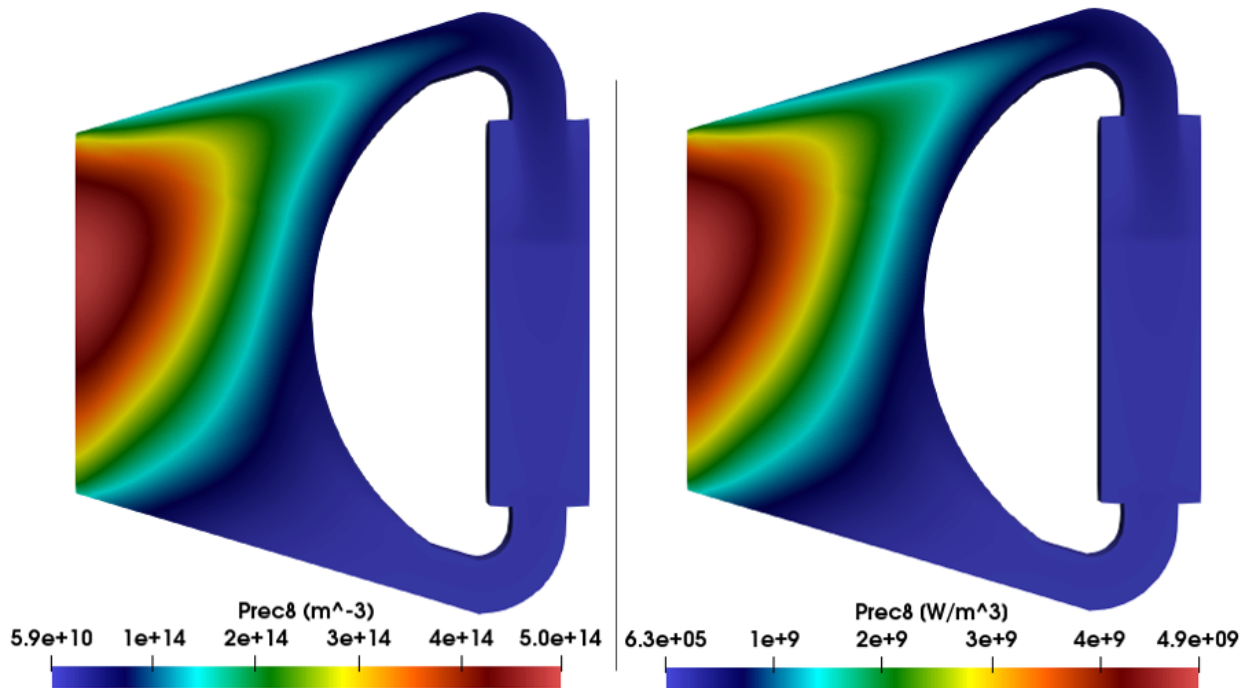


Figure 4.23: Initial distributions of the eighth group of precursors: On the left the distribution obtained with the diffusion, on the right the one obtained with the PK

#### 4. COMPARISON OF THE POINT KINETICS MODEL WITH DIFFUSION RESULTS

---

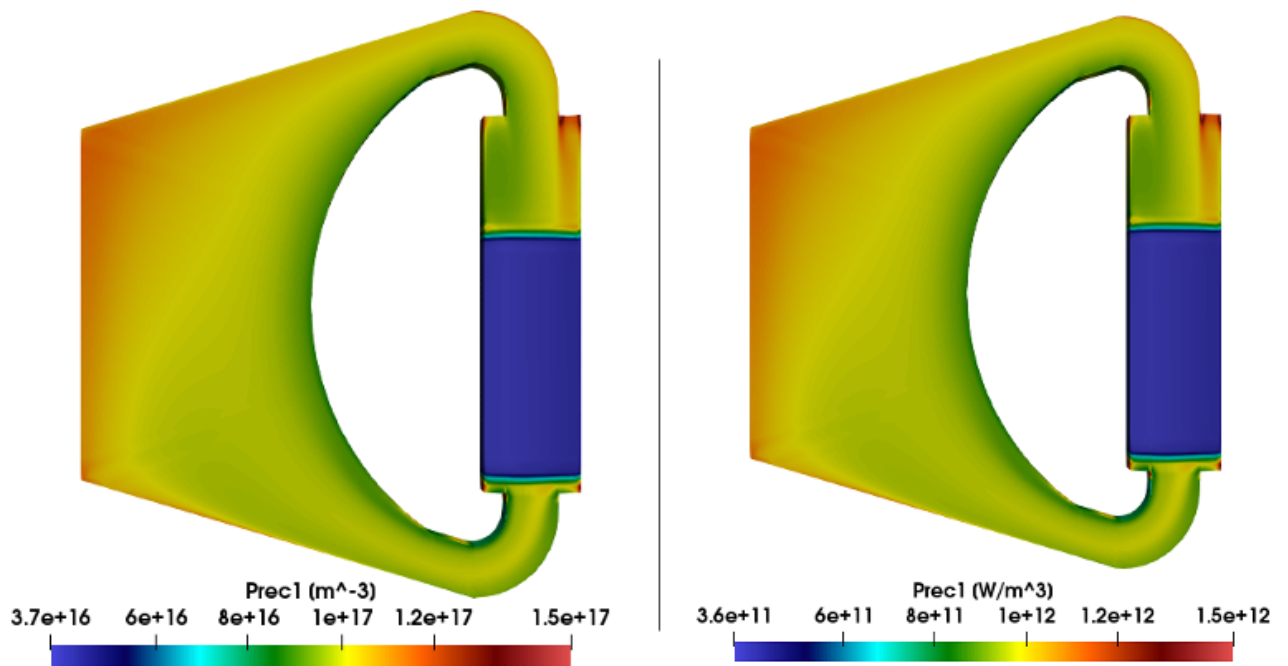


Figure 4.24: Final distributions of the first group of precursors for a reactivity insertion equal to 53.35 pcm: On the left the distribution obtained with the diffusion, on the right the one obtained with the PK

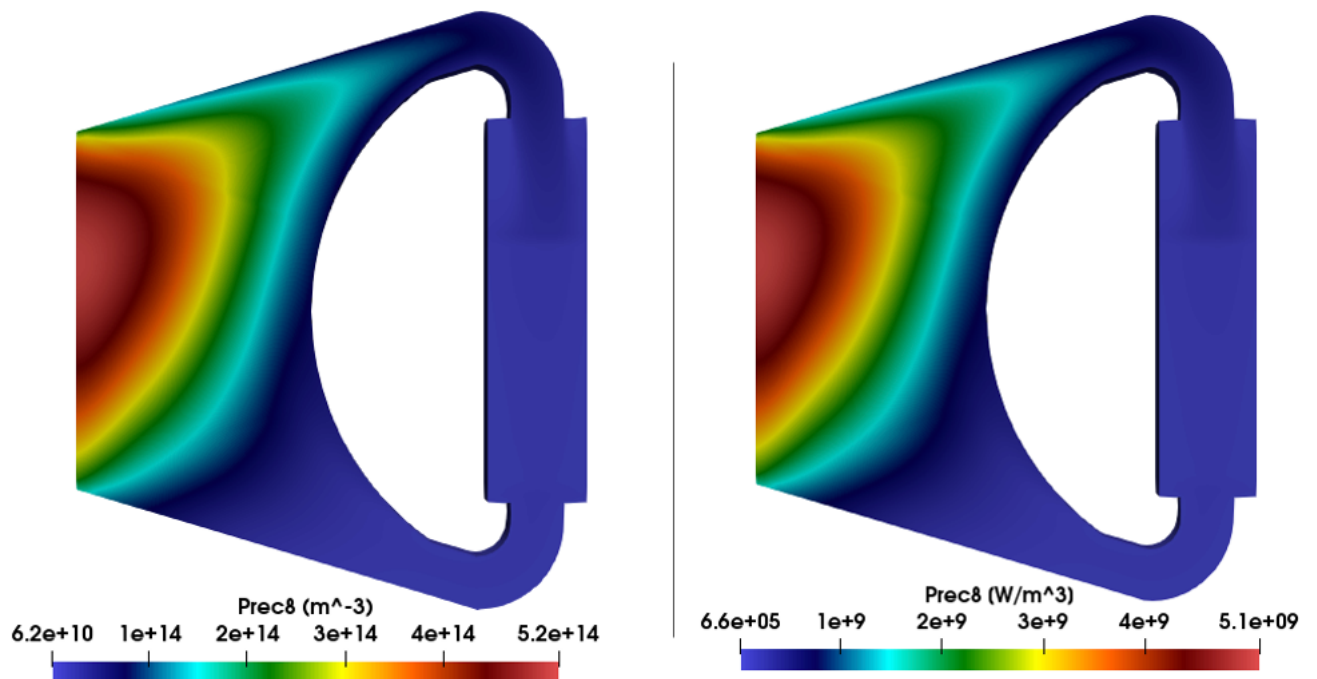


Figure 4.25: Final distributions of the eighth group of precursors for a reactivity insertion equal to 53.35 pcm: On the left the distribution obtained with the diffusion, on the right the one obtained with the PK

Looking at the Figures 4.26 and 4.27 one can note the different behaviour of the precursors in the system respect to the previous case. In fact a decrease of the precursors can be noted both for the first group and for the eighth group. This decrease seems to be in entire system also in the heat exchanger region. Therefore this behaviour is in agreement with the decrease of the power of the system at the end of the transients taken into consideration.

However beyond that there is to comment better the shapes of these spatial distributions respect to the initial shapes. In fact, there are several changes in these terms regarding precursors. These changes are related to the velocity fields (see Figure 4.20) and also on the temperature fields (see Figure 4.19).

Regarding the first group of precursors for the first exponential transient, one can note that in the core there is a decrease of the concentration respect to the initial conditions but in relation to the whole system the precursors are mostly present on the bottom of the core and on the wall of the hot leg. Even in the region near the inlet of the pump and near the outlet of the heat exchanger, there are some changes from before. However these results depends, as told before, to the velocity fields hence it isn't strange that the results for the second transient are little different.

In fact, as the temperature and the velocity fields of the two cases are different the same goes for the precursors distributions. In the second case one can look at a major decrease of the concentration in the area that goes from the outlet of the exchanger to the core through the cold leg. There is also a different distribution in the core region and near the reflector where the concentration is even lower than before, trying to agree with the final velocity and temperature fields. Hence for the first group the concentration decreases during the exponential reduction but the precursors start to become more present in the core region and on the wall of the hot leg where the temperature is higher.

Instead for the eighth group there is a general decrease but this decrease is more localised in the regions out of the core hence in the heat exchanger and in the pump. This is due to high decay constant of this group of precursors. Even so a behaviour due to the reduction of the velocity, which reduces the transport of the precursors into the system, can be seen also for this group. Focusing on the core region in the different situations a change of the spatial shape can be noted.

In fact, respect to the initial spatial distribution, the final distributions show that more the velocity decreases more the spatial distributions of the precursors of the eighth group tend to the distribution of the power. Obviously this is due to reduction of the transport of these precursors into the system.

Therefore it has been shown that this point kinetics solver manages to obtain the same results of the neutron diffusion solver also with regard to the spatial distributions of the precursors even if the geometry isn't simple as in this case where there are zones where there can be turbulent regimes.

However this kind of physical problem is linked to several aspect, for example the grid chosen and the complexity of the geometry and also to turbulent regimes of the fluid. Hence it is a good idea to the compare the results obtained in this chapter with a case with a simpler geometry and with an other type of grid.

#### 4. COMPARISON OF THE POINT KINETICS MODEL WITH DIFFUSION RESULTS

---

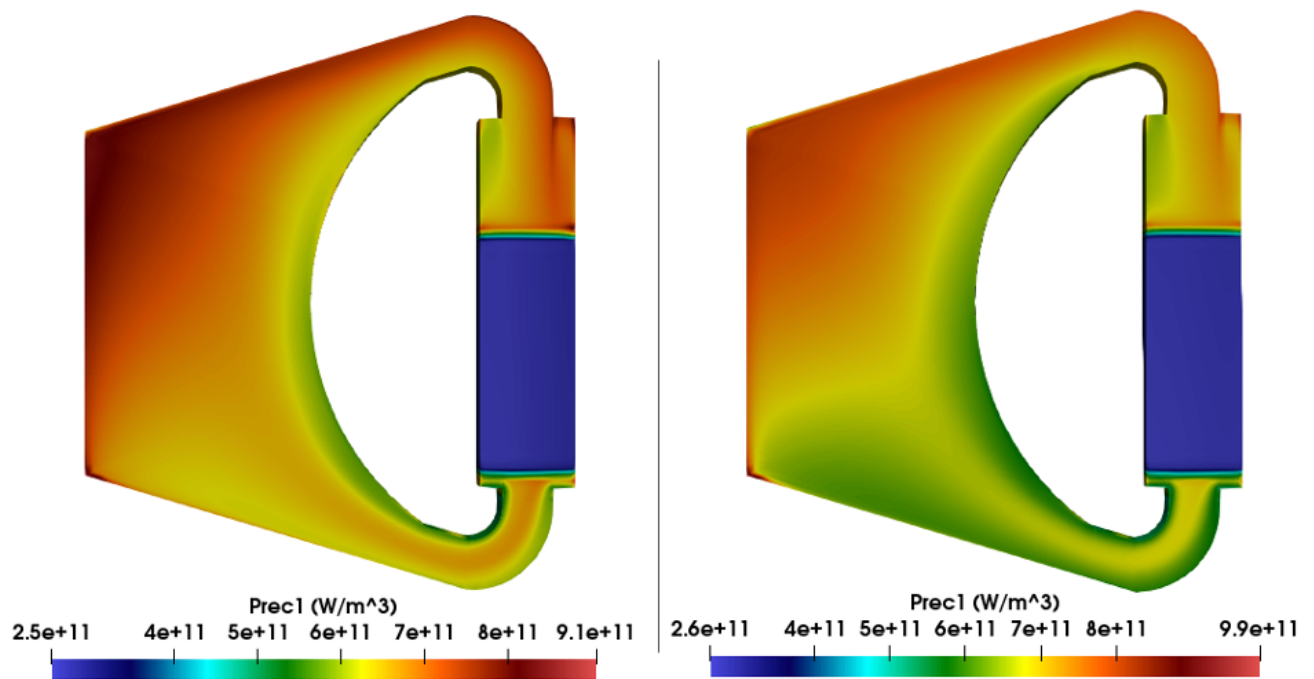


Figure 4.26: Final distributions of the first group of precursors obtained with the point kinetics for the exponential reduction of velocity transients: On the left the PK-10s transient, on the right the PK-15s transient

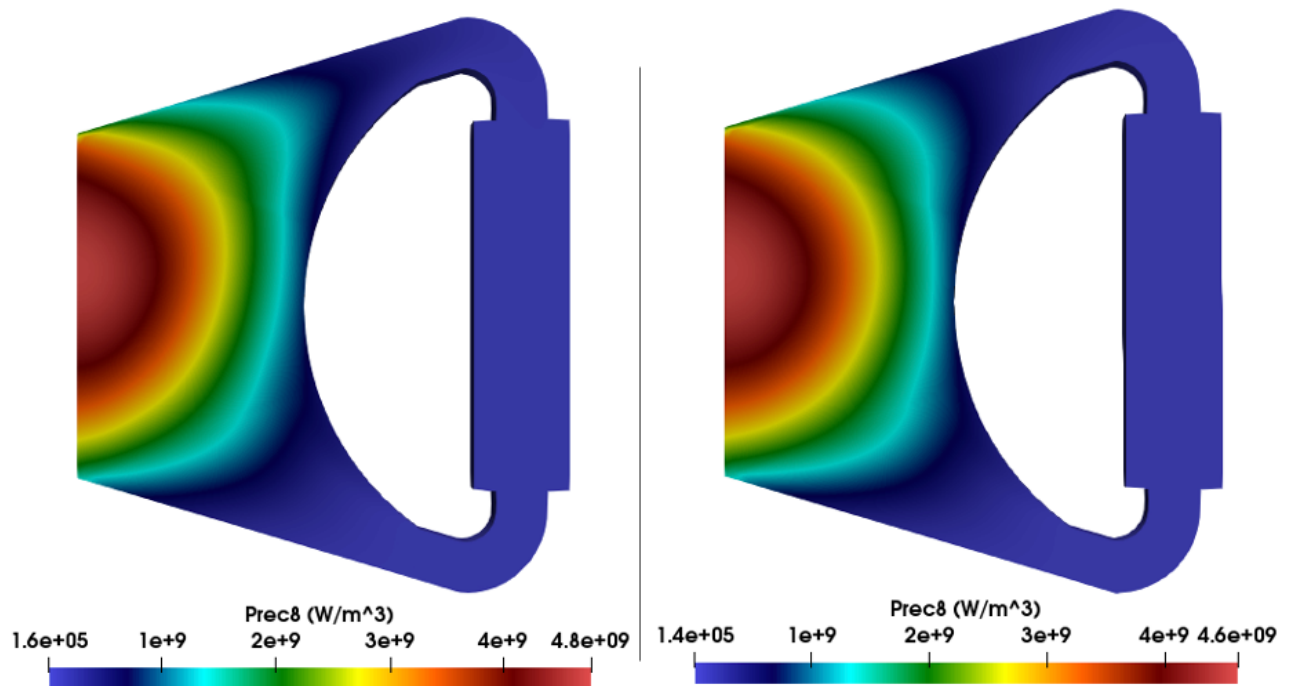


Figure 4.27: Final distributions of the eighth group of precursors obtained with the point kinetics for the exponential reduction of velocity transients: On the left the PK-10s transient, on the right the PK-15s transient

## 4.6 Conclusion

As seen in the results of the simulations reported, the point kinetics solver gets results very similar to the multi-group diffusion solver of GeN-Foam, i.e., solver that has already been verified.

The comparison between the point kinetics and the diffusion provides good results both for a simple transient, triggered by an insertion of external reactivity, and also for more complex transients such as those shown in the section 4.4:

- The exponential reduction of the velocity which lasts ten seconds;
- The other exponential reduction which lasts fifteen seconds.

It was also shown as the solver is able to obtain the spatial distributions of the precursors similar to those obtained by diffusion and that this characteristic of the model allows a study of the system linked to these distributions while using a point kinetics approach.

Furthermore there are other remarks to underline. The first is that the simulations with the diffusion solver are more accurate than those with the point kinetics solver. However this major accuracy corresponds to an higher computational time, as one can see from the summary tables 4.12 and 4.13. The second point is that the point kinetics model and its implementation use the hypothesis of having a mono-energetic case, instead in the diffusion simulations this hypothesis hasn't be used. In fact, it works with six energy groups to compute the neutron fluxes and then it compute the mono-energetic flux. In fact, this approximation is the main cause of the different prediction of  $\beta_{fluid}$  for the diffusion and the point kinetics and it is the reason of the differences in the power trends of the second kind of transient during the exponential reduction of the velocity.

#### 4. COMPARISON OF THE POINT KINETICS MODEL WITH DIFFUSION RESULTS

---

# Investigation of dimensional effects

## 5.1 Introduction

As told previously one of the most important features of this point kinetics model is the capacity to compute the spatial distributions of the precursors in the system. Then it is interesting to investigate the differences due to dimensional effects due to the precursors between two different geometries.

In this chapter, this kind of problem, the dimensional effects due the precursors, will be discussed. The problem will be faced through a comparison between a one dimensional case and a two dimensional one.

In order to remove effects due to a complex geometry, for the 1D simulation a simple geometry has been chosen and it has been build starting from the 2D geometry of the molten salt fast reactor, used in the chapter 4, in a such way to comply with these conditions:

- the volumes of each zone remain unchanged between the two geometries;
- the residence times of the fluid in each zone remain constant.

Then the mean goal is to see and to underline the differences between an 1D and 2D geometry, in order to show the importance of computing the spatial distributions of the precursors also in a point-like approach. This is also important when dealing with system codes that usually employ a monodimensional approach.

In conclusion the geometries used for this comparison are:

- The 2D molten salt fast reactor geometry used in the chapter 4;
- A closed channel system built based on some quantities of the 2D geometry.

As usual the transients used for the comparison are:

- A transient with an insertion of external reactivity;
- An exponential reduction of velocity.

The results of the 2D geometry are the same of the chapter 4 but with a difference on the external reactivity used in the first transient. So only a brief discussion of 1D geometry is reported.

## 5.2 The 1D geometry

For the 1D simulations the geometry chosen is very similar to the one used in the chapter 3, i.e., a closed channel system. However, as told before, the geometry is build having as reference the 2D geometry of the molten salt reactor.

The inlet area of the channel is the area of the heat exchanger of the molten salt fast reactor. Then all the zones are built based on this area in a such a way to have the same volumes of the 2D geometry (see Figure 5.1). It is worth remembering that in the molten salt reactor the region called main includes the core, the hot leg and the cold leg. Hence this zone has been divided in a such way to have the same volume both for the cold leg and for the hot leg. The heights of each zone are then defined accordingly:

- Inlet area of the channel equal to  $0.07 \text{ m}^2$ ;
- Height of the core equal to 1.95 m;
- Height of the cold leg equal to 0.42 m;
- Height of the hot leg equal to 0.42 m;
- Height of the pump equal to 0.39 m;
- Height of the heat exchanger equal to 1.10 m;
- Height of the intermed zone equal to 0.09 m.

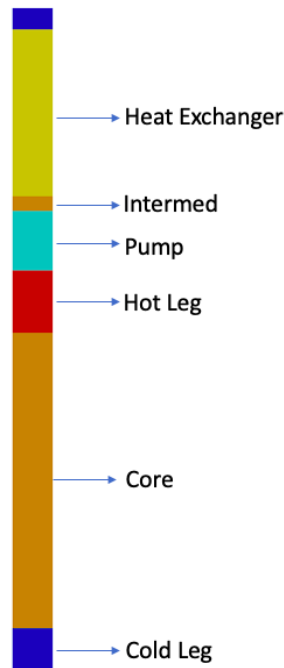


Figure 5.1: The 1D-MSFR geometry and the zones

So with a total volume of  $0.31 \text{ m}^3$ , the height of the system is equal to about 4.36 m. Regarding the thermal characteristics of the fluid and of the heat exchanger, they are the same used in the chapter 4 (see Table 4.1 and 4.2). Obviously, the same goes for the eight groups of precursors, listed in the Table 4.3.

In order to respect the transit times in the different zones of the system, the mass flow rate in the 1D geometry is the same present in the heat exchanger of the molten salt fast reactor. Then for a fluid dynamics point of view the 1D and 2D model are equivalent.

Also on the neutron point of view the two cases are equivalent because they are working with the same point neutron kinetics data,  $\Lambda$  and the feedback coefficients ( $K_d$  and  $\alpha_{rho}$ ).

Furthermore for the one dimensional geometry, there are two different cases which differ according to the power distribution (and then also to the starting steady states):

- A case with an imposed power on the core (called in the plots as 1D-MSFR-uniform);
- The other with a power distribution computed by an eigenvalue calculation (called in the plots as 1D-MSFR-eigenvalue).

For completeness, six energy groups were used in the eigenvalue calculation. The eigenvalue calculation is made in such a way as to have a cosine power distribution only on the core and not on the entire system. The different power distributions can be seen in the Figure 5.2.

The boundary conditions used for the fluid region are the same used in the simulations of the chapter 3 as one can see in the Table 5.1:

Boundary Condition of the fluid region			
	Top	Bottom	Walls
U	cyclic	cyclic	slip
p	cyclic	cyclic	calculated

Table 5.1: Boundary conditions of the fluid problem

Instead, for the neutron region the boundary conditions are (Table 5.2):

Boundary Condition of the neutron region			
	Top	Bottom	Walls
defaultFlux	cyclic	cyclic	zeroGradient
defaultFlux2	cyclic	cyclic	zeroGradient
defaultPrec	cyclic	cyclic	zeroGradient

Table 5.2: Boundary conditions of the neutron problem

## 5. INVESTIGATION OF DIMENSIONAL EFFECTS

---

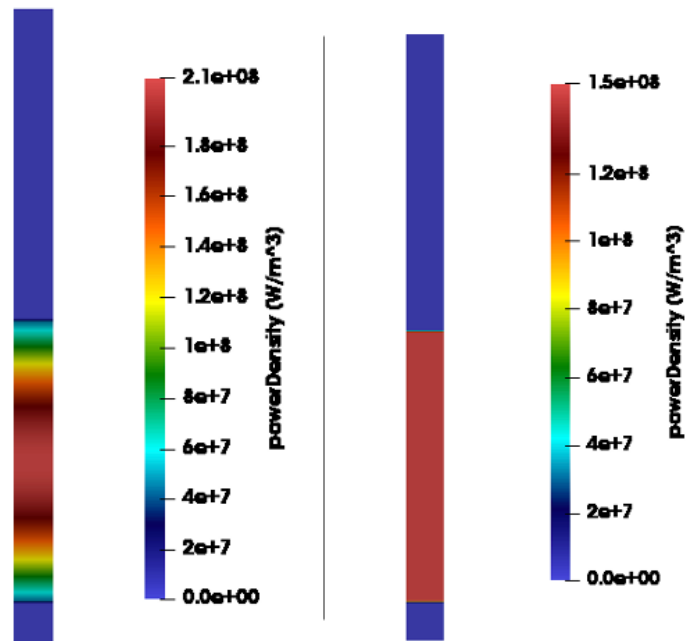


Figure 5.2: Power distributions at steady states: on the right the one for the imposed power on the core [Imposed Power system] on the core, on the left the one obtained with the eigenvalue calculation [Eigenvalue System]

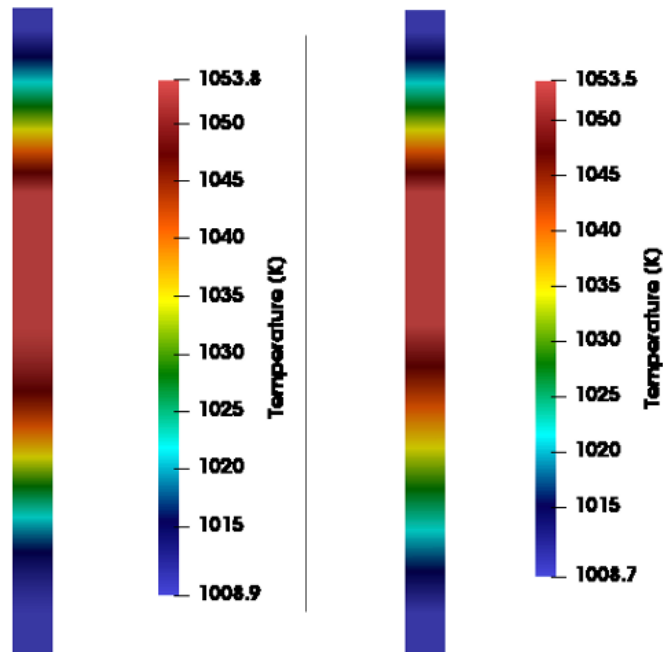


Figure 5.3: Temperature fields at steady states: on the right the one for the imposed power on the core [Imposed Power system] on the core, on the left the one obtained with the eigenvalue calculation [Eigenvalue System]

As for the steady-state temperatures fields shown in the Figure 5.3, no significant differences are present between the two cases. This is confirmed also for the average values as shown in Table 5.3.

	Imposed Power system	Eigenvalue system
$k_{eff}$	//	1.02888
$T_{fuel,avg,ini} [K]$	1031.3	1031.6
$\rho_{fluid,avg,ini} [kg\ m^{-3}]$	4016.7	4016.4

Table 5.3: Initial mean values of the initial steady states of the 1D geometry

A test on the initial steady states of the 1D cases is made in order to check if they are consistent initial conditions points for the transient simulations (Figure 5.4):

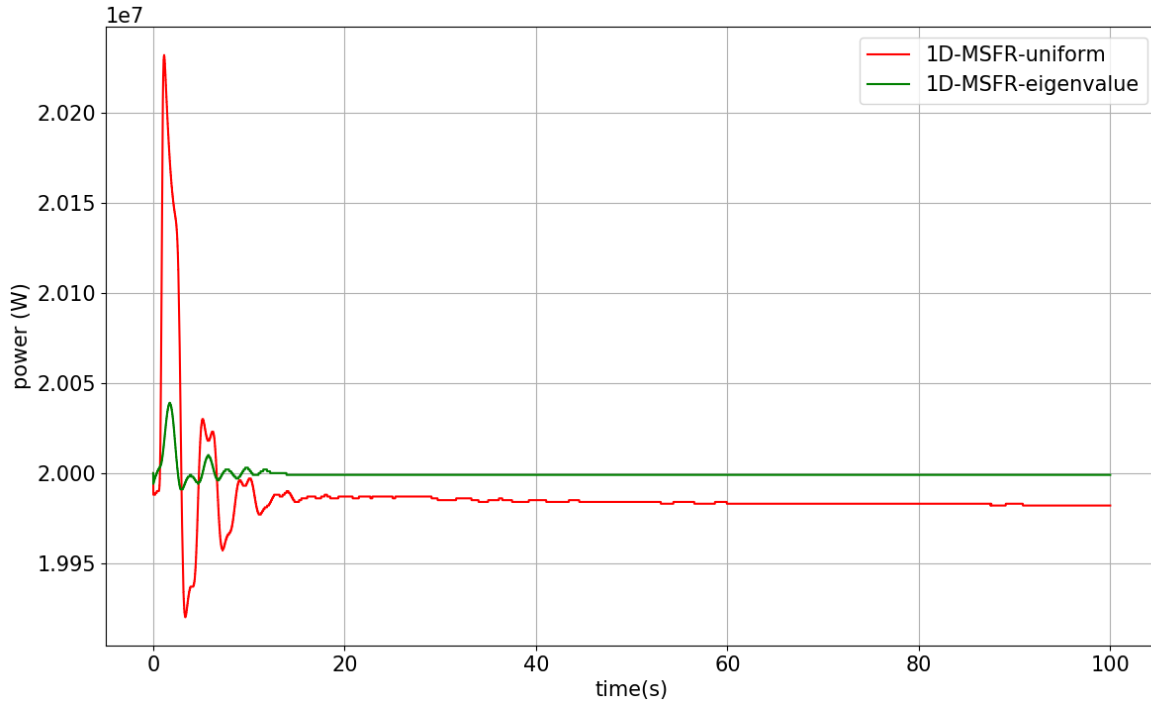


Figure 5.4: Check of the steady states through the point kinetics

These stationary states are not as good as those found in chapter 4 but anyway the maximum variation of the power is approximately less than 1 percent. Then these starting steady states can be considered as good starting points for the simulations of the transients. It is important to underline that for the 1D-MSFR-eigenvalue system better results are expected respect to the 1D-MSFR-uniform system, just see the major oscillations that occur in the case with a uniform power on the core.

### 5.3 Insertion of external reactivity transients

For a proper comparison in the reactivity transient, the external reactivity provided in the two cases must be equal in terms of dollars. In particular in these cases an external of reactivity equal to 0.1 \$ has been chosen.

This concept is very important because for three systems the equilibrium reactivity are different. The equilibrium reactivity for the three different systems are:

- $\rho_0 = 183.532$  pcm for the 2D simulation;
- $\rho_0 = 128.249$  pcm for the 1D simulation with a uniform power distribution on the core;
- $\rho_0 = 135.012$  pcm for the 1D simulation with the eigenvalue calculation.

Instead, the  $\beta_{eff,tot}$  is the same for the three systems, i.e., equal to 285.277 pcm.

Then the value of one dollar for each case is computed through this formula:

$$1\text{\$}[pcm] = \beta_{fluid} = \beta_{eff} - \rho_0 \quad (5.1)$$

The max difference between these reactivity are almost equal to 55 pcm. Tf we use the reactivity insertion of the previous simulation, this will lead to three different transient simulations.

In order to make a meaningfull comparison, the external reactivity inserted in each case are the following:

- $\rho_{external} = 10.174$ pcm for the 2D simulation;
- $\rho_{external} = 15.703$ pcm for the 1D simulation with a uniform power distribution on the core;
- $\rho_{external} = 15.027$ pcm for the 1D simulation with the cosine power distribution on the core.

On the Table 5.4 the most important values of the trends of the Figure 5.5 are reported.

	Power Peak [MW]	time peak [ms]	Final Power [MW]
1D-uniform power	22.20	6.38	20.32
1D-eigenvalue	22.20	5.90	20.32
2D-MSFR	22.17	6.25	20.18

Table 5.4: Values of the power of the simulations of the 1D and 2D MSFR

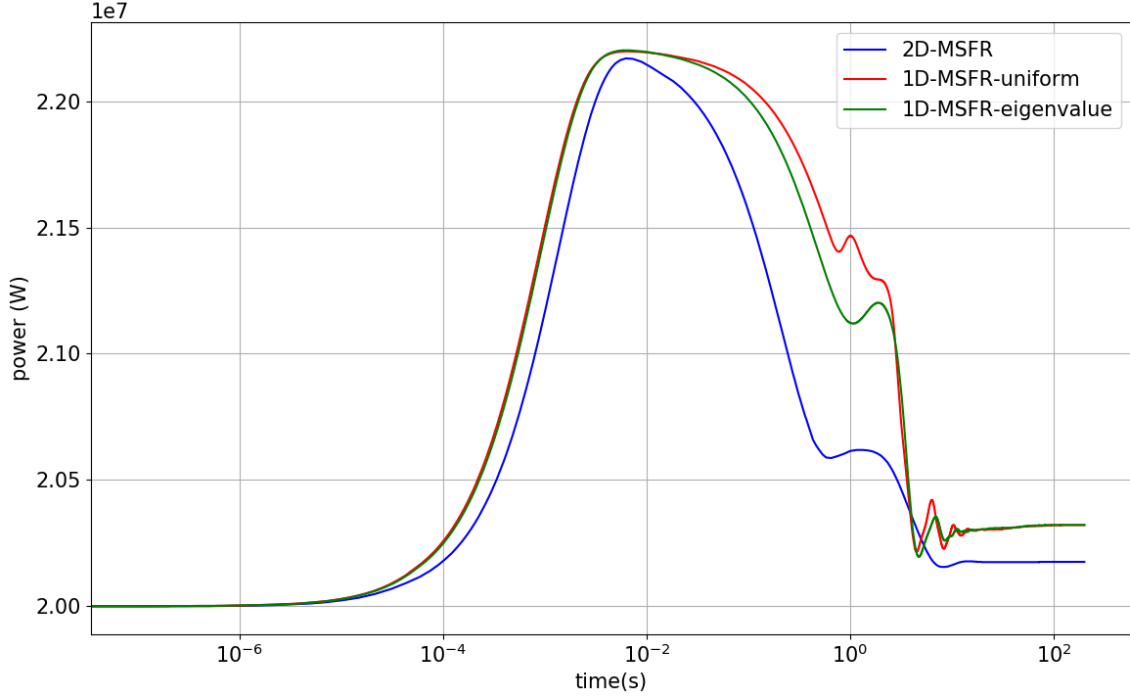


Figure 5.5: Power evolution for the three cases predicted by the point kinetics for an insertion of reactivity equal to 0.1 \$

Starting from the two 1D cases, their power trends are very similar apart for a peak and a minimum present after the peak power (respectively for the uniform power case and the cosine power one).

As for the comparison between the 2D case and the 1D cases the values of the power peaks are almost the same. The same applies for the values of the times peak of the three simulations. On the other hand, the peaks of the 1D cases have a greater amplitude than the peak of the 2D MSFR.

The most interesting aspect is the presence of the oscillations after the peak power, or better when the system approaches a new steady configuration after the perturbation, for the 1D simulations. These oscillations are due to the recirculating of the fluid in the primary circuit as can be explained with a point equation for the precursors (Eq. 5.2), taken from the point kinetics model represented by the Eq. 1.14 and 1.15 of the section 1.3.

$$\frac{dC_i(t)}{dt} = -\lambda_i C_i(t) + \frac{\beta_i}{\Lambda} P(t) - \frac{C_i(t)}{\tau_c} + \frac{C_i(t - \tau_e)}{\tau_c} e^{-\lambda_i \tau_e} \quad (5.2)$$

where  $\tau_c$  and  $\tau_e$  are the circulation time of the fluid through the core and through out of core, the  $\frac{C_i(t - \tau_e)}{\tau_c} e^{-\lambda_i \tau_e}$  is the term of the re-entering of the precursors in the core and the  $\frac{C_i(t)}{\tau_c}$  is the term of the exit precursors of the core.

Hence in a fluid system a re-entering term is presented, which is a production term, and the cause of the increase of the power in these oscillations.

The other thing to notice is that in the two dimensional simulation these oscillations seem to be damped and they can't be noticed in the power plot.

## 5. INVESTIGATION OF DIMENSIONAL EFFECTS

At the end of the transient, the power of the 1D simulations is greater than the final power in the 2D MSFR but anyway their values are very close. Lastly one can note that for the 1D geometry the power is always greater than the power on the 2D geometry.

Also the trends of the average fuel temperatures and average density of the fluid, together with the final values for the three cases are reported (Figure 5.6 and Table 5.5).

Also these results are expected but it should be noted that there are also reactivity oscillation in the 1D cases. These oscillations correspond, in terms of time, to the power oscillations seen before. This is a further proof that the power oscillations is due to the re-circulation of the precursors in the core. In fact, in the average fuel temperature there aren't oscillations so the same goes for the density and for the neutron feedback related to these physical quantities.

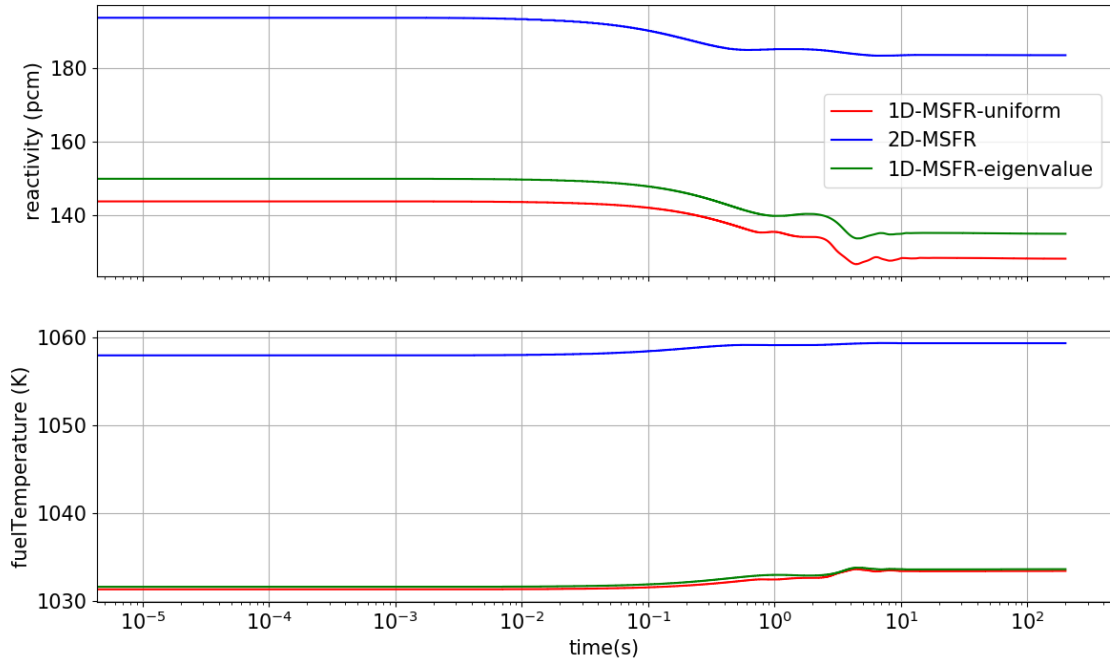


Figure 5.6: Total reactivity and average fuel temperature evolutions for the three cases predicted by the point kinetics for an insertion of reactivity equal to 0.1 \$

	$T_{fuel,avg,fin}$ [K]	$\rho_{fluid,avg,fin}$ [kg m <sup>-3</sup> ]
1D-uniform power	1033.4	4014.9
1D-eigenvalue	1033.6	4014.8
2D-MSFR	1059.3	3993.6

Table 5.5: Final values of the systems at the end of the transient

## 5.4 Exponential reduction of velocity transients

For the exponential reduction of velocity, the exponential reduction lasts 10 seconds with a characteristic time of the pump equal to 2 seconds and after the first 10 seconds of the simulations the velocity remains constant along all the system.

In the Figure 5.7 the trends of the three cases are reported and the Table 5.6 summarises the most important results.

About the shape, the trends of the powers (for the 1D cases) are very similar but for the trends 1D-MSFR-eigenvalue a lower power minimum and a higher power peak (the second peak power in the table) than in the 1D-MSFR-uniform case can be noted. This is probably due to the different power distributions of the two systems. In fact, in the plots of the Figure 5.8 there aren't significant differences which can relate this behaviour to the temperature distributions.

Moving on to the comparison between 2D and 1D, the results of the peak power, of the minimum and of the power at the end of the simulations are good. As for the transient evolution, small temporal shifts can be seen for the minimum of the power and for the peak. In the 1D simulations one more peak is present in the power trends and it is present during the exponential reduction of the velocity. This behaviour represents the main difference .

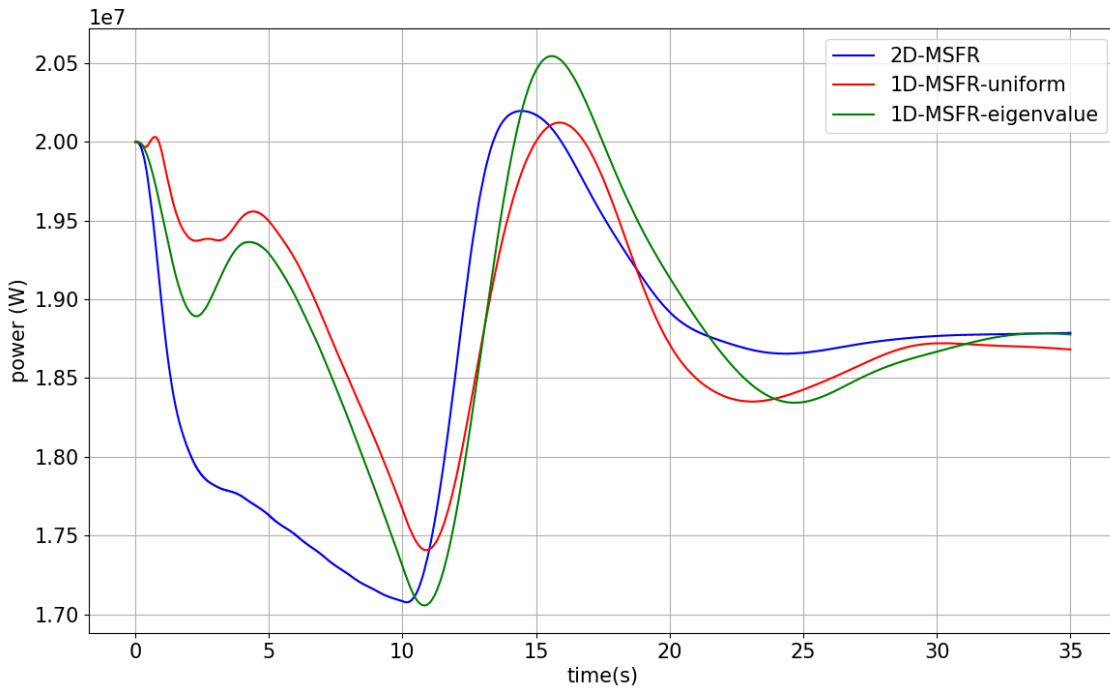


Figure 5.7: Power evolution for the three cases predicted by the point kinetics for an exponential reduction of the velocity of 10 seconds

## 5. INVESTIGATION OF DIMENSIONAL EFFECTS

	1D-uniform power	1D-eigenvalue	2D-MSFR
Minimum Power [ $MW$ ]	17.41	17.06	17.08
Time minimum [ $s$ ]	10.86	10.79	10.13
First peak power [ $MW$ ]	19.56	19.36	20.196
Time first peak [ $s$ ]	4.38	4.21	14.385
Second peak power [ $MW$ ]	20.12	20.54	//
Time second Peak [ $s$ ]	15.82	15.53	//
Power end transient [ $MW$ ]	18.64	18.78	18.79

Table 5.6: Interesting values of trends power

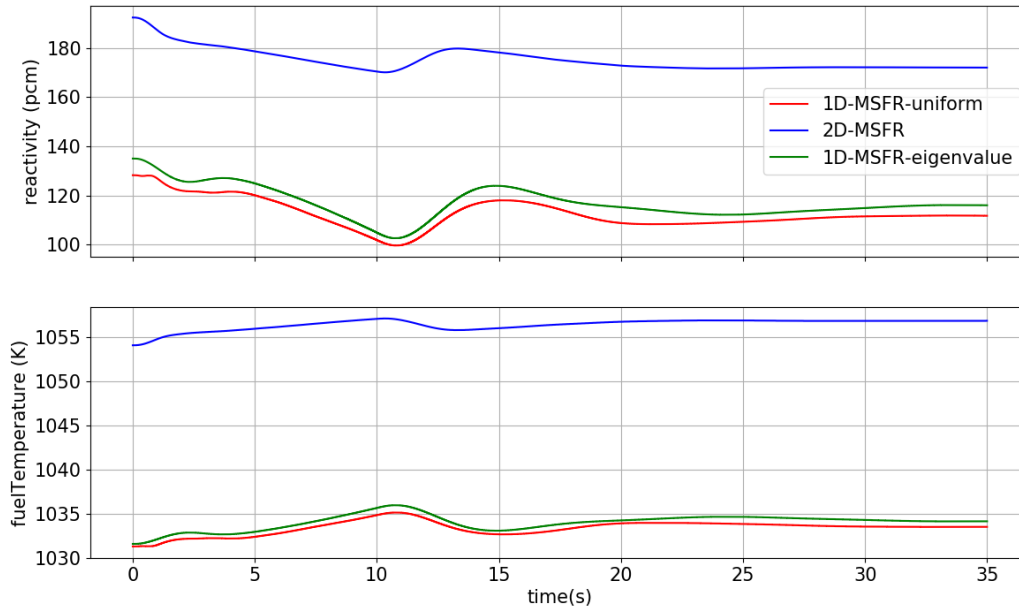


Figure 5.8: Total reactivity and average fuel temperature evolutions for the three cases predicted by the point kinetics for an exponential reduction of the velocity of 10 seconds

	$T_{fuel,avg,fin}$ [K]	$\rho_{fluid,avg,fin}$ [ $kg\ m^{-3}$ ]	Final total reactivity [pcm]
1D-uniform power	1033.6	4014.8	111.528
1D-eigenvalue	1034.2	4014.3	116.026
2D-MSFR	1056.9	3995.6	171.967

Table 5.7: Final values of the systems at the end of the transient

## 5.4. EXPONENTIAL REDUCTION OF VELOCITY TRANSIENTS

From the plot of the total reactivity, it can be noted a more reduction of the total reactivity during the exponential reduction transient for the 1D cases than in the 2D case. This behaviour can not be linked to the feedback of the fuel temperature, as their trends show.

Because the temperature feedback can't be responsible for this behaviour, the same is true for the density. The behaviour can be explained looking at the trends of the the quantity, called *liquidFuelBeta*, for the different cases (Figure 5.9). The *liquidFuelBeta* is the effective fraction of precursors with the inclusion of the re-circulation of the precursors.

$$\beta_{fluid}(t) = \frac{\Lambda}{P_{old}} \sum_{i=1}^R \lambda_i c_i(t) \quad (5.3)$$

Then between the 1D and 2D transients the increase of the reactivity due to the precursors is much greater in the 1D systems than in the 2D one. This means that in the 1D systems a greater increase of the precursors occurs than in the 2D one, of course this increase is located in the core region.

This behaviour explains the first peaks during the 1D transients because this term, which is increasing and it is a positive term in the power equation. Then it can justify those power peaks during the transient even if the peaks are during the exponential reduction of the velocity. This effect doesn't appear in the 2D simulation, obviously due to a smaller increase of this quantity.

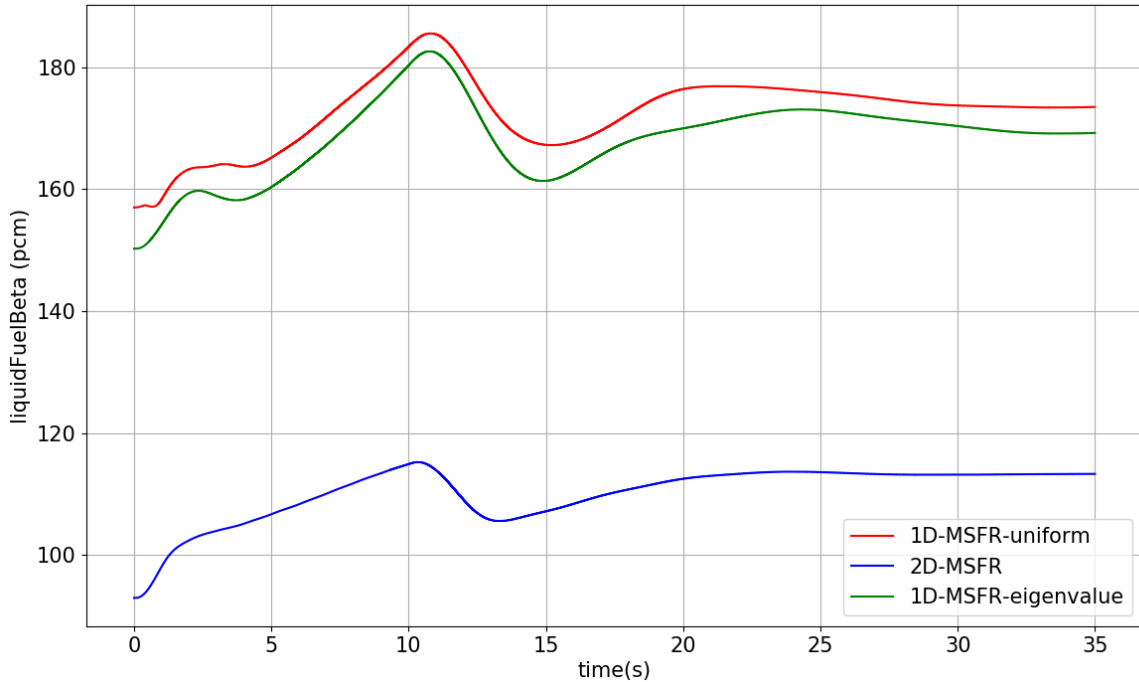


Figure 5.9:  $\beta_{fluid}$  evolution for the three cases predicted by the point kinetics for an exponential reduction of the velocity of 10 seconds

## 5.5 Conclusion of the comparison

There are some differences between the results of the two dimensional approach and the one dimensional one. Both for the insertion of reactivity and for the reduction of the velocity these differences can be seen in the plots for the power.

Furthermore these differences have also physical explanations which are related to the distributions of the precursors in the system.

The oscillations seen in the section 5.3 can be brought back to the re-entering and exit terms of the balance of precursors (Figure 5.10).

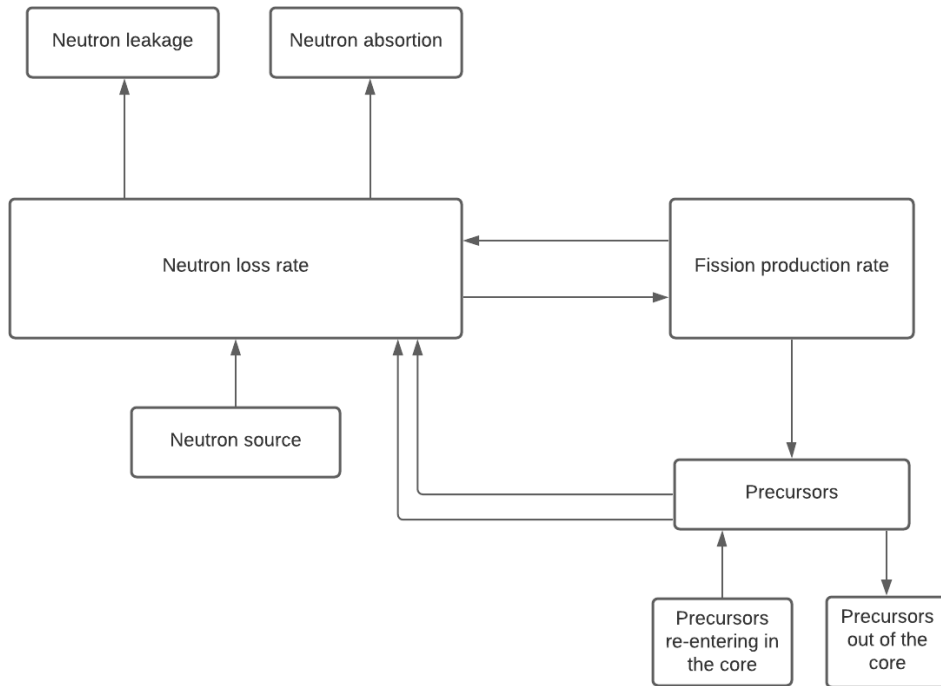


Figure 5.10: Kinetics balance of a fluid fuel nuclear system

However the most interesting difference seen in this comparison between the 2D and the 1D approach is the presence of a peak during the exponential reduction of velocity for the 1D cases. As explain before, the reason of these peaks are linked to the precursors which are getting in the core region. This phenomenon is linked to the different spatial distributions of the precursors in the different systems. In conclusion, this section shows in more details an important feature of this modified point kinetics models, that is the capacity to compute the spatial distributions or the precursors. Thanks to this feature is possible to see behaviours which can not be seen with a classical point kinetics formulation. In particular, in a classical point kinetics formulation the precursors will be seen as a point-like quantity in the reactor and for this reason the spatial information will be lost and this comparison, which is made in order to investigate the multi-effect scale, is impossible with a classical approach. Also, this approach makes it possible not to lose information regarding the importance of precursors which, as seen in the results, are important during the development of the transients.

# Conclusions

The spatial description of precursors is important in fluid fuel nuclear systems, as seen in the 5. Regarding the point kinetics models for these types of systems, there are not models with a fully spatial description of the precursors. The goal of this thesis is precisely to obtain a modified point kinetics model with this characteristic. Therefore, the point kinetics model with the fully spatial description of the precursors is derived with the introduction of some hypothesis regarding some neutronic parameters of the multi-group diffusion. After, it has implemented in GeN-Foam in order to use it as a neutronic sub-solver for the liquid fuel nuclear system.

Then, in the second section of the thesis a test of the point kinetics model is made through a comparison with an analytical model in a closed channel with a one dimensional mesh. The comparison shows as the new point kinetics model manages to predict the final state of the system after different transients with different perturbations, in more details a transient with an insertion of external reactivity and after a exponential transient on the velocity where it is reduced. The results show that even using a coarse mesh the neutronic solver developed manages to get errors very low. Obviously these errors can be reduced with a mesh refinement, even if they slightly decrease.

After an additional comparison of the point kinetics on a two dimensional model of the MSFR is made. This comparison has the goal to test the point kinetics during some transients through a more complex and already verified neutronic solver, that is the multi-group diffusion solver implemented on GeN-Foam. The comparison shows as the point kinetics model manages to predict very well the dynamic evolution of the system during the transients, both for a simple transient, the external reactivity insertion transient, and for other more complex ones, the exponential reduction of velocity transients. Also, the comparison shows as the feature of describing the precursors as spatial distributions of the system works very well. This can be seen by the comparison between the spatial distributions of precursors obtained by the diffusion and by the point kinetics which are very similar. Furthermore, through a comparison with the different transients, involving the velocity fields, it has been shown as the new neutronic solver manages to describe quite well the fully spatial evolution of the different precursors in the system.

Finally, the investigation of the dimensional effects is faced through the two dimensional MSFR and the one dimensional closed channel built based on the MSFR. The results show how important it is to properly treat the precursors in these nuclear systems. In fact, from the analysis of the results it can be noted that the differences during the transients between the 2D and 1D systems are related to precursors. For the transient with the insertion of external reactivity, the oscillations due to re-entering of the precursors on the

## 6. CONCLUSIONS

---

core can be noted. In the closed channel instead in the 2D system these oscillations are damped. Also, in the transient with the exponential reduction of velocity the peak power presents during the decrease of velocity is due to the precursors, that in the 1D cases they increase more in the core region than in the 2D case.

Hence, the point kinetics model, developed and implemented on GeN-Foam in this thesis work, achieves very good results as seen thanks to the different comparisons made and it manages to obtain interesting results regarding the dimensional effects due to the precursors in the liquid fuel nuclear system.

Regarding future works this point kinetics model could be used to investigate the dimensional effects of the precursors in a three dimensional (3D) description of the system and of the precursors with a comparison with the results obtained in the last section of this thesis. Also, a validation with experimental data can be made as future works in order to test in more details the model and its limits.

# Appendix

## A.1 solvePointKineticsLiquidFuel.H

```
//- Get solution contro
const dictionary& neutronTransport =
mesh_.solutionDict().subDict("neutronTransport");

scalar neutronIterationResidual =
neutronTransport.lookupOrDefault<scalar>
(
    "neutronIterationResidual",
    0.00001
);
int maxNeutronIterations =
neutronTransport.lookupOrDefault<int>("maxNeutronIterations", 10);

//- Update reactivity coefficients
#include "computeFeedbackFieldValues.H"
#include "correctReactivity.H"

//- Update old time step values if time step has changed
if(timeIndex_ != mesh_.time().timeIndex())
{
    timeIndex_ = mesh_.time().timeIndex();
    powerOld_ = power_;
}

scalar dt(mesh_.time().deltaT().value());

//- prepare fields necessary to weight precursors
PtrList<scalar> weightedPrec(delayedGroups_);

//- Iterate precursors and power till sufficiently small prec residual
int neutroIter = 0;
scalar neutroResidual = 0.0;

//- Check if you need to initialize precurosr distribution
bool initialize = false;
```

## APPENDIX A. APPENDIX

---

```
if(initPrecursorsLiquidFuel_ &&
    (mesh_.time().timeIndex() == mesh_.time().startTimeIndex()+1) && neutroIter==0)
{
    initialize = true;
}

//Calc equilibrium precPK at the steady-state
if(initialize)
{
    forAll(precPK_,precI)
    {
        fvMatrix<scalar> precEq
        (
            fvm::Sp(dimensionedScalar("",dimless/dimTime, lambdas_[precI])*alphaPtr_(),
                precPKStar_[precI])
            - initOneGroupFluxN_*dimensionedScalar("",dimPower,power_)*betas_[precI]/
            dimensionedScalar("",dimTime,promptGenerationTime_)
            + fvm::div(phiPtr_(), precPKStar_[precI], "div(phi_,precStar_)")
            - fvm::laplacian(diffCoeffPrecPtr_(), precPKStar_[precI])
        );
        precEq.solve();
        precPKStar_[precI].storePrevIter();
    }
}

//Calc the precEquilibriumReactivity
if(initialize)
{
    precEquilibriumReactivity_=0.0;
    precEquilibriumReactivity_ += beta_;

    forAll(precPKStar_,precI)
    {
        //- Conver to precs per total volume
        precPK_[precI] = precPKStar_[precI] * alphaPtr_();
        precPK_[precI].correctBoundaryConditions();

        weightedPrec.set(precI,new scalar(fvc::domainIntegrate(
            initOneGroupFluxN_*precPK_[precI]).value()/domainIntegratedInitOneGroupFluxN_ ));

        precEquilibriumReactivity_ -= weightedPrec[precI] * lambdas_[precI] *
            promptGenerationTime_ / powerOld_;
    }
    #include "correctReactivity.H"
    Info << "precEquilibriumReactivity[pcm] = " << precEquilibriumReactivity_ *1e+5 << nl << endl;
}
}
```

```

do
{
  Info << "Neutron iteration no:  " << neutroIter << nl << endl;

  //- Solve for precursors
  neutroResidual = 0.0;

  forAll(precPK_,precI)
  {
    //- Solve precursors
    fvMatrix<scalar> precEq
    (
      fvm::ddt(alphaPtr_(), precPKStar_[precI])
      + fvm::Sp(dimensionedScalar("",dimless/dimTime,lambdaS_[precI])*alphaPtr_(),
        precPKStar_[precI])
      - initOneGroupFluxN_*dimensionedScalar("",dimPower,power_)*betas_[precI]/
        dimensionedScalar("",dimTime,promptGenerationTime_)
      + fvm::div(phiPtr_(), precPKStar_[precI], "div(phi_,precStar_)")
      - fvm::laplacian(diffCoeffPrecPtr_(), precPKStar_[precI])
    );

    scalar initRes = precEq.solve().max().initialResidual();
    neutroResidual = max(neutroResidual,initRes);

    //- Conver to precs per total volume
    precPK_[precI] = precPKStar_[precI] * alphaPtr_();
    precPK_[precI].correctBoundaryConditions();

    //- Calculate weighted precursors to be fed to power equation
    weightedPrec.set(precI,new scalar(fvc::domainIntegrate(
      initOneGroupFluxN_*precPK_[precI]).value()/domainIntegratedInitOneGroupFluxN_ ));
  }

  scalar liquidFuelBeta= 0.0;

  forAll(precPKStar_,precI)
  {
    //- Conver to precs per total volume
    precPK_[precI] = precPKStar_[precI] * alphaPtr_();
    precPK_[precI].correctBoundaryConditions();

    scalar weightedPrecI = (fvc::domainIntegrate(
      initOneGroupFluxN_*precPK_[precI]).value()/domainIntegratedInitOneGroupFluxN_ );

    liquidFuelBeta += weightedPrecI * lambdaS_[precI] *
      promptGenerationTime_ / powerOld_;
  }

  Info << "liquidFuelBeta[pcm] =  " << liquidFuelBeta*1e+5 << nl << endl;
}

```

## APPENDIX A. APPENDIX

---

```
//- Calc power
scalar sumPrecLamda = 0.0;
forAll(precPK_,precI)
{
    sumPrecLamda += weightedPrec[precI] * lambdas_[precI];
}

power_ = (powerOld_/dt+sumPrecLamda)/
(
    1.0/dt - (totalReactivity_-beta_)/promptGenerationTime_
);

Info<<"Intermediate Power for the next iteration in the precursors equation[W] =
"<< power_ <<nl <<endl;

neutroIter++;

//- Some info on iterations
Info<< "neutroResidual (couplingIter: " << couplingIter
<< ", neutroIter: " << neutroIter << "): " << neutroResidual
<< endl;
}
while((neutroResidual > neutronIterationResidual)
    && (neutroIter < maxNeutronIterations)
    );

//- Re-scale fluxes, volFuelPower
scalar fluxScaleFactor = power_/powerOld_;

for (int i = 0; i < energyGroups_; i++)
{
    fluxes_[i] *= fluxScaleFactor;
    fluxes_[i].correctBoundaryConditions();
}

oneGroupFlux_ *= fluxScaleFactor;
oneGroupFlux_.correctBoundaryConditions();

volFuelPower_ *= fluxScaleFactor;
volFuelPower_.correctBoundaryConditions();

Info << endl << "pointKinetics: " << endl;
#include "pointKineticsInfo.H"
```

## A.2 computeFeedbackFieldValues.H

```

//- Create field for weighting. This is currently done on the oneGroupFlux,
// rather than on the energy-dependent adjoint. It will be changed in the
// future
volScalarField oneGroupFluxSqr(sqr(oneGroupFlux_));

scalar domainIntegratedFluxSqrFuel
(
    fvc::domainIntegrate(oneGroupFluxSqr*fuelFeedbackCellField_).value()
);
scalar domainIntegratedFluxSqrCool
(
    fvc::domainIntegrate(oneGroupFluxSqr*coolFeedbackCellField_).value()
);

//- Compute average perturbed values
scalar TFuelValue
(
    fvc::domainIntegrate
    (
        oneGroupFluxSqr*TFuel_*fuelFeedbackCellField_
    ).value()/
    domainIntegratedFluxSqrFuel
);
scalar TCladValue
(
    fvc::domainIntegrate
    (
        oneGroupFluxSqr*TClad_*fuelFeedbackCellField_
    ).value()/
    domainIntegratedFluxSqrFuel
);
scalar TCoolValue
(
    fvc::domainIntegrate
    (
        oneGroupFluxSqr*TCool_*coolFeedbackCellField_
    ).value()/
    domainIntegratedFluxSqrCool
);
scalar rhoCoolValue
(
    fvc::domainIntegrate
    (
        oneGroupFluxSqr*rhoCool_*coolFeedbackCellField_
    ).value()/
    domainIntegratedFluxSqrCool
);
scalar TStructValue
(
    fvc::domainIntegrate
    (
        oneGroupFluxSqr*TStruct_*structFeedbackCellField_
    ).value()/

```

```
    fvc::domainIntegrate(oneGroupFluxSqr*structFeedbackCellField_).value()
);
scalar TDrivelineValue
(
    fvc::domainIntegrate
    (
        oneGroupFluxSqr*TStruct_*drivelineFeedbackCellField_
    ).value()/
    fvc::domainIntegrate(oneGroupFluxSqr*drivelineFeedbackCellField_).value()
);
```

### A.3 correctReactivity.H

```
scalar DopplerReactivity =
    -coeffFastDoppler_*
    Foam::log(max(TFuelValue, SMALL)/max(TFuelRef_, SMALL));

scalar TFuelReactivity =
    coeffTFuel_*(TFuelValue - TFuelRef_);

scalar TCladReactivity =
    coeffTClad_*(TCladValue - TCladRef_);

scalar TCoolReactivity =
    coeffTCool_*(TCoolValue - TCoolRef_);

scalar rhoCoolReactivity =
    coeffRhoCool_*(rhoCoolValue - rhoCoolRef_);

scalar TStructReactivity =
    coeffTStruct_*(TStructValue - TStructRef_);

scalar drivelineExpValue
(
    coeffDrivelineExp_*(TDrivelineValue - TDrivelineRef_)
);
scalar drivelineReactivity(calcDrivelineReactivity(drivelineExpValue));

Pair<scalar> GEMLevelAndReactivity(calcGEMLevelAndReactivity());
scalar GEMSodiumLevel(GEMLevelAndReactivity.first());
scalar GEMReactivity(GEMLevelAndReactivity.second());

(void) GEMSodiumLevel;

totalReactivity_ =
    precEquilibriumReactivity_
    + externalReactivity_
    + DopplerReactivity
    + TFuelReactivity
    + TCladReactivity
    + TCoolReactivity
    + rhoCoolReactivity
    + TStructReactivity
    + drivelineReactivity
    + GEMReactivity;
```

# Bibliography

- [1] M. Brovchenko, D. Heuer, E. Merle-Lucotte, M. Allibert, V. Ghetta, A. Laureau, and P. Rubiolo, “Design-related studies for the preliminary safety assessment of the molten salt fast reactor,” *Nuclear Science and Engineering*, vol. 175, no. 3, pp. 329–339, 2013.
- [2] G. I. Bell and S. Glasstone, “Nuclear reactor theory,” tech. rep., US Atomic Energy Commission, Washington, DC (United States), 1970.
- [3] M. Zanetti, A. Cammi, L. Luzzi, J. Křepel, and K. Mikityuk, “Extension of the fast code system for the modelling and simulation of msr dynamics,” in *Proceedings of ICAPP*, pp. 03–06, 2015.
- [4] J. Serp, M. Allibert, O. Beneš, S. Delpech, O. Feynberg, V. Ghetta, D. Heuer, D. Holcomb, V. Ignatiev, J. L. Kloosterman, *et al.*, “The molten salt reactor (msr) in generation iv: overview and perspectives,” *Progress in Nuclear Energy*, vol. 77, pp. 308–319, 2014.
- [5] T. J. Dolan, *Molten salt reactors and thorium energy*. Woodhead Publishing, 2017.
- [6] C. Fiorina, I. Clifford, M. Aufiero, and K. Mikityuk, “Gen-foam: a novel openfoam® based multi-physics solver for 2d/3d transient analysis of nuclear reactors,” *Nuclear Engineering and Design*, vol. 294, pp. 24–37, 2015.
- [7] Z. Akcasuh, *Mathematical methods in nuclear reactor dynamics*. Elsevier, 2012.
- [8] D. L. Hetrick, “Dynamics of nuclear reactors.,” 1971.
- [9] C. R. GUERRIERI, “Investigation of the dynamic behaviour and of control issues of circulating fuel reactors,” 2013.
- [10] G. Lapenta, F. Mattioda, and P. Ravetto, “Point kinetic model for fluid fuel systems,” *Annals of Nuclear Energy*, vol. 28, no. 17, pp. 1759–1772, 2001.
- [11] C. Guerrieri, A. Cammi, and L. Luzzi, “An approach to the msr dynamics and stability analysis,” *Progress in Nuclear Energy*, vol. 67, pp. 56–73, 2013.
- [12] S. Dulla, P. Ravetto, and M. Rostagno, “Neutron kinetics of fluid–fuel systems by the quasi-static method,” *Annals of Nuclear Energy*, vol. 31, no. 15, pp. 1709–1733, 2004.
- [13] C. Guerrieri, A. Cammi, and L. Luzzi, “A preliminary approach to the msfr control issues,” *Annals of Nuclear Energy*, vol. 64, pp. 472–484, 2014.

## BIBLIOGRAPHY

---

- [14] J. Krepel, U. Rohde, U. Grundmann, and F.-P. Weiss, “Dynamics of molten salt reactors,” *Nuclear Technology*, vol. 164, no. 1, pp. 34–44, 2008.
- [15] A. Cammi, C. Fiorina, C. Guerrieri, and L. Luzzi, “Dimensional effects in the modelling of msr dynamics: moving on from simplified schemes of analysis to a multi-physics modelling approach,” *Nuclear Engineering and Design*, vol. 246, pp. 12–26, 2012.
- [16] C. Fiorina, A. Cammi, C. Guerrieri, L. Luzzi, and B. Spinelli, “Development of a simulation tool for a preliminary analysis of the msr core dynamics,” in *Proceedings of the International Conference Nuclear Energy for New Europe 2010*, 2010.
- [17] S. Ball and T. Kerlin, “Stability analysis of the molten-salt reactor experiment,” tech. rep., Oak Ridge National Lab., Tenn., 1965.
- [18] A. F. Henry *et al.*, *Nuclear-reactor analysis*, vol. 4. MIT press Cambridge, Massachusetts, 1975.
- [19] C. Fiorina, N. Kerkar, K. Mikityuk, P. Rubiolo, and A. Pautz, “Development and verification of the neutron diffusion solver for the gen-foam multi-physics platform,” *Annals of Nuclear Energy*, vol. 96, pp. 212–222, 2016.